Technological University Dublin
ARROW@TU Dublin

Doctoral | Science

2013-8

Studies of Shrinkage in Photopolymerisable Materials for Holographic Applications

Mohesh Moothanchery
Technological University Dublin, moheshm@gmail.com

Follow this and additional works at: https://arrow.tudublin.ie/sciendoc

 Part of the Physics Commons

Recommended Citation

Moothanchery, M. (2013). *Studies of Shrinkage in Photopolymerisable Materials for Holographic Applications*. Doctoral Thesis. Technological University Dublin. doi:10.21427/D7859T

This Theses, Ph.D is brought to you for free and open access by the Science at ARROW@TU Dublin. It has been accepted for inclusion in Doctoral by an authorized administrator of ARROW@TU Dublin. For more information, please contact arrow.admin@tudublin.ie, aisling.coyne@tudublin.ie, vera.kilshaw@tudublin.ie.

STUDIES OF SHRINKAGE IN PHOTOPOLYMERISABLE MATERIALS FOR HOLOGRAPHIC APPLICATIONS

Mohesh Moothanchery M.Sc (Integrated)

A thesis submitted for the degree of Doctor of Philosophy to the Dublin Institute of Technology

Supervisors:

Dr. Izabela Naydenova , Prof. Vincent Toal

Centre for Industrial and Engineering Optics
School of Physics
Dublin Institute of Technology
Kevin Street, Dublin 08, Ireland

August 2013

ABSTRACT

Holography is now firmly established as a tool for scientific and engineering studies and also as a display medium. Holographic performance mainly depends on the choice of recording wavelengths, recording material, recording conditions and experimental setup as well as environmental conditions in the laboratory. Acrylamide based photopolymer has significant advantages as a holographic recording material such as self-development, low scatter, high diffraction efficiency, ease of preparation and low cost.

The main objective of this project is to determine and minimise the shrinkage of an acrylamide based photopolymer developed in the Centre for Industrial and Engineering Optics for holographic recording. This recording material is sensitized in the visible spectrum with Erythrosine B, a green sensitive dye. The shrinkage of the material is determined for different exposure intensities and thicknesses using different techniques in order to determine the optimum conditions for holographic recording. We also have carried out experiments at different spatial frequencies of recording. The influence of nanoparticle dopants on the shrinkage, diffraction efficiency and the dynamic range of the photopolymer system is also studied.

The results shows that careful consideration is needed to attain maximum efficiency and minimum shrinkage during holographic recording. Incorporation of zeolite nanoparticles shows improvement in holographic recording characteristics in the photopolymer material. Diffraction efficiency is improved up to 40% and shrinkage is reduced to one half with increased concentration of nanoparticles.

Using Electronic Speckle Pattern Interferometry (ESPI) phase shifting technique a 3D map due to shrinkage has been calculated. The shrinkage map has the same circular symmetry as the profile of the recording beam as expected.

Declaration

I certify that this thesis which I now submit for examination for the award of Doctor of Philosophy is entirely my own work and has not been taken from work by any other person. All the relevant works or quotations or paraphrase of another person has been duly acknowledged in the work.

This thesis was prepared according to the regulations for the postgraduate study by research of the Dublin Institute of Technology and has not been submitted either in part or in whole for an award at any other Institute or University.

The work reported in this thesis conforms to the principles of the Institute's guidelines for ethics in research.

The Institute has permission to keep, to lend or to copy this thesis in whole or in part, on condition that any such use of the material of the thesis is duly acknowledged.

Signature _____ Date_____

Acknowledgements

I would like to take this opportunity to thank a number of people who gave suggestions who encouraged me and who helped with valuable advice and assistance.

First and foremost, I would like to express my respect and gratitude to Dr. Izabela Naydenova and Prof. Vincent Toal, my supervisors for their valuable suggestions and encouragement all through my project.

I would like to thank my colleague Dr. Viswanath Bavigadda for his valuable help in writing LabVIEW programme and MATLAB codes.

I would like to thank my research colleagues from Centre for Industrial and Engineering Optics, Dr. Suzanne Martin, Dr. Emilia Mihaylova, Dr. Chakrapani Meka, Dr. Elsa Leita, Dr. Raghavendra Jallapuram, Dr. Pavani Kotakonda, Mr. Dennis Bade, Ms. Dervil Cody, Ms. Tatsiana Mikulchyk, Ms. Amanda Creane, Ms. Hoda Akbari, Dr. Lina Persechini and everyone else from the IEO and FOCAS for their friendship and technical advice.

Also, I would like to thank Prof. Svetlana Mintova for providing the nanoparticles and SEM images.

Additionally I would like to thank the technical staff from School of Physics and the FOCAS building.

Finally I would like to acknowledge scholarships provided by the Technological Sector Research: Strand I - Post-Graduate R&D Skills Programme, DIT Fiosraigh PhD Scholarship Extension scheme, SPIE student scholarship, Travel grant from COST ACTION MP0604 Optical Micro-Manipulation by Nonlinear Nanophotonics, FOCAS Institute and School of Physics, DIT Kevin Street for providing laboratory facilities.

List of Abbreviations

CCD - Charged Coupled Device

CMOS - Complementary Metal Oxide Semiconductor

DAPP - Diallyl Phthalate Pre-Polymer

DC - Direct Current

DCG - Dichromated Gelatin

DLS - Dynamic Light Scattering

Er.B - Erythrosine B

ESPI - Electronic Speckle Pattern Interferometry

GERI - General Engineering Research Institute

HBP - Hyperbranched Polymer

He -Ne - Helium- Neon

HPEMA - Hyperbranched Poly (Ethyl Methacrylate)

IEO - Industrial and Engineering Optics

IPN - Interpenetrating Network

SHPE - Silver Halide Photographic Emulsion

LCD - Liquid Crystal Display

LS-CAS - Low Shrinkage Cyclic Allylic Sulfides

MEX - Matlab Executable

Nd-YVO_4- Neodymiun-Doped Yttrium Orthovanadate

NI - National Instruments

PMMA - Polymethylmethacrylate

POSS - Polyhedral Oligomeric Silsesquioxane

PVC - Polyvinyl Chloride

PVCz - Poly-N-Vinyl Carbazole

PZT - Piezoelectric Transducer

TEA - Triethanolamine

TEOS - Tetraethyl Orthosilicate

TSPEG - Triethoxysilylpropyl Polyethyleneglycol Carbamate

TEM - Transmission Electron Microscopy

VI - Virtual Instrument

2D-SRNCP - Two-Dimensional Phase-unwrapping algorithm, based on Sorting by Reliability, following a Non-Continuous Path

Table of Contents

List of figures

List of Tables

Summary of thesis

Chapter 1: focuses on the theory of holography, different hologram types, applications of holography, challenges in holography and different materials used for holographic recording.

Chapter 2: focuses on photopolymer material and the mechanisms involved in holographic recording and also the advantages and disadvantages of photopolymer as holographic recording media.

Chapter 3: focuses on the shrinkage occurring in photopolymer as a result of holographic recording, models used to determine shrinkage and an overview of the shrinkage determined in different photopolymer material.

Chapter 4: deals with the shrinkage study in acrylamide photopolymer developed at IEO, and includes intensity, spatial frequency and thickness dependence of shrinkage in photopolymer material determined from the shift of Bragg curve. The effect of incorporating zeolite nanoparticles on photopolymer shrinkage is also reported.

Chapter 5: deals with theory of holographic interferometry and different techniques and sensitivities.

Chapter 6: deals with the real time shrinkage study in photopolymer films using holographic interferometry and also the influence of nanoparticles on photopolymer shrinkage.

Chapter 7: deals with electronic speckle pattern interferometry (ESPI) principles and different techniques and sensitivities.

Chapter 8: deals with the shrinkage study in photopolymer films by ESPI technique.

Chapter 9: summarises the achievements and also discusses the future scope of this work.

Appendix: The MATLAB and LabVIEW codes used during the work are discussed.

CHAPTER 1

HOLOGRAPHY

1.1 History of Holography

The theory of holography was developed by Gabor in 1947 [1] when he was working to improve the resolution of the electron microscope. The basic idea was that for perfect optical imaging, the object should be recorded as a whole, both the amplitude and phase of the electron wave from the object needs to be recorded. In this manner a significantly magnified picture can be obtained when the recording is illuminated at visible wavelength. Gabor used the term hologram from the Greek word ‘holos’ meaning ‘whole’ or ‘entire’ and ‘graphein’ ‘to write’. Holography is a technique which records not only the irradiance at each point in an image but also the direction in which the wave propagates at that point. That is what the name holography means, a ‘whole record’, whereas conventional photography records only the intensity of the optical wave at each point. In 1971 Gabor was awarded the Nobel Prize in Physics for the invention and development of the holographic method [1, 2]. Gabor’s technique, also called in-line holography, had the drawback of formation of twin images (normal and conjugate) which are always both in the viewer’s line of sight during reconstruction. Further development in the field occurred during 1960 with the invention by Maiman while working at Hughes Research Laboratory [3] of the ruby laser which can emit a very powerful burst of light which lasts a few nanoseconds. The first hologram of a person was made using a pulsed laser in 1967 [4].

It was in 1962 Leith and Upatnieks [5, 6] developed the first laser transmission hologram of a 3D object. They used a separate reference beam from the same source to record the hologram. The technique they developed is called off-axis holography since the reference beam illuminates the photographic plate at an angle offset to the object beam. The transmission holograms produced were of good clarity but the drawback was that it required a laser light to view the holographic image. The technique that they developed is still the basis of holographic methodology.

In 1962 Denisyuk [7] combined holography with Lippmann's [8] work in natural colour holography and produced a white light reflection hologram which can be viewed by an ordinary incandescent lamp.

Benton [9] in 1968 invented white light transmission holography which was a major advance in display holography. This is a type of hologram which can be viewed in ordinary white light creating rainbow colours. This technique created a wide awareness of holography because of its importance for mass production of holograms.

1.2 Theory of Holography

Holography is basically a two-step process which involves

1) Writing the hologram which involves recording amplitude and phase information on a photographic plate
2) Reading the hologram by illuminating it with the reference beam used during the time of recording

The basic idea behind the recording process is that the intensity distribution in the interference pattern from two or more coherent electromagnetic waves is a function of the relative phases of the waves. The interference pattern contains both information about the amplitude of light reflected or scattered by the object, that is the object beam, and information about the relative phase of the object and reference beams. Using the phenomenon of interference it is possible to encode both amplitude and phase information in a recording device such as a film which is sensitive only to the intensity of the exposing light field.

1.2.1 In-Line holography

Gabor's technique [2] also known as in-line holography uses a collimated beam from a monochromatic point source (a mercury lamp filtered to isolate the 546 nm spectral line) to illuminate a semi-transparent object. A Fresnel diffraction pattern of the object is recorded on a photographic plate as shown in Fig.1.1.

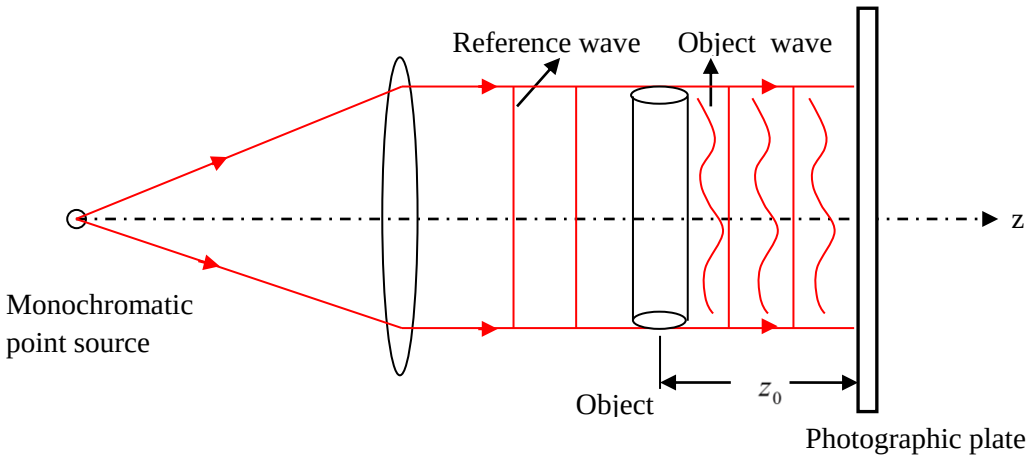

Figure 1.1. Gabor's in-line holography set up

The beam that passes through the semi-transparent object consists of both scattered and unscattered beams of light

Let $$u_o(x,y) = a_o(x,y)e^{-i\varphi_o(x,y)} \quad (1.1)$$

represent the complex amplitude of the object beam at any point *(x, y)* on the surface of photographic plate and

$$u_r(x,y) = a_r(x,y)e^{-i\varphi_r(x,y)} \quad (1.2)$$

represent the complex amplitude of the reference beam.

where a_o and φ_o are the amplitude and phase of the object beam and

a_r and φ_r those of the reference beam.

The two wavefronts interfere and the resulting intensity on the photographic plate is

$$\begin{aligned} I(x,y) &= [u_o(x,y)+u_r(x,y)][u_o^*(x,y)+u_r^*(x,y)] \\ &= a_r^2 + a_o^2 + u_o^* u_r + u_o u_r^* \end{aligned} \quad (1.3)$$

where * denotes complex conjugate

The photosensitive material is exposed to the interference pattern described by equation 1.3, and the amplitude transmittance (ratio of the transmitted light amplitude to incident light amplitude) of the material changes as a result.

It is considered for simplicity that the amplitude transmittance *t (x, y)* is proportional to *I (x, y)*

$$t(x,y) = t_0 + \beta It \quad (1.4)$$

t_0 - constant background transmittance, *t*- exposure time, β - a constant determined by the recording material and processing conditions

$$t(x,y) = t_0 + \beta t[a_r^2 + a_o^2 + u_o^* u_r + u_o u_r^*] \quad (1.5)$$

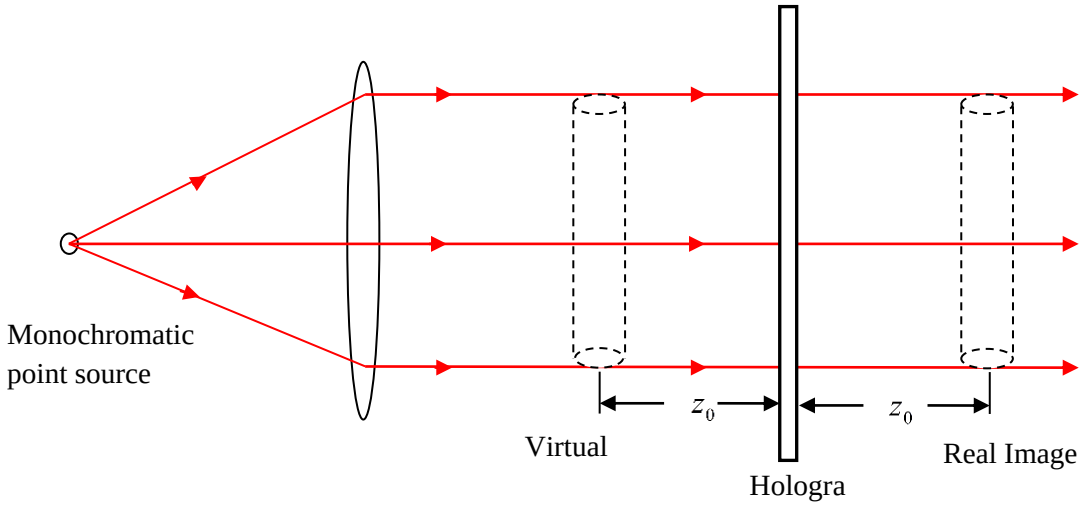

Figure 1.2. Reconstruction of image from an in-line hologram

Reconstruction from the hologram is by illuminating with a reference beam whose complex amplitude is $u_r(x,y)$

The complex amplitude transmitted by the hologram can be written as the product of the illuminating plane wave and the amplitude transmittance.

$$\begin{aligned} r(x,y) &= u_r(x,y)t(x,y) = u_r(x,y)\{t_0 + \beta t[a_r{}^2 + a_o{}^2 + u_o{}^* u_r + u_o u_r{}^*]\} \\ &= u_r(x,y)(t_o + \beta t a_r{}^2) + \beta t u_r(x,y) a_o{}^2 + \beta t a_r{}^2 u_o + \beta t a_r{}^2 u_o{}^* \end{aligned} \quad (1.6)$$

The first term in the above equation $u_r(x,y)(t_o + \beta t a_r{}^2)$ is the directly transmitted beam. The second term is extremely small and can be neglected because the object beam intensity (scattered beam) is very small compared to that of the reference beam (unscattered beam). The third term is similar to the original object wavefront incident on the photographic plate during the recording and gives rise to the reconstructed wavefront from the hologram to form a virtual image of the object behind the hologram. The fourth term is similar to the third one but contains the complex conjugate of the object wavefront. It has opposite wavefront curvature and forms a real image in front of the hologram. A hologram is not a recording of the

image; unlike a photograph it is the recording of the pattern of interference between the object and the reference waves. The type of holograms made here are referred to as transmission holograms because the object beam and reference beam are incident on the same side of the film, and reconstruction of the image occurs with the reference beam incident on the opposite side of the film from which the reconstruction is normally viewed.

1.2.2 Off-axis holography

The introduction of a laser with longer coherence length made possible for a new recording geometry in holography. The recording arrangement for the off-axis holographic technique developed by Leith and Upatnieks [2, 3] is shown in Fig 1.3. A separate reference beam is used during the recording process. The success of holography is mainly associated with the introduction of this technique. The reference beam is a beam with uniform intensity from the same source that is used to illuminate the object.

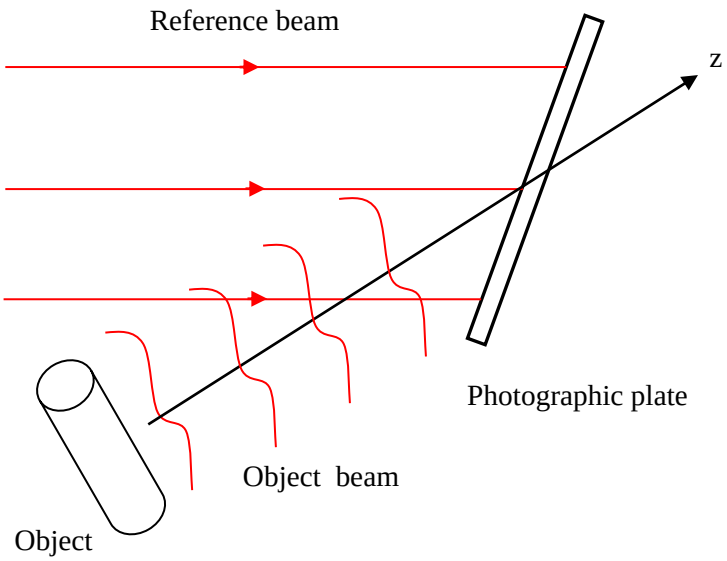

Figure 1.3. Off-axis holography setup

Considering the object and reference beam are incident on the photographic plate at an offset angle θ to each other.

The complex amplitude at any point *(x, y)* due to reference wave can be written as

$$u_r(x,y) = a_r e^{i2\pi\xi x} \tag{1.7}$$

where $\xi = (\sin\theta)/\lambda$,

For the reference beam we assume that only the phase varies across the photographic plate

whereas the object wave varies in phase and amplitude and can be written as

$$u_o(x,y) = a_o(x,y)e^{-i\varphi(x,y)} \tag{1.8}$$

The resultant intensity is therefore

$$\begin{aligned} I(x,y) &= [u_o(x,y) + u_r(x,y)]^2 \\ &= a_r{}^2 + [a_o(x,y)]^2 + 2a_r[a_o(x,y)]\cos[2\pi\xi x + \varphi(x,y)] \end{aligned} \tag{1.9}$$

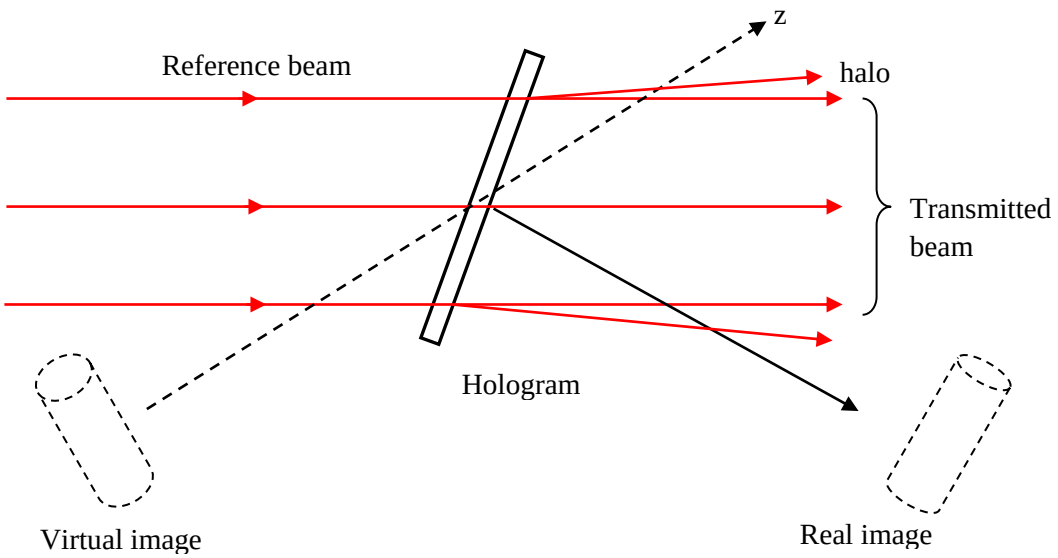

Figure 1.4. Reconstruction from off axis hologram

By considering the amplitude transmittance as a linear function of intensity, the resultant amplitude transmittance of the hologram can be written as

$$t(x,\ y)\ =\ t_0'\ +\beta T\ \begin{Bmatrix}\left[a_o(x,\ y)\right]^2+\ a_r\left[a_o(x,\ y)\right]e^{-i\varphi(x,y)}e^{-i2\pi\xi x}\\ +\ a_r\left[a_o(x,\ y)\right]a_o(x,\ y)e^{i\varphi(x,y)}e^{i2\pi\xi x}\end{Bmatrix} \quad (1.10)$$

$t_0' = t_0 + \beta T r^2$ is the constant background transmittance

The complex amplitude transmittance of the reconstructed beam is

$$\begin{aligned} u(x,\ y)\ &=\ u_r(x,\ y)t(x,\ y)\\ &=\ t_0' a_r\ e^{i2\pi\xi x}+\beta T a_r\left[a_o(x,\ y)\right]^2 e^{i2\pi\xi x}\\ &\quad +\beta T {a_r}^2 a_o(x,y)+\beta T {a_r}^2 {a_o}^*(x,y)e^{i4\pi\xi x}\end{aligned} \quad (1.11)$$

The first term corresponds to the directly transmitted beam, while the second term corresponds to a halo surrounding the transmitted beam having approximately twice the angular spread of the object wave. The third term is similar to the original object wave and forms a virtual image of the object. The fourth term corresponds to the conjugate image which is real. The virtual image can be separated from the conjugate image if we make the offset angle of the reference beam large enough. In this arrangement, corresponding points on the real and virtual images are located at equal distances from the hologram and on opposite sides.

1.3 Hologram types

This section discusses different types of holograms according to their recording geometry

1.3.1. Transmission Hologram

Transmission holograms can be made if the object and the reference beam are incident on the recording medium from the same side. Fig.1.5 shows the basic

geometry of recording a transmission holographic grating. The interference pattern which is produced as a result of the superposition of collimated beams consists of a set of straight parallel fringes.

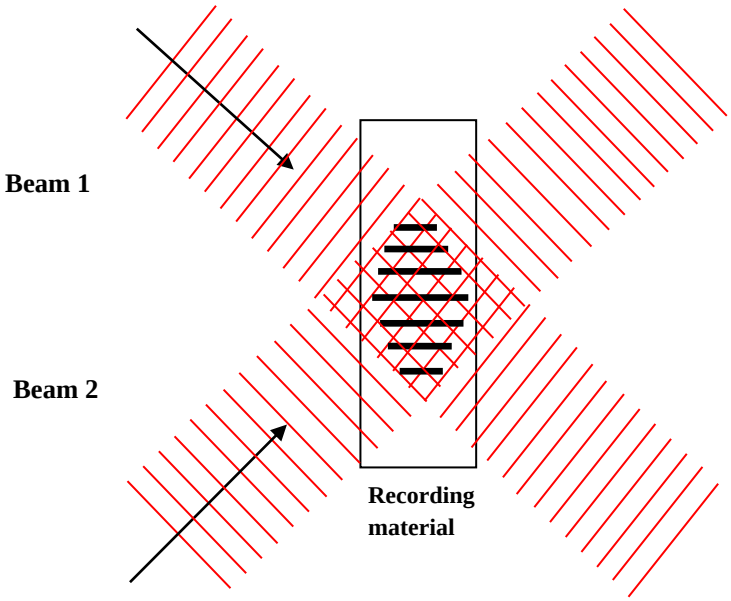

Figure 1.5. Recording geometry of transmission grating

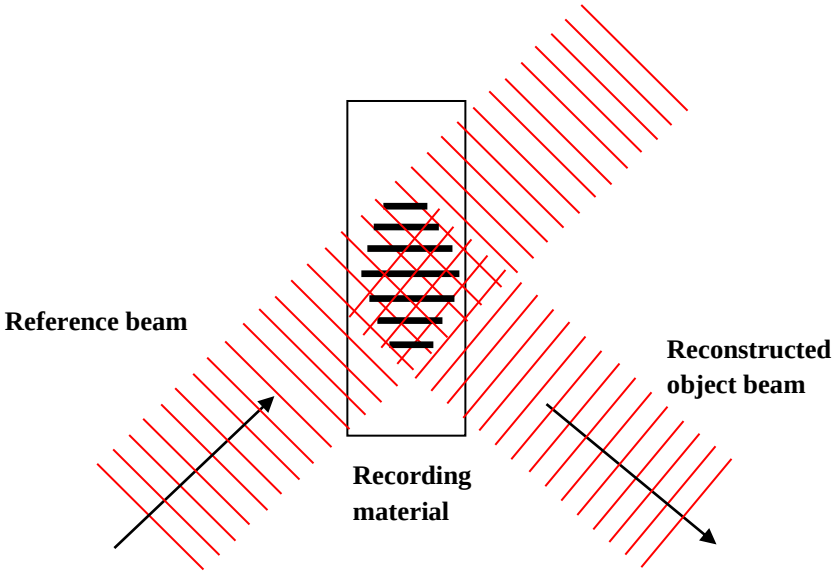

Figure 1.6 Reconstruction of beam from a holographic transmission grating

Reconstruction is the process of reconstructing one beam by illuminating the recorded hologram only with the other as shown in Fig.1.6. This can be done by blocking the beam which is to be reconstructed. The holographic grating will diffract the illuminating beam to reconstruct the other beam.

1.3.2 Reflection holograms

Reflection holograms are recorded using two beams (object and reference) illuminating the recording medium from opposite sides. Fig.1.7 illustrates how a reflection holographic grating is recorded and Fig.1.8 shows reconstruction of the object beam.

Reflection holography is the most common method for producing display holograms.

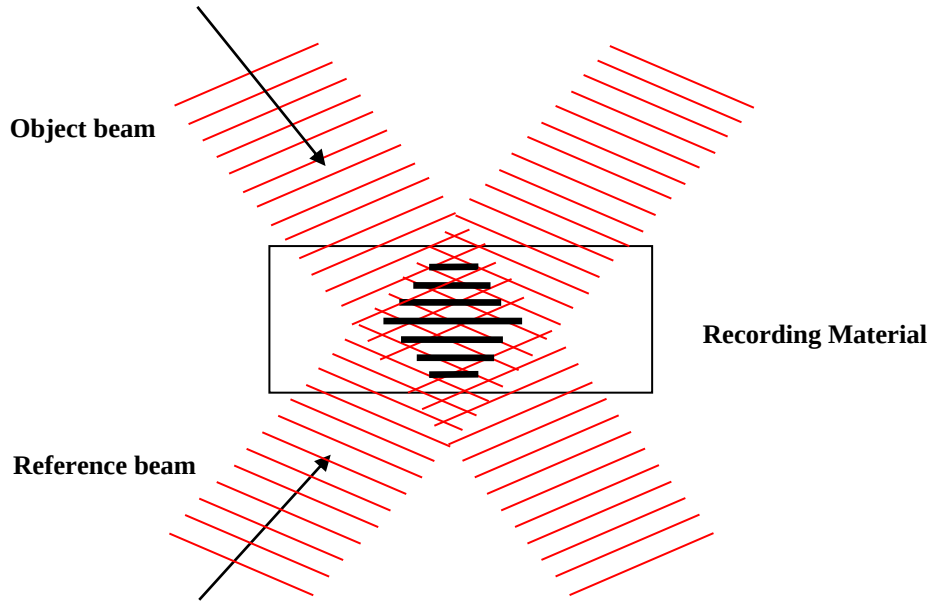

Figure 1.7. Recording geometry for reflection hologram

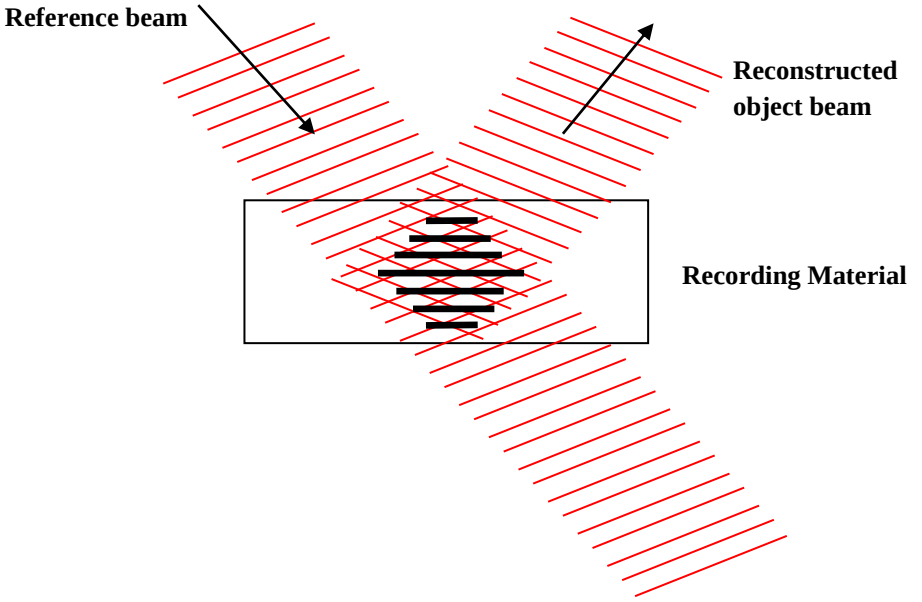

Figure 1.8. Reconstruction of reflection hologram

1.3.3 Thin and Thick Holograms

Depending on the thickness of the recording medium and also the fringe spacing of the interference pattern holograms can be classified as thin or thick (volume) holograms.

Using the Q parameter [10] holograms can be classified according to

$$Q = \frac{2\pi\lambda d}{n\Lambda^2} \tag{1.12}$$

where λ - wavelength of the source, d - thickness of the recording material, Λ - fringe spacing , n- refractive index of the material

Q < 1 corresponds to a thin (Raman Nath) grating

Q > 10 corresponds to a thick (Bragg) grating

1 < Q < 10 corresponds to intermediate holograms whose properties lie between 3D and 2D.

1.3.3.1 Thin amplitude hologram

Assuming the recording process will result in the spatial modulation of the transmissivity of the recording material.

let $$t(x,y) = at(x,y)n\exp[-i\varphi(x,y)] \quad (1.13)$$

be the complex amplitude transmittance of the grating.

For an amplitude hologram it is the amplitude of the wave that varies upon reconstruction. Low diffraction efficiency (ratio of diffracted to incident intensity) makes these holograms not widely used.

1.3.3.2 Thin phase hologram

The complex amplitude transmittance of a phase hologram with no loss is given by the equation

$$t(x) = \exp[-i\varphi(x)] \quad (1.14)$$

If the thickness or refractive index of the material is changed upon illumination by light such holograms are phase holograms whose complex amplitude transmittance is given by

$$t(x) = \exp(-i\varphi_0)\exp[-i\varphi_1\cos(Kx)] \quad (1.15)$$

where $K = \frac{2\pi}{\Lambda}$ is the grating vector, Λ is the fringe spacing

The grating vector expresses the direction and spacing of grating planes and the relation between the incident and diffracted propagation vectors. Consider k_i and k_d as the incident and diffracted wave vector. Maximum diffraction efficiency is attained when $k_i + K = k_d$ the so called Bragg matching condition.

Applications of phase holograms include communication, fabrication of Holographic Optical Elements (HOEs) and holographic interferometry [11-13].

1.3.3.3 Volume gratings

Holographic recording in thick material is important for data storage applications [14-16].

Here the thickness of the recording medium is much larger than the recording wavelength.

Let $$\Lambda\left[\sin(\theta_1 - \theta_2)\right] = n\lambda \qquad (1.16)$$

where θ_1 and θ_2 are the angles of incidence and diffraction,

be the grating equation for a volume transmission grating. There are many factors which determine the diffracted beam order including thickness of the grating, contrast and deviation from Bragg angle [17].

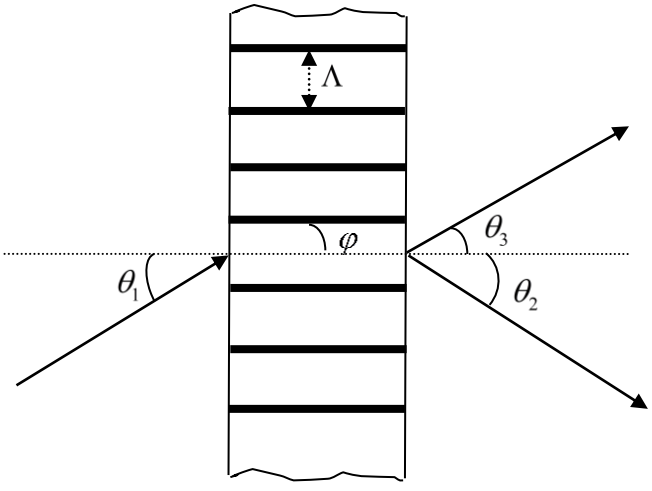

Figure 1.9. Unslanted transmission grating

Fig. 1.9 shows the fringe pattern for an unslanted transmission grating, recorded with two beams at equal angles to the surface normal and illuminating the

recording material from the same side. Maximum diffraction efficiency (ratio of diffracted intensity to incident intensity) will be obtained if the one beam is incident on the grating at a particular angle of incidence θ called the Bragg angle.

The Bragg condition [18] for an unslanted grating is given by

$$n\lambda = 2\Lambda \sin\theta \qquad (1.17)$$

Λ - Fringe spacing, θ - Bragg angle inside the medium

The Bragg condition is satisfied when *n* is an integer (n=1 for first order) and also the wavelength and fringe spacing are such that the angles of incidence and diffraction are equal and opposite with respect to surface normal.

Figure 1.10 shows the fringe pattern for a slanted transmission grating, recorded with two beams at unequal angles to the surface normal and illuminating the recording material from the same side.

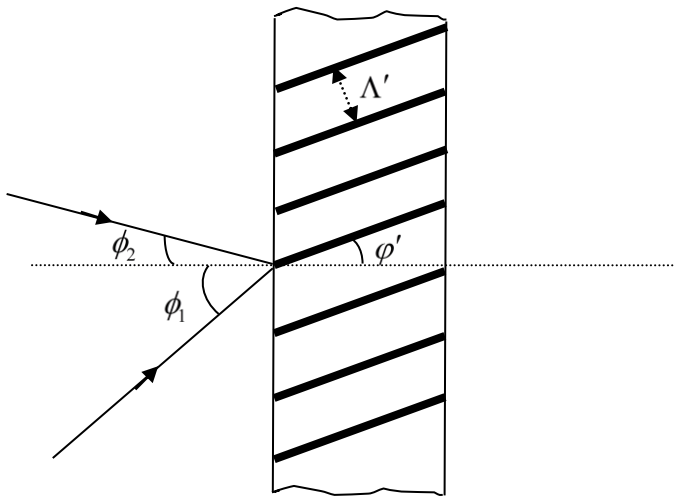

Figure 1.10. Slanted transmission grating

The fringe spacing in the case of slanted holographic grating is given by [19]

$$\Lambda' = \frac{\lambda / n}{2\sin\left(\frac{\phi_1 + \phi_2}{2}\right)} \tag{1.18}$$

$$\varphi' = \frac{\pi - (\phi_1 - \phi_2)}{2} \tag{1.19}$$

ϕ_1 and ϕ_2 are the angles of incidence of the two beams; λ - recording wavelength ; n - average refractive index of the material ; Λ' - fringe spacing ; φ' - slant angle inside material.

1.4 Major Applications of Holography

1.4.1 Holographic Data storage

The introduction of Compact Disc technology makes optical data storage technology a great success. Advances in the technology made it possible to increase storage capacity by the introduction in 1995 of the digital versatile disc (DVD) which can store up to 17 GB in a double sided dual layer [20]. The introduction of the blue laser for reading discs (blue ray disks) enabled further increase of storage capacity by a factor of 2.5. By decreasing the spot size blue lasers achieve approximately 25 GB of storage capacity per layer. Up to four layers increase storage capacity up to 100 GB per disk (quadruple layers) [21]. The increasing magnitude of storage requirements makes data storage one of the biggest challenges in the multimedia market.

Further efforts to increase storage capability by increasing numerical aperture and increasing layer number face several obstacles. The use of holographic technology to store information throughout the three dimensional volume of the recording material further improves storage capacity. Volume holography offers capacities of

approximately 1 TB (terabyte) with data transfer rate of 1GB/s with access times less than 100 μs/bit [22,23].

Data to be stored in the material is impressed on an optical beam by means of a spatial light modulator or a page composer. The data carrying beam (object beam) interferes with a reference beam in the recording medium to produce an interference pattern which represents a data page. Bragg selectivity allows multiple holograms to be recorded in the same material by varying the angle of the reference beam, a process referred to as angular multiplexing, or by applying other appropriate multiplexing methods such as shift multiplexing, peristrophic multiplexing, polytopic multiplexing etc.[24-26]. In order to retrieve data a single reference beam or read out beam is incident on the medium under the same conditions as used for storage, producing a diffracted beam representing the stored data page. The output devices used to detect the diffracted beam are either a charge-coupled device (CCD) camera or CMOS camera which allows the extraction of the stored data from its measured intensity pattern. Holographic data storage (HDS) offers high storage capability, low cost, short access time, high transfer rate and high data security [27].

Shrinkage in the recording material is a major issue which needs to be considered in HDS [28]. Controlling shrinkage is the major challenge. Shrinkage occurring in the material results in re-orientation of gratings recorded in the material and thereby changes the grating spacing of previously recorded data. This results in Bragg mismatch during reconstruction and the readout beam needs to be altered otherwise only a portion of data page can be read out for a particular readout geometry, which leads to large data errors. Attempts were made to make reversible polymer media with high sensitivity but these falls short of the requirements for

holographic data storage systems (HDSSs) [30]. A medium with high sensitivity and a low level of shrinkage is needed [29]. Data capacities exceeding 250 GB on a DVD-like disk have been obtained and data rates exceeding 10 GB/s have been demonstrated at Stanford University [31,32].

1.4.2 Holographic Optical elements

Holographic optical elements (HOE's) are basically diffractive elements which work on the principle of interference and diffraction. Optical elements such as lenses, mirrors, beam splitters, diffraction gratings and spectral filters can be produced holographically by interfering two laser beams and are called holographic optical elements. A HOE can also work as a lens, beam splitter and spectral filter simultaneously as shown in Fig.1.11.

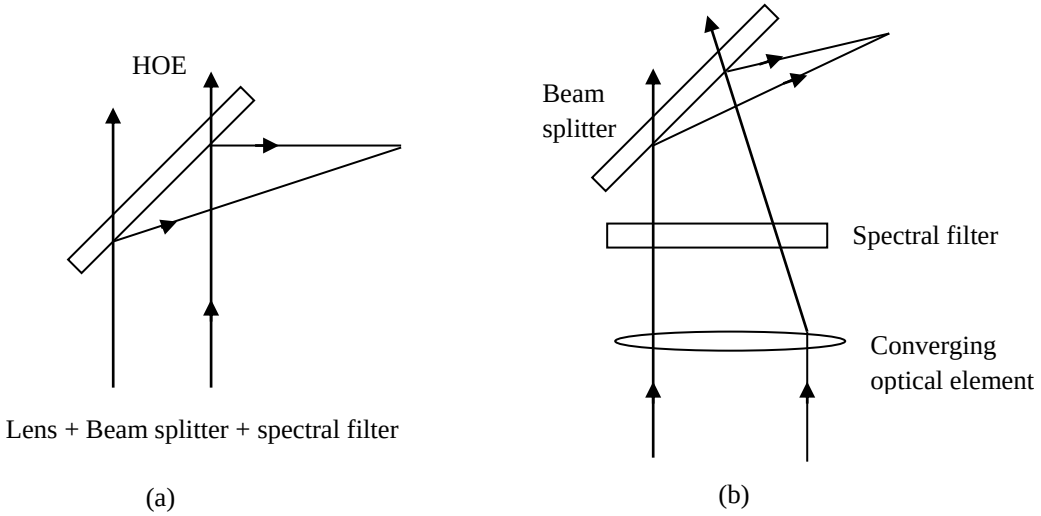

Figure 1.11. Characteristics of Holographic optical elements

Kock et al. [33] in 1966 analysed the imaging properties of the hologram. Schwar et al. [34] experimentally demonstrated its function as a lens. The interference

pattern can be recorded in a holographic material as a spatial variation of absorption or thickness or refractive index.

High quality HOE's are difficult to make because any defects in the optics will be recorded in the HOE. Hence the recording optics should be stable and of high quality. Multiple reflections between the surfaces of the construction optics and scattered light should be minimized. The optics must be kept free from dust and other noise sources.

In order to reduce aberrations due to emulsion shrinkage during recording of holographic lenses the holographic plates were arranged in such a way that the two beams made almost equal angles with the plate normal [35, 36]. Deliberately overexposing the plates is also a means of reducing emulsion shrinkage [35].

1.4.2.1 Head-up display

Head-up displays (HUD) are an important example of holographic optical elements. HUD's are transparent displays which project data onto a windscreen [37]. The major application is in aircraft. A HUD projects the display image (of the instrument panel) onto a partially transparent screen, so called combiner which reflects the display to the viewer as in Fig.1.12. The ability to reflect very narrow wavelength spectrum is the main advantage of a holographic HUD combiner. The reflectivity will be high for the display wavelength and will remain very low for all other wavelengths in the field of view. Shrinkage occurring in the material will lead to distortions in both phase and in amplitude of the reconstructed image which results in reduced image resolution of the reconstructed image.

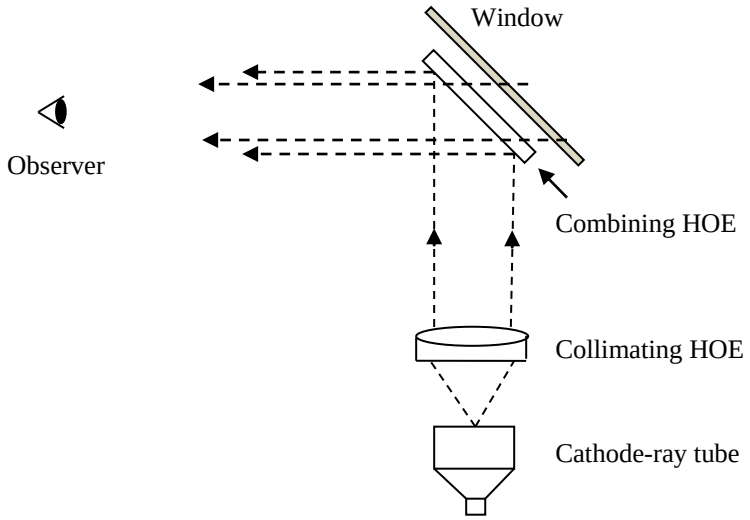

Figure 1.12. Head-up display

1.4.3 Holographic display

Holographic display is a three dimensional display which incorporates a true parallax element so that the viewer can move around the image in any direction without changing the image clarity. This technology can be implemented by creating holograms on a flat surface which are capable of diffracting light beams of different colors and intensity in various directions, in a controlled manner The light beams are generated through a light modulation system arranged in a specific geometry and the holographic screen makes the necessary optical transformation to compose these beams into a perfectly continuous 3D view. Shrinkage occurring in the recording material will change the grating spacing and angle of the recorded holograms and hence will decrease the image clarity during reconstruction.

1.4.4 Holographic interferometry

The advantage of holographic interferometry is mainly due to the capability of holography for storing a wavefront for reconstruction at a later time. Wavefronts

that are separated in time or space and also wavefronts of different wavelengths, can be compared by holographic interferometry. As a result, changes in shape due to deformations can be studied with interferometric precision. One important application of holographic interferometry is non-destructive testing which visually reveals structural defects without damaging the specimen. Holographic interferometry has applications in aerodynamics, heat transfer studies, and plasma diagnostics etc. [38]. Shrinkage occurring in the material will affect measurements of the change occurring in the object under observation.

1.4.5 Holographic sensors

A holographic sensor consists of a hologram recorded in any holographic material which is capable of detecting certain molecules or relative environmental changes [39-41]. The operation of holographic sensors is based on the fact that when the physical or chemical properties of the holographic recording medium are changed due to the presence of an analyte, the optical properties of the recorded hologram also change. This usually leads to a visual change in the recorded holographic image that can be easily detected simply by looking at it. The detection can be made possible by certain changes in the material such as change in the refractive index or change in the fringe spacing of the recorded grating. Shrinkage occurring in the material will result in the change in fringe spacing and hence is an advantage in developing certain sensors [41]. The advantages of holographic sensors include low price, flexible design and small format.

1.5 Holography – Major challenges

1.5.1 Laser

A variety of lasers have been used for holography over the years. There are certain properties that the laser should have in order to produce good quality holograms.

1.5.1.1 Coherence: For holographic applications the main requirement is the coherence. The coherence of a beam depends on the characteristics of the source. For waves propagating through space, spatial coherence describes the correlation between waves at different points on space. Mostly lasers produce beams which are of high spatial coherence and the beam divergence is consequently small (< 1milliradian).

Consider a source which emits light with wavelength in the range $\lambda \pm \Delta\lambda$. Suppose that at some point in space, waves with wavelength λ and $\lambda \pm \Delta\lambda$ constructively interfere. They will destructively interfere after some further optical path length L_c called the coherence length.

$$L_c = \lambda^2 / 2\pi\Delta\lambda \tag{1.20}$$

For waves travelling through space with speed *c*, coherence time T_c is given by

$$T_c = L_c / c \tag{1.21}$$

Temporal coherence describes the correlation between phases of light waves at different moments in time. Temporal coherence gives information on how monochromatic a source is. A good holography laser will have a coherence length of several meters.

1.5.1.2 Polarisation: Linear polarisation is one of the other main requirements that a laser beam should satisfy, which means the electric field vector should lie in a single plane and the magnetic field vector will lie orthogonal to this. Two beams will interfere to form a pattern only if they are mutually coherent i.e. they should be plane polarized in the same plane, from the same source and have similar path length. A beam that is depolarised (i.e. scattered from any rough surfaced object) will produce an interference pattern with a reference beam polarised in any direction. Two beams which are polarised perpendicular to their plane of incidence (plane containing the direction of propagation of a wave incident on a surface and a line perpendicular to the surface) or at an angle to each other will only interfere depending on the cosine of the angle between the polarisation vectors.

1.5.1.3 Power: Laser power is one another thing to be noted in case of holographic recording. The power should be stable. The exposure required for recording a hologram mainly depends on the laser power available and on the type and thickness of the medium. All the elements within the optical system have to be stable during the period of recording. Holograms of less stable objects can be made by using a pulsed laser which produces a large amount of energy in a very short time (μs or less) [42].

1.5.2 Beam expansion

Since the laser beam is 1mm-2mm in diameter, it is necessary to expand the beam by means of lens as shown in Fig.1.12. A spatial filter consists of a lens with a pinhole which is positioned at the focal point of the lens in order to remove the random diffraction patterns due to dust or any defect in the optical components. Randomly diffracted light will be blocked at the pinhole and the transmitted beam

will be smooth. The pinhole position can be adjusted vertically, horizontally and longitudinally.

The minimum pinhole size can be calculated from the formula

$$D = 600\lambda / Md \qquad (1.22)$$

D- Pinhole diameter in μm , λ -Wavelength of laser in μm , *d*- diameter of beam in mm

M- Magnification of objective

$$M = 250 / f \qquad (1.23)$$

f- Focal length of lens in mm

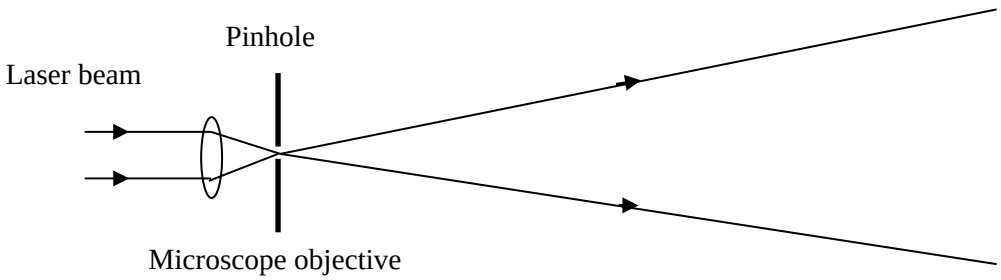

Figure 1.13. Spatial filtering of laser beam

1.5.3 Materials/Media

Media for holographic recording have long been one of major challenges for researchers [43]. Although a number of materials have been developed, none meet all the requirements and hence the lack of ideal recording material remains one of the main obstacles to the success of holographic technology [44].

In materials for recording amplitude holograms the absorption constant changes as a result of exposure, while in materials for recording phase holograms thickness or refractive index (RI) changes due to exposure.

1.5.3.1 Photosensitive material requirements

The performance of the material is mainly described in terms of parameters such as diffraction efficiency , sensitivity, resolution, signal to noise ratio , temporal stability etc. [45].

There are several criteria that an ideal holographic recording material should satisfy:

- High optical quality
- High light sensitivity (100-1000 mJ/cm^2)
- High resolution (>5000 mm^{-1} in reflection mode)
- High Refractive index contrast $\Delta n > 5x10^{-3}$
- Self-developing and free from wet processing
- Large dynamic range ($\geq$10)
- Good environmental stability
- Low cost
- Low shrinkage (<0.5%)

1.6 Holographic recording materials

1.6.1 Silver halide photographic emulsions

Silver halide emulsions are the oldest and the most commercially available holographic material because of their high sensitivity, range of spectral sensitivity, good shelf life and good stability of holograms after processing. This emulsion

consists of silver halide (usually AgBr) microcrystals dispersed in gelatin. [46]. These materials can record phase, amplitude and colour holograms. The need for wet chemical processing is the major drawback of the material.

1.6.2 Dichromated gelatin (DCG)

Low scattering and high refractive index modulation makes DCG a prospective candidate in holography. DCG consists of a gelatin layer that contains ammonium dichromate which becomes hardened on exposure to light due to the photochemically produced Cr3+ ions forming localized cross-links between the carboxylate groups of neighbouring gelatin chains [38]. DCG is ideal for recording volume phase holograms [47]. The need for complex wet chemical processing, short shelf life and environmental instability are the major drawbacks.

1.6.3 Photoresist

Photoresists are materials which can form surface relief holograms. The phase change produced between high and low intensity areas in a photoresist is produced by thickness variation, opposed to refractive index variation, creating a thin phase hologram. Positive and negative photoresist are two types of photoresist. In negative photoresists the areas exposed to light becomes insoluble to the developing solution whereas in positive photoresist areas exposed to light are soluble and are dissolved away during processing [38]. Relatively long exposures are necessary, usually through the back side of the plate, to ensure that the exposed negative photoresist adheres to the substrate during development. Photoresists are preferable for making master holograms needed for embossing [48]. This material has low scattering and low sensitivity.

1.6.4 Photochromics

Photochromic material can undergo reversible colour change after exposure to light [38]. These materials don't need any processing. The hologram can be erased and the material can be used again. Properties like high resolution, lack of grain (no inherent resolution limit) and self-development makes them promising holographic materials. Low diffraction efficiency, poor sensitivity and short storage time (stored hologram is degraded during readout) are the main disadvantages [49].

1.6.5 Photothermoplastics

Photothermoplastic material has a multilayered structure consisting of glass substrate coated successively with a transparent electrode, an organic photoconductor and a thermoplastic layer [50]. The thermoplastic is sensitized by applying a uniform electric charge before recording. A pulse of electric current, passing through the photoconductor provides the heating of the thermoplastic that becomes soft enough to be deformed by an electric field generated in a recharging step and finally cooled to fix the pattern of deformations. Holograms recorded in this material have high diffraction efficiency and high stability at room temperature. They don't require any wet processing.

1.6.6 Photorefractives

The hologram is formed in photorefractive crystals by the electro-optic effect. Free electrons are generated upon exposure and will move to areas in which the illumination intensity is lower and get trapped. Charge migration takes place by diffusion. The resulting spatially varying electric field modulates the refractive index and creates a phase hologram. Good availability, high robustness, large

storage capacities and reversibility make LiNbO3 and LiTaO3 the best among inorganic photorefractive materials [51].

1.6.7 Photopolymers

Photopolymer systems [23,40] typically comprise one or more monomers, a photoinitiation system and an inactive component often referred as a binder. The material doesn't require any post processing. The history of photopolymers, recording mechanism advantages and disadvantages of photopolymer are explained in detail in the next chapter.

1.7 Characteristics of holographic materials

Different characteristics of holographic recording material were shown in Table 1.1 [38]

Table 1.1. Characteristics of holographic recording materals

Material	Reusable	Exposure (mJ/cm^2)	Resolution (mm^{-1})	Processing	Type	Maximum efficiency (%)
Photographic emulsions	No	1.5	6000	Wet	Amplitude	6
				Bleached	Phase	60
Dichromated gelatin (DCG)	No	100	10000	Wet	Phase	100
Photoresists	No	100	3000	Wet	Phase	30
Photopolymers	No	10000	6000	Dry	Phase	100
Photochromics	Yes	1	2000	Dry	Amplitude	6
Photo thermoplastics (PTP)	Yes	0.1	500-1200	Dry	Phase	30
Photorefractives	Yes	10	10000	No need	Phase	100

References

[1] D.Gabor, “A New Microscopic Principle,” Nature.161, 777-778 (1948)

[2] D.Gabor, “Microscopy by reconstructed wavefronts,” Proceedings of the Royal Society London. Series A.197, 454-487(1949)

[3] Maiman.T.H. “Stimulated Optical Radiation in Ruby,” Nature.187, 493-494 (1960).

[4] L.Siebert, “Front-lighted pulsed laser holography,” Appl.Phys.Lett.11, 326 (1967)

[5] E.Leith and J.Upatnieks, “Reconstructed Wavefronts and Communication Theory,” Journal of the Optical Society of America.52, 1123-1128 (1962)

[6] E.Leith and J.Upatnieks, “Wavefront Reconstruction with Continuous-Tone Objects,” Journal of the Optical Society of America. 53, 1377-1381 (1963)

[7] Yu.N.Denisyuk, "Photographic reconstruction of the optical properties of an object in its own scattered radiation field,” Sov. Phys, Doklady. 7, 543-545(1962)

[8] G.Lippmann, “Sur la theorie de la photographie des couleurs simples et composees par la methode interferentielle,” J. Physique.3, 97- 107 (1894).

[9] S.A.Benton, "Hologram reconstructions with extended incoherent sources,” JOSA. 59, 1545- 1546 (1969).

[10] R.Collier, C.B.Buckart, and L.H.Lin, “Optical Holography,” Academic Press, New York, (1971).

[11] A.Lonnqvist, J.Mallat, E.Noponen, J.Ala-Laurinaho, J.Saily, T.Koskinen, J.Hakli and A.Raisanen, “A Phase Hologram Compact RCS Range for Scale Model Measurements,” Proceedings of 3rd ESA Workshop on Millimetre Wave Technology and Applications, Espoo, Finland, 511-516 2003)

[12] M.Collados, J.Atencia, J.Tornos and M.Quintanilla, "Construction and Characterization of Compound Holographic Lenses for Multichannel One-Dimensional Fourier Transformation and Optical Parallel Processing," Optics Communications.249, ,85–94 (2005)

[13] S.Martin, C.Feely, J.Sheridan and V.Toal, "Applications of a Self Developing Photopolymer Material: Holographic Interferometry and High Efficiency Diffractive Optical Element," Optical Memory and Neural Networks.7, No. 2, 79-87 (1998)

[14] P.J.Van Heerden, "Theory of Optical information storage in solids," Appl. Optics.2, 393-400(1963)

[15] F.M.Smiths and L.E.Gallaher, "Design Considerations for a semipermanent optical memory," B.S.T.J. 46, 1267-1278 (1967)

[16] V.A.Vitols, "Hologram memory for storing digital data," IBM Technical Disclosure Bull. 8 (1966)

[17] S.C.Barden, J.A.Arns, W.S.Colburn, "Volume phase holographic gratings and their potential for astronomical applications," SPIE Proc. 3355, 866-876 (1998)

[18] F.A.Jenkins, H.E.White, "Fundamentals of Optics," Chap.31 4th Edition, McGrawHill (1981)

[19] Gallo J.T and Verber C. M, "Model for the effects of material shrinkage on volume holograms," Appl.Opt.33, 6797-6804 (1994)

[20] http://www.mpeg.org/MPEG/DVD/Book_A/Specs.html (14-02-2013)

[21] http://www.bit-tech.net/hardware/2011/02/23/pioneer-bdxl-bdr-206-review/1(14-02-2013)

[22] K.Singh, Proc. 31st OSI symposium on contemporary optics and applications, Vadodara, India 176 (2007)

[23] H.Sherif, I.Naydenova, S.Martin, C.McGinn, V.Toal "Characterisation of an Acrylamide-based Photopolymer for Data Storage Utilizing Holographic Angular Multiplexing," J.Opt.A. Pure Appl.Opt.7, 255-260 (2005).

[24] D.Psaltis, M. Levene, A. Pu, G.Barbastathis and K.Curtis "Holographic storage using shift multiplexing," Opt lett.20,782-784 (1995).

[25] K.Cutis, A.Pu and D.Psaltis, "Method for holographic storage using peristrophic multiplexing,"Opt.Lett. 19, 993-994 (1994)

[26] K.Anderson and K.Curtis, "Polytopic multiplexing,"Opt.Lett. 29, 1402-1404 (2004)

[27] S.Orlic, J.Rass, E.Dietz and S.Frohmann, "Multilayer recording in microholographic data storage," J. Opt. 14 (2012)

[28] N.Ishii, T.Muroi, N.Kinoshita, K.Kamijo, N.Shimidzu," Wavefront compensation method using novel index in holographic data storage,"Journal of the European Optical Society- Rapid Publications. 5 (2010)

[29] M.Ortuno, S.Gallego, A.Marquez, C.Neipp, I.Pascual and A.Belendez , "Biophotopol: A Sustainable Photopolymer for Holographic Data Storage Applications," Materials. 5, 772-783 (2012)

[30] T.Bieringer, "Photoaddressable polymers," in Holographic Data Storage, H.Coufal, G.T.Sincerbox, and D.Psaltis, Eds. Berlin, Germany: Springer-Verlag, , pp. 209–230(2000)

[31] S.S.Orlov, W.Phillips, E.Bjornson, L.Hesselink, and R.Okas, "10 Gigabit/second sustained optical data transfer rate from a holographic disk digital data storage system," OSA Annual Meeting 2000, Paper MK3.

[32] S.S.Orlov, "Volume holographic data storage," Commun. ACM, 43, 46–55 (2000)

[33] W.E.Kock, L.Rosen, J.Rendeiro, “Holograms and zone plates,” Proc.IEEE, 54, 1599-1601 (1966).

[34] M.J.R.Schwar, T.P.Pandya, and F.J.Weinberg, “Point Holograms as Optical Elements,” Nature .215, 239-241 (1967).

[35] P.C.Mehta, S.Swami, V.V.Rampal, “Compact optical data processor employing holographic reflective lenses,” Appl.Opt., 16, 445-453 (1977).

[36] D.H.R.Vilkomerson and D.Bostwick, “Some effects of emulsion shrinkage on a hologram's image space,” Appl.Opt. 6, 1270-1272 (1967).

[37] R.R.A.Syms, “Practical Volume Holography,” Oxford Engineering Series 24, Clarendon Press, Oxford, p. 248 (1990)

[38] P.Hariharan, “Optical holography principle techniques and applications,” Cambridge, University Press (1987)

[39] J.L.Martínez-Hurtado , C.A.B. Davidson , J.Blyth , and C.R. Lowe, “Holographic Detection of Hydrocarbon Gases and Other Volatile Organic Compounds,” Langmuir. 26, 15694–15699 (2010)

[40] I.Naydenova, H.Sherif, S.Martin, R.Jallapuram and V.Toal, “A Holographic Sensor”, Patent number: IE20060856 (A1) (2007)

[41] A.V.Kraiskii, V.A.Postnikov, T.T.Suitanov and A.V.Khamidulin, “Holographic sensors for diagnostics of solution components,” Quantum Electronics.40, 178 -182 (2010)

[42] J.L.Martínez-Hurtado , C. A. B. Davidson , J. Blyth , and C. R. Lowe , “Holographic Detection of Hydrocarbon Gases and Other Volatile Organic Compounds,” Langmuir. 26 ,15694–15699 (2010)

[43] R.B.Johnson , R.G. Driggers, Marcel Dekker, Encyclopedia of Optical Engineering, Ed. New York (2002)

[44] G. W. Burr and M. Neifeld, “Gray-scale data pages for digital holographic data storage,” in Holographic Data Storage, pp 319-328, H. Coufal, D. Psaltis, and G. Sincerbox, ed., Springer-Verlag, Berlin (2000).

[45] L.Carretero, S.Blaya, R.Mallavia, R.F.Madrigal, A.Fimia, “A theoretical model for noise gratings recorded in acrylamide photopolymer materials used in real-time holography,” J. Mod. Opt. 45, 2345-2354 (1998)

[46] H.Bjelkhagen, New Recording Materials for Holography, Conference of Holography, Art and Design (Holography and Three-Dimensional Displays), London (1998)

[47] B.J.Chang and C.D.Leonard, “Dichromated gelatin for the fabrication of holographic optical elements,” Appl. Opt. 18, 2407-2417 (1979).

[48] F.Iwata, J.Tsujiuchi, “Characteristics of a photoresist hologram and its replica,” Appl.Opt.13, 1327-1336 (1974)

[49] I.Pascual, C.Garcia, A.Belendez and A.Fimia, “PVA/acrylamide photopolymers as holographic recording materials at short wavelengths,” Recent Research. Developments in. Optics.1 , 177-191(2001)

[50] J.C.Urbach and R.W.Meier, “Thermoplastic Xerographic Holography,”Appl. Opt. 5, 666-667 (1966).

[51] H.J.Coufal, D.Psaltis and G.T.Sincerbox, Holographic Data Storage, Springer, New York (2000).

CHAPTER 2

HOLOGRAPHIC RECORDING IN PHOTOPOLYMERS

2.1 Brief history of photopolymers

The characteristics that an ideal recording material should satisfy for most holographic applications are high spatial resolution, large dynamic range, low scattering, high optical quality and high sensitivity. For commercial purposes the material should be recyclable, have long shelf life, good environmental stability and be of low cost. Silver halide photographic emulsion (SHPE) and dichromated gelatin (DCG) are commercially available materials for making high efficiency holograms. The need for wet chemical post-processing is one of the most limiting properties of these materials. The property of self-development makes photopolymers a promising medium for holographic recording and their use in mass production.

Photopolymers have been under investigation for several years for holographic applications including LCD displays [1] data storage [2, 3] optical elements [4] etc. because of their easy processing, high light sensitivity, relatively high refractive index contrast and low cost [5].

There are two types of photopolymers, crosslinking and polymerisable photopolymers. In crosslinking photopolymer the phase change in hologram is caused by modification in refractive index modulation when crosslinks between new polymer strands break or are formed due to the change in molecular polarizibility of these bonds. Examples of crosslinking photopolymer materials are dichromated gelatin (DCG), metal ion doped polymers (dichromated polyvinyl

alcohol, dichromated polyacrylic acid), Poly-n-vinyl carbazole (PVCz) and Polymethylmethacrylate (PMMA).

In polymerisable photopolymer when light of appropriate wavelength is incident on the photosensitive medium, a dye molecule absorbs photon and enters a single excited state. This singlet excited state dye molecule enters a triplet excited state through intersystem crossing. The dye molecule in the excited state reacts with an electron donor to generate a free radical. This free radical in the presence of monomer initiates a polymerisation reaction. During polymerisation the monomer in regions of higher intensity illumination is polymerized to a greater extent than in lower intensity areas which gives rise to diffusion of monomer molecules from regions of higher concentration to regions of lower concentration. As a result spatial density redistribution of material occurs. This redistribution results in refractive index modulation corresponding to an interference pattern resulting in a phase hologram.

Photopolymers which can be either liquid or dry layer systems, generally consist of a monomer, a photosensitive dye and an initiator. It is the lack of binder that differentiates liquid photopolymer from dry photopolymer layers.

Initial investigations on dye sensitised polymerisation reaction were made by Oster and Oster [6-8] in 1962. From these initial studies Close et al. [9] in 1969 introduced a liquid photopolymer system consisting of a mixture of acrylamide and methylacrylates as monomers and methylene blue and p-toluene sulfinic acid sodium salt as a photocatalyst. The holograms were made using a ruby laser of wavelength 694nm and a diffraction efficiency of 45% was observed in a 10-20 μm layer with an interbeam angle of 30° outside the material and exposure energy of approximately 1-30 mJ/cm^2.

Jenney [10] in 1970 optimised this system and improved the sensitivity by adding lead or barium acrylate along with acrylamide monomer in order to achieve higher sensitivity. Phase holograms were recorded in the material with diffraction efficiency of 45% at 3000 lines/mm spatial frequency at 0.6 mJ/cm^2

Van Renesse [11] in 1972 improved the acrylamide based photopolymer by adding N,N-methylene-bis-acrylamide which can act as a cross linker to the polymer network. Lack of adhesion to the substrate was a drawback with this system.

Sugawara et al. [12] developed a system consisting of acrylamide monomer, N,N methylene-bis-acrylamide as crosslinker and acetyl acetone or triethanolamine (TEA) as initiator. They achieved a diffraction efficiency of 65% in layers of thickness of 50 μm for an exposure energy of 50 mJ/cm^2 and resolution of 550 lines/mm. Addition of t-butyl hydrogen peroxide as electron donor and ferric ammonium citrate for green sensitisation further improved diffraction efficiency [13].

The instability of recorded holograms was a problem with liquid photopolymers. During the initial stage of exposure inhibitor molecules (such as oxygen) suppress the polymerization process [14]. The chain reaction of polymerisation begins only when the concentration of such molecules becomes less than some critical value. The inhibition period will affect the quality of holograms by lowering maximum diffraction efficiency. The inclusion of a binder material transforms liquid photopolymers to solid dry photopolymers.

Sadlej et al. [15] improved the original system developed by Jenney by introducing polyvinylalcohol as a binder in the system which produced dry photopolymer layers. This improved the shelf life of the material. Spatial frequency of up to 4700 lines/mm could be recorded, but they achieved low diffraction efficiency of 4% for

layers having surface deformation and 0.5 % for layers without thickness modulation.

Jeudy et al. [16] in 1975 made an interesting development of the Sugawara liquid system by using polyvinylalcohol as binder and a reversible photochrome (indoline-spiropyran) as sensitiser. The photochrome which is transparent in visible light could be activated by UV light, shifting the absorption band to allow recording at 633nm. Diffraction efficiency of 90 % was achieved with exposure energy of 100 mJ /cm^2 and resolution of 3000 lines/mm.

Calixto [17] in 1980 developed a photopolymer composition that included acrylamide monomer, triethanolamine (electron donor), methylene blue dye (photosensitizer) and polyvinylalcohol (binder). Diffraction efficiency was as low as 10 % with exposure energy of 94 mJ/cm^2. The system developed in our laboratory is based on this composition.

Fimia et al. [18] introduced a photopolymer solution containing two photosensitive dyes, Methylene Blue sensitive to 633nm and Rose Bengal sensitive to 546nm. The photosensitive layer was uniformly pre-exposed with 546 nm laser wavelength. The Rose Bengal dye generates free radicals which react with the oxygen present in the photopolymer and consume it thereby reducing the inhibition time due to oxygen. Then a 633 nm red laser was used for holographic recording to polymerise the monomer. There is a reduced amount of oxygen and sufficient Methylene Blue dye to polymerise the monomer. Diffraction efficiency of 40% was achieved with exposure energy of 3 mJ/cm^2 at a spatial frequency of 1000 lines/mm.

Zhao et al [19] proposed a material containing acrylamide and acrylic acid as monomers, Methylene Blue as photosensitizer, TEA and p-toluenesulfonic acid as sensitizers and gelatine as binder. The material was capable of recording up to a

spatial frequency of 4000 lines/mm. Diffraction efficiency of greater than 80 % was obtained and the exposure energy density was 2 mJ/cm^2.

Martin et al. [20, 21] improved Calixto's photopolymer composition by the addition of a cross-linking agent N-N, methylene-bis-acrylamide to stabilise and speed up the polymerisation reaction. They used 5 xanthene dyes, Fluorescein, Erythrosine B, Phloxine B, Eosin Y and Rose Bengal as sensitisers to record at 514 nm wavelength. An improved formulation was then prepared with erythrosine B. Diffraction efficiency of greater than 80% was obtained in 150 μm thick layers with exposure 80 mJ/cm^2.

Naydenova et.al. [23] and Raghavendra [22] studied diffusion processes that occur immediately after an exposure of short duration. Transmission gratings were recorded at different spatial frequencies using exposure times of a fraction of a second and the diffraction efficiency growth was studied in real time. It was observed that two diffusion processes occur in the material [23, 24], monomer diffusion from the unexposed regions to the exposed regions and a second diffusion process involving short terminated and unterminated polymer chains diffusing from exposed regions to unexposed regions. By selecting a binder with low permeability and suppressing the short chain polymer diffusion the photopolymer composition was optimized to make reflection holograms at 532 nm. Diffraction efficiencies of 35 % were achieved in reflection mode of recording at 3500 lines/mm [25]. The recording mechanism in this photopolymer is explained below.

2.2 Recording mechanism

2.2.1 Photopolymerisation

Free radical polymerisation is what occurs in photopolymer materials. Polymerisation can be divided into three steps, initiation, propagation and termination [26, 29]. Propagation or chain growth consists of a series of repeating similar reactions as shown below each adding a monomer molecule *(M*) to a molecule having an unpaired electron which is a reactive site (R^*).

Initiation

$$R^* + M \longrightarrow RM^* \qquad (2.1)$$

Propagation

$$M_i^* + M \longrightarrow M_{i+1}^* \qquad (2.2)$$

Termination

$$M_i^* + M_j^* \rightarrow \text{Terminated polymer chain} \qquad (2.3)$$

R^* - free radical, M -single unreactive monomer, M_i^* - Single reactive monomer

M_j^* - unterminated polymer with *i* monomer units.

2.2.1.1 Initiation

Generation of a free radical initiates the polymerisation process. When a dye molecule (*D*) absorbs a photon of light of a particular wavelength within its absorption band it gets excited to a singlet state D_1^* .

$$D + h\upsilon \longrightarrow D_1^* \qquad (2.4)$$

This excited singlet dye can return to the ground state with the emission of a photon by process called fluorescence.

$$D_1^* \longrightarrow h\upsilon + D \tag{2.5}$$

It can return to the ground state by non-radiative energy transfer to another molecule (electron donor- ED) by the process called fluorescence quenching

$$D_1^* + ED \longrightarrow D + ED^* \tag{2.6}$$

or else the singlet state can also undergo inter-system crossing into the excited triplet state whose life time is longer and more stable.

$$D_1^* \longrightarrow D_3^* \tag{2.7}$$

This triplet state dye molecule can revert to the ground state by non radiative transfer or by delayed emission of a photon. At high dye concentration it can be deactivated by collision with another dye molecule (concentration quenching).

$$D_3^* + D \longrightarrow 2D \tag{2.8}$$

A free radical is generated when the exited triplet state dye molecule reacts with the electron donor.

$$D_3^* + ED \longrightarrow R^* \tag{2.9}$$

R^* -Free radical,

Triethanolamine (TEA) $(HOCH_2CH_2)_3N$ is used as an electron donor in our photopolymer system. TEA donates an electron to the exited triplet state dye molecule D_3^* leaving the dye with one unpaired electron and overall negative charge.

$$D_3^* + (HOCH_2CH_2)_3N \rightarrow D^- + (HOCH_2CH_2)_3N^+ \tag{2.10}$$

The TEA radical then loses a proton and becomes a free radical

$$(HOCH_2CH_2)_3N^+ \rightarrow (HOCH_2CH_2)_2NCH^{\bullet}CH_2OH + H^+ \quad (2.11)$$

These free radicals attach to the monomer to initiate the polymerization reaction. The initiating free radical breaks the carbon-carbon double bond of the monomer and shares the free electron with one of the π electrons of the carbon atom in the double bond leaving the other carbon bond with an unpaired electron. The monomer (*M*) in this case is acrylamide.

$$R^* + M \xrightarrow{k_a} RM^* \quad (2.12)$$

These free radicals can also react with dye radicals resulting in dye bleaching to form a transparent dihydro dye (or leuco dye).

2.2.1.2 Propagation

The free radical generated in the initiation reaction reacts with another monomer in a similar manner by breaking the carbon-carbon double bond. Each time the free radical reacts with a monomer the number of molecules in the polymer chain increases. This process continues until either all the monomer is consumed or a termination reaction occurs.

$$RM^* + M \xrightarrow{k_p} RMM^* \quad (2.13)$$

$$RMM^* + M \xrightarrow{k_p} RM_nM^* \quad (2.14)$$

M_n - unterminated polymer with *n* monomer units.

where k_p is the propagation constant. The rate of propagation is as follows

$$R_p = k_p[M][M^*] \quad (2.15)$$

2.2.1.3 Termination

Termination in free radical polymerization occurs either by disproportionation or combination.

Combination occurs when free radicals at the ends of two propagating chains meet and share their single free electrons forming a covalent bond resulting in a single long polymer chain. Termination by combination is shown below, with the symbol **(***R*) representing the rest of the chain.

$$(R)-CH_2\overset{\overset{H}{|}}{\underset{\underset{X}{|}}{C}}\cdot + \cdot\overset{\overset{H}{|}}{\underset{\underset{X}{|}}{C}}CH_2-(R) \rightarrow (R)-CH_2\overset{\overset{H}{|}}{\underset{\underset{X}{|}}{C}}-\overset{\overset{H}{|}}{\underset{\underset{X}{|}}{C}}CH_2-(R) \qquad (2.16)$$

$$M_m^* + N_n^* \xrightarrow{k_{tc}} M_m - N_m \qquad (2.17)$$

Disproportionation occurs when a growing polymer chain abstract one hydrogen atom from another growing polymer chains thereby reacting with the free radical to reform the carbon- carbon double bond on the first chain, causing the termination reaction. Termination by disproportionation is shown below.

$$(R)-CH_2\overset{\overset{H}{|}}{\underset{\underset{X}{|}}{C}}\cdot + \cdot\overset{\overset{H}{|}}{\underset{\underset{X}{|}}{C}}CH_2-(R) \rightarrow (R)-CH_2\overset{\overset{H}{|}}{\underset{\underset{X}{|}}{C}}-H + \overset{\overset{H}{|}}{\underset{\underset{X}{|}}{C}}=CH-(R) \qquad (2.18)$$

$$M_m^* + N_n^* \xrightarrow{k_{td}} M_m + N_m \qquad (2.19)$$

k_{tc} - Rate constant of termination by combination

k_{td} - Rate constant of termination by disproportionation.

Termination may also occur by a mixture of disproportionation and combination [24].

$$M_m^* + N_n \xrightarrow{k_t} dead\ polymer \tag{2.20}$$

The rate of termination will be

$$R_t = k_t[M^*]^2 \tag{2.21}$$

where $$k_t = k_{tc} + k_{td} \tag{2.22}$$

As a result of this polymerization mechanism each carbon double bond is converted into a carbon-carbon single bond lowering the molar refractivity. However, this is accompanied by an increase in polymer density leading to a change in refractive index. The combination of these two processes results in higher refractive index in polymerised regions compared to non-polymerised regions so that a refractive index modulation occurs between exposed and unexposed region [30]. It is also observed and accepted that during exposure monomer diffuses into bright regions as a result of a concentration gradient. This causes a further difference in density and refractive index between bright and dark regions.

The next section gives a detailed physical explanation of the refractive index modulation during hologram formation in photopolymers.

2.3 Hologram formation mechanism

When a photopolymer recording material is illuminated with a light interference pattern the bright regions are polymerized as explained in Section 2.2. This results in a concentration gradient of the monomer resulting in the diffusion of monomer from the dark unexposed regions (high monomer concentration) to the bright

exposed regions (low monomer concentration). Due to these processes the molar refractivity and polymer density changes in the bright and dark regions resulting in spatial modulation of refractive index. Holograms recorded by this mechanism are known as phase holograms. The diffraction efficiency growth depends on several chemical and physical factors. Tomlinson and Chandross [27] have given a detailed explanation regarding physical and chemical changes occurring in the material as a result of polymerization which lead to change in refractive index. The refractive index modulation depends on the local composition of the material, that is the volume fractions of the concentrations of monomer (ϕ^m) polymer (ϕ^p) and the background polymer matrix (binder (ϕ^b)). Their sum is assumed to remain conserved at any point and at all times [28].

$$\phi^m + \phi^p + \phi^b = 1 \tag{2.23}$$

The Lorentz-Lorentz relation [27] shows the relation between refractive index, *n* and the optical polarizability per unit volume P.

$$\frac{n^2 - 1}{n^2 + 2} = \frac{4}{3}\pi \mathrm{P} \tag{2.24}$$

where the polarizability per unit volume for a pure substance is equal to the polarizability per molecule times the number density of molecules and is expressed as

$$\frac{n^2 - 1}{n^2 + 2} = \frac{4\pi\rho N\alpha}{3M} = \frac{\rho R}{M} \tag{2.25}$$

where *M* is the molecular weight, ρ is the density of the substance, *N* is Avogadro number, α is the mean polarizability and *R* is the molar refractivity.

The molar refractivity of the photopolymer composition can be approximately related to the molar refractivities of its individual components and is given as

$$R = N_m R_m + N_P R_p + N_b R_b \tag{2.26}$$

where, N_m, N_p and N_b are the number of molecules of monomer, polymer and binder per unit volume respectively.

Aubrecht et al. [28] assume that each particular density is proportional to the corresponding concentration and is given by

$$N_m = \frac{\phi^m \rho_m N}{M_m}, N_p = \frac{\phi^p \rho_p N}{M_p}, N_b = \frac{\phi^b \rho_b N}{M_b}, , \tag{2.27}$$

where ϕ^m, ϕ^p and ϕ^b are the volume fractions and M_m, M_p and M_b are the molecular weights of monomer, polymer and binder respectively.

The refractive index modulation can be considered as a linear function of the refractive indices and concentrations of monomer, polymer and binder

Refractive index modulation can be written as

$$\Delta n = \Delta\phi^m \left[\frac{n_m^2 - 1}{n_m^2 + 2} - \frac{n_b^2 - 1}{n_b^2 + 2} \right] + \Delta\phi^p \left[\frac{n_p^2 - 1}{n_p^2 + 2} - \frac{n_b^2 - 1}{n_b^2 + 2} \right] \tag{2.28}$$

where $\Delta\phi^m$ and $\Delta\phi^p$ are the change in volume fractions of monomer and polymer concentration respectively. It can be seen that the greater the difference between the refractive indices of the monomer or polymer and the binder, the greater the refractive index modulation.

2.4 Advantages and disadvantages of photopolymers as holographic recording material

2.4.1 Advantages

- Photopolymers can spontaneously develop during recording without the need of post-exposure processing steps. This real-time recording characteristic eliminates the need for complicated development procedures and makes them promising candidates for data storage applications.
- Photopolymer materials can be used for recording phase holograms whose applications in mass-production of display holograms and optical elements are of primary interest.
- Use of photopolymerisable compositions for holograms permits the recording of very high spatial frequencies free of any particle size limitation, since the photosensitive composition does not contain any particulate material.
- Photopolymer materials are self-processing and thus, non-latent, [31], hence diffractive properties are immediately available as the grating is being formed. This allows the evolution of the grating to be monitored by replaying the grating with a probe beam having a wavelength, which lies outside the absorption spectrum of the photosensitiser used, thereby not affecting the fabrication process.
- Thick photopolymer layers can be fabricated to act as volume materials giving high diffraction efficiency and good angular selectivity, which makes photopolymers suitable for applications such as holographic embedded photopolymer waveguides, [32-35] and holographic data storage [2,3].

Hence the properties that make photopolymer a good recording medium are

- ❖ High sensitivity, high diffraction efficiency (DE), large dynamic range, real-time imaging capabilities, minimum fabrication steps, low scattering loss and low cost.

2.4.2 Disadvantages

- ➢ Photopolymerisation is not a reversible process and hence photopolymer holograms cannot be erased and reused. Hence photopolymers are suitable materials for write-once-read-many (WORM) applications only.
- ➢ Volume shrinkage that occurs during photopolymerisation remains a major obstacle to the practical application of photopolymers [36, 37]. Shrinking of the photopolymer layers results in a change in the fringe spacing [38]. Due to this it is required to alter the readout beam angle to achieve the maximum diffraction efficiency

The main aim of this project is to determine and minimise the shrinkage of an acrylamide based photopolymer developed at Centre for Industrial and engineering Optics. The techniques used to determine shrinkage precisely after holographic recording and also in real time during holographic recording will be explained in the following chapters.

References

[1] J.Biles, “Holographic Color Filters for LCDs”, SID 94 Digest, 403-406(1994)

[2] A.Pu and D.Psaltis, “High-density recording in photopolymer based holographic three-dimensional disks,” Appl. Opt. 35, 2389–2398 (1996)

[3] U.S.Rhee, H.J.Caulfield, J.Shamir, C.S.Vikram, and M.M.Mirsalehi, “Characteristics of the DuPont photopolymer for angularly multiplexed page-oriented holographic memories,” Opt. Eng. 32, 1839–1847(1993)

[4] J.Ludman, H.J.Caulfield, and J.Riccobono, Eds, “Holography for the New Millennium,” Springer,179–189(2002)

[5] I.Naydenova, H.Sherif, S.Mintova, S.Martin and V.Toal “Holographic recording in nanoparticle doped photopolymer,” Proc. SPIE 6252, (2006)

[6] G.Osterand A.H.Adleman, “Long-lived states in photochemical reactions,” Analytical Chemistry.25, 913-916 (1953)

[7] G.K.Oster and G.Oster, “Photochemical modifications of high polymers by visible light,” Journal of Polymer Science. 48, 321-327(1960)

[8] G.Oster and N.L.Yang, “Photopolymerization of vinyl monomers,” Chemical Reviews.68, 125-151(1968)

[9] D.H.Close, A.D.Jacobson, J.D.Margerum, R.G.Brault, and F.J.McClung, “Hologram Recording on Photopolymer Materials,” Appl. Phys. Lett. 14, 159-160 (1969)

[10] A.Jenney, “Holographic recording in photopolymers,” J. Opt. Soc. Am. 60, 1155-1161 (1970).

[11] R.L.VanRenesse, “Photopolymers in Holography,” Opt. Laser.Tech. 4, 24-27 (1972).

[12] S.Sugawara, K.Murase, and T.Kitayama, “Holographic Recording by Dye-Sensitized Photopolymerization of Acrylamide,” Appl. Opt. 14, 378-382 (1975).

[13] K.Sukegawa, S.Sugawara, K.Murase, “Holographic recording by Fe3+ sensitized photopolymerization,” Electronics and Comminications in Japan. 58-C(11),132-138 (1975)

[14] D.J.Lougnot, C.Truck, “Photopolymer for holographic recording: II self-developing materials for real-time interferometry,” Pure and applied optics. 1, 251-268 (1992)

[15] N.Sadlej and B.Smolinska, “Stable photo-sensitive polymer layers for holography,” Opt. Laser Tech. 7, 175–179 (1975).

[16] M.J.Jeudy and J.J.Robillard, “Spectral Sensitization of a Variable Index Material for Recording Phase Holograms with High Efficiency,” Opt. Comm. 13, 25-28 (1975).

[17] S.Calixto, “Dry polymer for holographic recording,” App.Opt.26, 3904–3909 (1987).

[18] A.Fimia, N.Lopez and F.Mateos, “Acrylamide photopolymers for use in real time holography: Improving energetic sensitivity,” Proc. SPIE1732, 105–109 (1992).

[19] F.Zhao, E. E. E. Frietman, and X. Li, “Novel type of red sensitive photo-polymer system for optical storage,” SPIE 3468. 317–321, July 1998.

[20] S.Martin, P.Leclere, Y.Renotte, V.Toal and Y.Lion, “Characterisation of an acrylamide-based dry photopolymer holographic recording material,” Opt. Eng.33, 3942–3946 (1994).

[21] S.Martin "A new photopolymer recording material for holographic applications: photochemical and holographic studies towards an optimized system," (PhD Thesis) University of Dublin (1995)

[22] R.Jallapuram,"Optimization of an acrylamide-based photopolymer for reflection holographic recording," Ph.D thesis, Dublin Institute of Technology (2005).

[23] I.Naydenova, R.Jallapuram, R.Howard, S.Martin and V.Toal, "Investigation of the diffusion processes in a self-processing acrylamide-based photopolymer system," Appl. Opt.43, 2900-2905 (2004).

[24] S.Martin, I.Naydenova, R.Jallapuram, R.Howard and V.Toal, "Two way diffusion model for the recording mechanism in a self developing dry acrylamide photopolymer," Proc.SPIE. 6252, 37-44 (2006).

[25] I.Naydenova, H.Sherif, S.Martin, J.Raghavendra, V.Toal, "A Holographic sensor," Patent number: WO2007060648A3.

[26] Krzysztof Matyjaszewski and Thomas P. Davis, "Handbook of Radical Polymerization," John Wiley and Sons (2002).

[27] W.Tomlinson and E.Chandross, "Organic photochemical refractive index image recording systems," in Advances in Photochemistry, T. N. Pitts, G. S. Hammond, K. Gallnik, and D. Grosjier, eds.,Wiley Interscience, London (1980).

[28] I.Aubrecht, M.Miler, I.Koudela, "Recording of holographic diffraction gratings in photopolymers: theoretical modelling and real-time monitoring of grating growth," J. Mod.Opt. 45, 1465–1477 (1998)

[29] Petr Munk, Tejraj M. Aminabhavi, "Introduction To Macromolecular Science," John Wiley & Sons Inc., New York, 135-178 (2002)

[30] W.S.Colburn, K.A.Haines, “Volume Hologram formation in photopolymer materials,” Applied Optics.10, 1636-1641 (1971)

[31] R.R.A.Syms, Practical Volume Holography, In Clarendon Press, Oxford.(1990)

[32] S.Maruo, O.Nakamura, S.Kawata, “Three-dimensional microfabrication with two-photon-absorbed photopolymerization,” Opt. Lett. 22, 132-134 (1997).

[33] K.Saravanamuttu, C.F.Blanford, D.N.Sharp, E.R.Dedman, A.J.Turberfield, R.G.Denning, “Sol-gel organic-inorganic composites for 3-D holographic lithography of photonic crystals with submicron periodicity,” Chem. Mater. 15, 2301-2304 (2003)

[34] M.Gu, M.Straub, L.H.Nguyen, “Complex-shaped 3-D microstructures and photonic crystals generated in a polysiloxane polymer by two-photon microstereolithography,” Opt. Mater. 27, 359-364 (2004).

[35] A.C.Sullivan, M.W.Grabowski, R.R.McLeod, “Three-dimensional direct-write lithography into photopolymer,” Appl. Opt. 46, 295-301 (2007)

[36] L.Dhar, M.G.Schnoes, T.L.Wysocki, H.Bair, M.Schilling and C.Boyd, “Temperature-induced changes in photopolymer volume holograms,” Appl. Phys. Lett. 73, 1337-1339 (1998)

[37] R.M.Shelby, D.A.Waldman and R.T.Ingwell, “Distortions in pixel-matched holographic data storage due to lateral dimensional change of photopolymer storage media,” Opt. Lett.25, 713-715 (2000).

[38] H.Sherif, I.Naydenova, S.Martin, C.McGinn and V.Toal, “Characterization of an acrylamide based photopolymer for data storage utilizing holographic angular multiplexing,” J.Opt.A:Pure Appl.Opt.7, 225-260 (2005)

[39] J.T.Gallo and C.M.Verber, “Model for the effects of material shrinkage o n volume holograms,” Appl. Opt. 33, 6797-6804, (1994).

CHAPTER 3

SHRINKAGE IN PHOTOPOLYMERISABLE MATERIALS

3.1 Introduction

Volume shrinkage occurring during photopolymerisation remains a major obstacle for practical applications of photopolymers [1, 2]. Up to now several models have been presented to describe the effect of material shrinkage including the fringe-plane rotation model [3, 4], the average refractive-index change model [5], fringe-plane rotation and average refractive-index change model [6, 7] and fringe bending model [8]. In all these models it is assumed that shrinkage in the lateral direction is smaller [1-9] due to the strong adhesion of photopolymer to the rigid glass substrate.

All of the models focused on shrinkage in photopolymers utilise the information provided by studies of volume holographic gratings recorded in these materials. In order to facilitate the discussion of the models and the methods used in the present thesis, a brief description of the coupled wave theory is given below. This theory, with a very good approximation, describes the properties of volume holographic gratings.

3.2 Coupled wave theory

Kogelnik's Coupled wave theory [10] gives information about the efficiency with which a volume grating diffracts incident light and also the angular and wavelength selectivity for all hologram types. The maximum achievable diffraction efficiency can be measured by illuminating the grating at the Bragg angle.

Coupled wave theory assumes, monochromatic light is incident on the holographic grating at or near the Bragg angle and polarised perpendicular to the plane of incidence. According to coupled wave theory the total field in the grating is due to incident light beam and the diffracted wave in the first order of diffraction. The other (higher) diffraction orders are negligible [10, 11].

$K = \frac{2\pi}{\Lambda}$ is the grating vector, which is normal to the fringe plane, where Λ is the period of the grating.

A wave propagating through the grating can be expressed by the following wave equation

$$\nabla^2 E + \left(\frac{\omega^2}{c^2} \varepsilon - j\omega\mu\sigma \right) E = 0 \qquad (3.1)$$

where E is the complex amplitude of the y component of electric field , ω is the angular frequency, c the velocity of light in free space and μ the permeability of the medium.

The holographic fringes are represented by spatial modulation of ε or σ

$$\begin{aligned} \varepsilon &= \varepsilon_0 + \varepsilon_1 \cos(K.x) \\ \sigma &= \sigma_0 + \sigma_1 \cos(K.x) \end{aligned} \qquad (3.2)$$

ε_1 and σ_1 are the amplitudes of spatial modulation

ε_0 and σ_0 are the average dielectric constant and average conductivity.

Substituting equation (3.2) in equation (3.1) gives

$$\nabla^2 E + \left(\beta^2 - 2J\alpha\beta + 4\chi\beta \cos k.r \right) E = 0 \qquad (3.3)$$

where β and α are the average propagation constant and average absorption constant respectively:

$$\beta = \frac{2\pi(\varepsilon_0)^{1/2}}{\lambda} \quad , \quad \alpha = \frac{c\mu\sigma_0}{2(\varepsilon_0)^{1/2}} \tag{3.4}$$

The coupling constant is given by the following expression:

$$\chi = \frac{1}{4}\left(\frac{2\pi}{\lambda} \frac{\varepsilon_1}{(\varepsilon_0)^{1/2}} - j \frac{\mu c \sigma_1}{(\varepsilon_0)^{1/2}} \right) \tag{3.5}$$

Optical materials are mainly characterised by their refractive index and their absorption coefficient. Under the assumptions that the absorption per wavelength and the change in refractive index of the medium are small compared with the average values in the material, equation (3.4) and (3.5) can be written as

$$\beta = \frac{2\pi}{\lambda} n \quad , \quad \chi = \left(\frac{\pi n_1}{\lambda} \right) - \frac{j\alpha_1}{2} \tag{3.6}$$

In equation (3.3) the coupling constant χ describes the coupling of light between the two beams. The total electric field *E* in the grating as a result of propagation of two coupled waves can be described as the sum of their complex amplitudes which vary along the *z* direction.

$$E = R(z)e^{-i\rho.r} + S(z)e^{-i\delta.r} \tag{3.7}$$

where ρ and δ are the propagation vectors of the reference and signal waves.

The relation between the incident and diffracted wave propagation vectors with the grating vector *K* is expressed as [10]

$$\delta = \rho - K \tag{3.8}$$

We combine equations (3.1) and (3.3) and insert equations (3.7) and (3.8) and compare the terms with exponentials $e^{-i.\rho.r}$ and $e^{-i.\delta.r}$ to obtain the equations

$$R'' - 2j\rho_z R' - 2j\alpha\beta R + 2\chi\beta S = 0 \tag{3.9}$$

$$S'' - 2j\delta_z S' - 2j\alpha\beta S + (\beta^2 - \delta^2)S + 2\chi\beta R = 0 \tag{3.10}$$

Prime indicates differentiation with respect to *z*.

We assume the energy interchange between *S* and *R* is slow which will allow us to neglect $R^{''}$ and $S^{''}$.

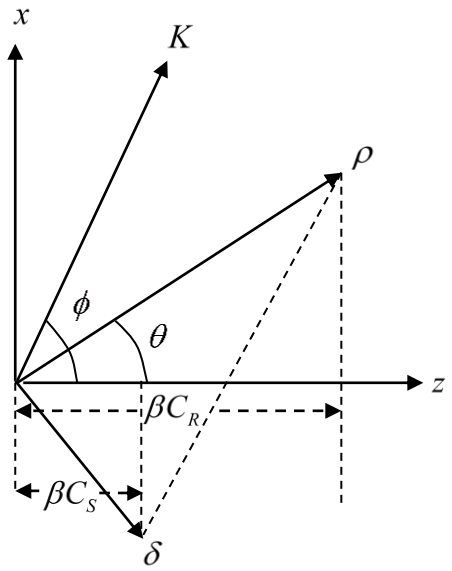

Figure 3.1. Relation of grating vector with propagation vectors

Rewriting equation (3.9) and (3.10) gives the coupled equations for basic analysis

$$C_R R^{'} + \alpha R = -JkS \tag{3.11}$$

$$C_S S^{'} + (\alpha + j\nu)S = -jkR \tag{3.12}$$

where,

$$\begin{aligned} C_R &= \rho_Z / \beta = \cos\theta \\ C_S &= \delta_Z \Big/ \beta = \cos\theta - \frac{K}{\beta}\cos\phi \\ \nu &= \beta\zeta 2\theta_0 \end{aligned} \tag{3.13}$$

The angles in equations 3.13 are defined in Fig.3.1 [10].

In the case of lossless transmission phase holograms having thickness *T*, the amplitude of the diffracted wave at $z=T$

$$S(T) = -j\frac{\exp(-i\xi)\sin(\xi^2+\upsilon^2)^{1/2}}{\left(1+\xi^2/\upsilon^2\right)^{1/2}} \tag{3.14}$$

When the incident light is exactly at the Bragg angle then the angular deviation from the Bragg angle $\zeta = 0$ and the wavelength deviation $\xi = 0$

Diffraction efficiency can now be written as

$$\eta = \frac{|S(T)|^2}{|R(0)|^2} = |S(T)|^2 = \sin^2\upsilon \tag{3.15}$$

The efficiency is 100% when $\upsilon = \pi/2$ beyond which the energy couples back to the reference beam and there will be a decrease of diffraction efficiency. When the incident beam deviates from the Bragg angle the diffraction efficiency is given by the following equation:

$$\eta = \frac{\sin^2(\xi^2+\upsilon^2)^{1/2}}{\left(1+\xi^2/\upsilon^2\right)^{1/2}} \tag{3.16}$$

$$\xi = \Delta\theta\frac{KT}{2}, \quad \upsilon = \pi\Delta nT/\lambda\cos\theta_0 \tag{3.17}$$

The normalised diffraction efficiency of a volume transmission grating as a function of parameter ξ for different values of υ is shown in Fig 3.2

In spite of being mathematically simple Kogelnik's Coupled Wave theory has the advantage that it predicts very accurately the diffraction efficiency of the first order for volume phase gratings

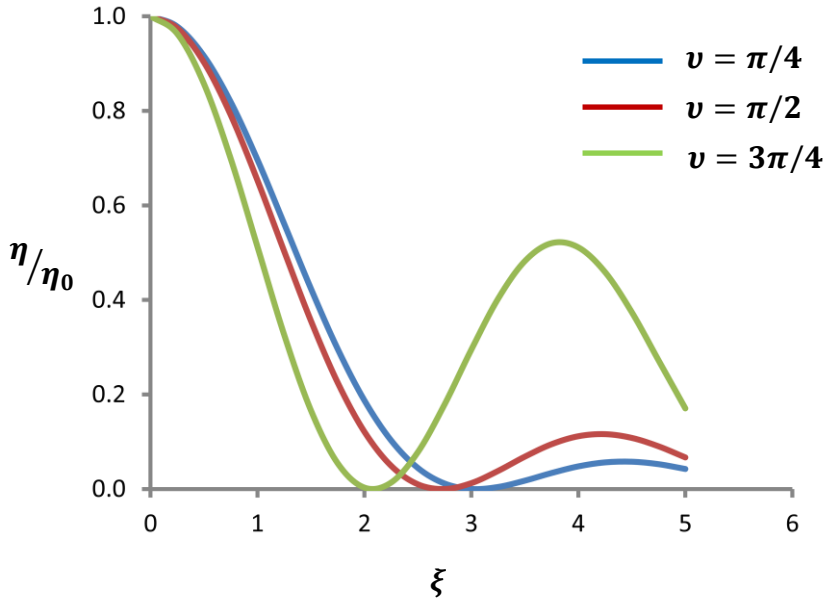

Figure 3.2. Normalised diffraction efficiency v/s ξ for different values of υ in the case of a volume transmission grating.

This angular Bragg selectivity curve can be used to estimate shrinkage in slanted transmission gratings, by measuring the shift of the peak position. The experimental details and the technique used to determine shrinkage in an acrylamide photopolymer will be shown in detail in the next chapter.

3.3 Fringe plane rotation model

We will consider two collimated beams interfering in a holographic medium to form a plane grating having a period Λ and slant angle φ given by [4]

$$\Lambda = \frac{\lambda / n}{2\sin\left(\frac{\theta_1 + \theta_2}{2}\right)} \tag{3.18}$$

$$\varphi = \frac{\pi - (\theta_1 - \theta_2)}{2} \tag{3.19}$$

θ_1 and θ_2 are the angles of incidence of signal and reference beams, λ is the recording wavelength, *n* is the average refractive index of the material.

Figure 3.3 shows the formation of plane wave fringes ($\theta_1 \neq -\theta_2$)

The material shrinks from its original thickness *d* to thickness d'. Due to the change in thickness of the recording material the orientation of the fringes will change in volume transmission grating as shown in Fig. 3.3

$$d' = (1-\tau)d \tag{3.20}$$

where τ is the coefficient of shrinkage (2% shrinkage corresponds to τ = 0.02)

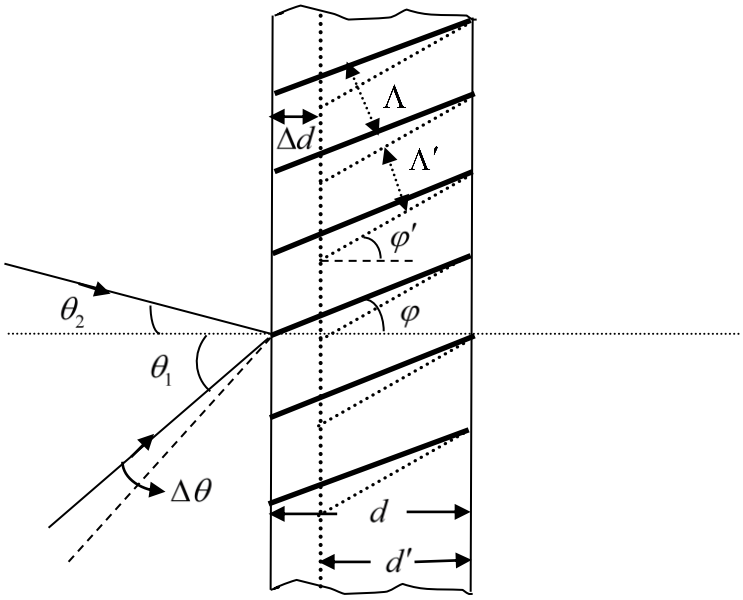

Figure 3.3. Re-orientation of fringes as a result of shrinkage

The assumption made here is that the holographic material is attached to a rigid substrate. The effect of shrinkage is modelled by the rotation of grating slant angle and reduction of grating period. The change in grating slant angle is equal to the rotation of Bragg angle required for maximum diffraction efficiency. Because of the change in Λ with shrinkage, maximum possible diffraction efficiency also changes.

The change in angle is

$$\Delta\varphi = \Delta\theta = \tan^{-1}\left(\tan\varphi \big/ 1-\tau\right) - \varphi \tag{3.21}$$

Thus the slant angle after shrinkage is

$$\varphi' = \varphi + \Delta\varphi = \tan^{-1}\left(\tan\varphi \big/ 1-\tau\right) \tag{3.22}$$

We can write the expression for the fractional change Δd in grating thickness d knowing the slant angles before (φ) and after shrinkage (φ') as

$$\frac{\Delta d}{d} = \frac{\tan\varphi'}{\tan\varphi} - 1 \tag{3.23}$$

3.4 Effective holographic grating model

The effective holographic grating model is based on 3 assumptions:

1) The average refractive index of the medium changes after processing
2) Due to shrinkage occurring in the material the fringes plane rotate
3) The point of contact of the fringe with the glass backing the material won't change as a result of shrinkage.

Consider a grating with spacing Λ recorded in a medium having thickness d with collimated beams having wave vectors along y component null ($\phi = 0$) [7]. The distance between the Bragg planes in the X and Z direction be d_x and d_z. After processing the medium thickness changes from d to d' and hence the Bragg plane changes its position from OP to OP' and the grating spacing also changes to Λ'. Let d_x' and d_z' be the distance between Bragg planes along X and Z direction after processing. According to the model Bragg planes change size but won't change shape hence $d_x = d_x'$

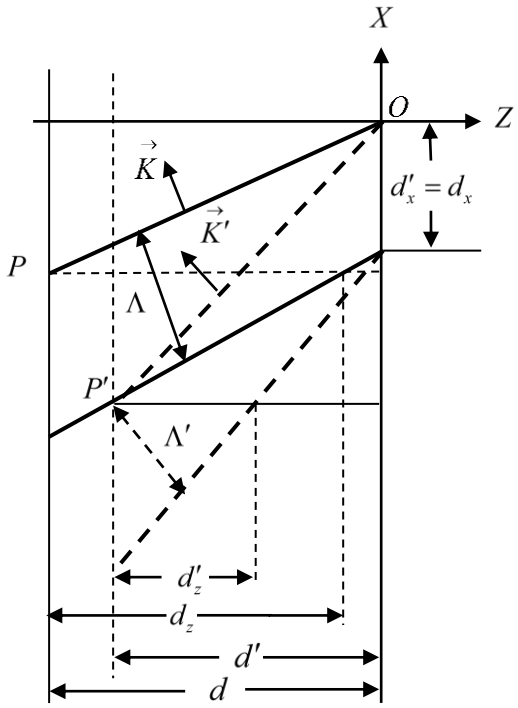

Figure 3.4. Holographic grating before and after processing

Figure 3.5 shows the schematic diagram to obtain the relation between grating parameters before and after processing.

The relation which exists between the coordinates of the points on the grating before and after processing can be expressed as [7]

$$x' = x + z\tan\theta, \quad z = D_z \tag{3.24}$$

Similarly the relation between grating vectors K and K'(before and after processing) is expressed as

$$K'_x = K_x \quad , \quad K'_z = \left(-K_x \tan\theta + K_z\right)/D \tag{3.25}$$

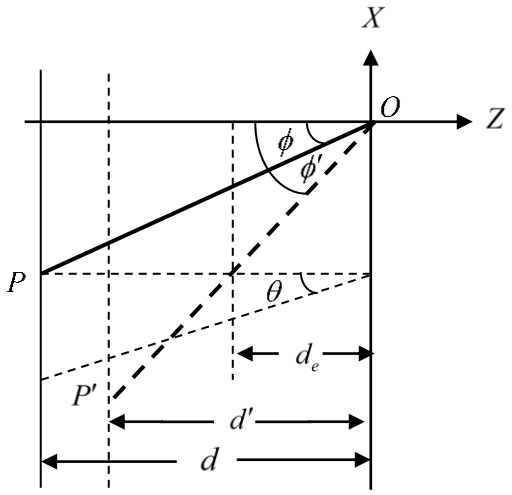

Figure 3.5. Schematic diagram to obtain relation between grating parameters before and after processing

From figure 3.5 we can derive

$$\tan\theta = D\tan\phi' - \tan\phi \qquad (3.26)$$

where, $D = d'/d$ (3.27)

ϕ and ϕ' are the Bragg plane inclinations before and after processing with respect to *z* axis,

d and d' the thickness of the material before and after processing, θ is the 'cut' or 'shear' angle due to inclination of Bragg planes which will be small (only a few degrees).

Using the relation $\tan\phi = -K_z / \mathrm{K}_x$ and equation (3.26) we can write equation (3.25) as

$$K_z' = \left(\tan\phi'/\tan\phi\right)K_z \qquad (3.28)$$

It can be seen that $\tan\phi'/\tan\phi = d/d_e$ (3.29)

If we postulate $D_e = d_e/d$ then $\tan\phi'/\tan\phi = 1/D_e$ equation (3.28) becomes

$$K_z' = K_z / D_e \tag{3.30}$$

d_e parameter is called as the effective thickness of holographic grating. The effective thickness plays a fundamental role in thick holographic gratings because it is directly related to the reconstruction angle which complies with Bragg law. If this angle is α_c the following equation can be obtained for transmission gratings [12]

$$\sin\alpha_c = \frac{1}{2}\left(\frac{N}{D_e} + \mu\right)\sin\alpha_R + \frac{1}{2}\left(\frac{N}{D_e} - \mu\right)\sin\alpha_O \tag{3.31}$$

And we can write

$$\frac{D_e}{N} = \frac{\sin\alpha_R + \sin\alpha_O}{2\sin\alpha_c + \mu(\sin\alpha_O - \sin\alpha_R)} \tag{3.32}$$

α_R and α_O are the reference and object beams angles, $N = n'/n$ and $\mu = \lambda/\lambda'$

n and n' are the refractive index of the material before and after processing.

λ and λ' are recording and reconstruction wavelengths.

The measurement of the recording angles and the reconstruction angle in compliance with Bragg's law gives not the actual thickness but rather the effective thickness.

Taking into account Equations (3.24)-(3.30), we express the parameters θ and D_e

$$\tan\theta = \frac{D - D_e}{D_e}\tan\phi \tag{3.33}$$

$$D_e = \frac{\tan\phi}{\tan\theta + \tan\phi} D \tag{3.34}$$

Equations (3.33) and (3.34) produce the following conclusions;

- The greater the difference between the angles θ and ϕ the more similar the values of D and D_e
- When ϕ is small, the difference between D and D_e is greater.
- When ϕ is ~ 90° (reflection grating), the D and D_e parameters coincide, so that, for reflection gratings, $D_e \approx D$
- If $\phi \approx \theta$ then $D_e \approx 0.5D$
- In symmetric gratings ($\phi = 0°$), θ will equal 0

3.5 Shrinkage studies in photopolymer material

Zhao et.al [13] successfully demonstrated shrinkage measurements in DuPont photopolymer having thickness 20μm. Holographic gratings were recorded using an Argon Ion laser (514.6 nm). The intensities of the two recording beams at the surface of the film were 2.21 mW and 0.67 mW. A thickness change of 1.05 μm (5.25% shrinkage) was observed by measuring the angular shift of the Bragg peak.

Cheah et al. [14] reported the effects of adding short glass fibers into an acrylic-based photopolymer used in laser solidification process. It was observed that the fiber reinforced specimens yielded higher measured values of elastic modulus and ultimate tensile strength. For determining shrinkage strain, square specimens having dimensions of 40mm × 40mm × 4mm were fabricated and the dimensions of the specimens were measured before and after the post-curing process using a two-axis travelling microscope. The amount of shrinkage obtained in the reinforced prototypes during post curing was also found to be less than in their non-reinforced counterparts. It was observed that shrinkages in both directions (longitudinal and

transverse) decrease with the use of high laser power and low layer thickness. The authors suggested that this may be due to the fact that the fibers added to the specimen have displaced some of the volume originally occupied by partially cured and uncured polymer within the structure. The reduced amount of these partially cured and uncured polymer results in a reduction in the shrinkage obtained on post-curing.

Trentler et al [15] reported photopolymer systems with epoxy resins as a matrix. The crosslink density of epoxy resins plays a crucial role in the holographic performance with regards to diffraction efficiency and volume shrinkage. Shrinkage was determined by measuring the Bragg detuning of the holograms. Epoxy resins with high crosslink density lead to low volume shrinkage, due to their high dimensional stability. It also results in reduced diffraction efficiency due to restricted monomer diffusion for photopolymerisation. Whereas epoxy resin with a low crosslink density makes monomer diffusion more efficient and high diffraction efficiency can be obtained. The relation between dimensional stability and diffraction efficiency is a challenging factor for high performance in a crosslinked polymeric matrix. Diffraction efficiency near 92% and volume shrinkage of 0.67% was also obtained by the addition of epoxy resin to the matrix [16]. It was found that the epoxy-resin based photopolymer with low cross-linking density could significantly enhance the energetic sensitivity without reducing both the diffraction efficiency and dimensional stability.

Vaia et.al [17] introduced the idea of incorporating nanoparticles to improve refractive index modulation, The inclusion of nanoparticles also results in substantial suppression of polymerization shrinkage, giving high dimensional stability. Nanoparticles are non-reactive components known for having low

scattering, stability in water suspensions and are available with a broad range of refractive index [18]. The incorporation of TiO_2 nanoparticles in methacrylate photopolymers by Suzuki et.al [19] in 2002 gained attention. The nanocomposite attained refractive index modulation (Δn) as high as 5.1×10^{-3}. Shrinkage of about 2.9% was determined with nanoparticle concentration of 15 vol.% by measuring Bragg angle detuning before and after holographic exposure as a function of an external angle between the sample normal and the bisector of the two writing beams. Sanchez et al [20] in 2005 reported a similar TiO2 nanoparticle (average diameter - 4 nm) dispersed in two kinds of acrylate monomers. Holographic recording was performed at 351 nm and Δn as large as 15.5×10^{-3} at 633 nm was obtained.

Tomita et al [21] in 2006 reported the use of hyperbranched polymers (HBPs), acting as mobile organic nanoparticles, dispersed in methacrylate photopolymers. Two types of reduced HBPs, hyperbranched poly (ethyl methacrylate) (HPEMA) and hyperbranched polystyrene (HPS), having average size of 10 nm were synthesized. The material provided diffraction efficiency near 100% at a recording intensity of 100 mW/cm^2 and wavelength 532 nm. The effective thickness differences of these samples were estimated by curve fitting of their Bragg-angle detuning data to Kogelnik's formula [10]. An approximately 60% reduction in the fractional volume change was obtained compared to the undoped material sample.

Later Hoque et.al [22] reported shrinkage in photopolymer by introducing epoxy cured silsesquioxane (hyper-branched POSS molecules) in PVC matrix. In order to determine volume shrinkage, slanted holographic gratings (slant angle 16^0) were fabricated. The degree of volume shrinkage noted in the material without POSS was 2.6 % and shrinkage with 15 % POSS hyper branched content was 1.64 %.

The contribution to the reduction in volume shrinkage was due to the dimensional stability enhancement of the medium by the hyper-branched POSS.

Lee et.al [23] reported a photopolymer material using organic/inorganic hybrid interpenetrating networks (IPNs) as matrix, which exhibits both high monomer diffusion and low volume shrinkage. Slanted gratings (slant angle 5°) were recorded in the material in order to determine shrinkage. It was shown that the hybrid IPNs enable the enhancement of dimensional stability (reduced volume shrinkage) without sacrificing monomer diffusion or diffraction efficiency in crosslinked matrix photopolymer system. The estimated volume shrinkage coefficients were 0.101–0.151 %.

Chen et.al [24] reported an organic-inorganic hybrid matrix with low shrinkage. The matrix is triethoxysilylpropyl polyethyleneglycol carbamate (TSPEG) homogeneously bonded with tetraethyl orthosilicate (TEOS) prepared by the sol-gel method. Diallyl phthalate pre-polymer (DAPP, 10 wt% of the matrix) was used as monomer and 9,10- Phenanthrenequinone (PQ, 2 wt% of the monomer) as photoinitiator. The mixture was stirred with a magnetic stirrer and filtered using membranes of 0.20μm pore size attached to a Teflon syringe. The filtrate was injected into the cell between two glass plates separated by a spacer, and then thermally cured for 3–7 days at 45°C. Optical data recording was performed with a blue laser source (405 nm) having intensity 2 mW/cm^2. In order to investigate the shrinkage of photopolymer, a set of 15 holograms were angle multiplexed in a 0.6 mm thick photopolymer sample. The shrinkage of photopolymer film obtained by measuring the Bragg detuning was 0.145 %. The relatively low shrinkage was explained by the presence of the silica inorganic component in the hybrid matrix,

which provided good mechanical properties to resist the deformation caused by shrinkage during photopolymerisation of DAPP monomer.

Gallego et al [25] reported different values of shrinkages or swelling in photopolymer layer using a reflection interferometer. Their results suggested that at higher spatial frequencies, monomer diffusion from the dark zones to the bright ones, together with surface tension effects, could considerably affect the material volume changes. In particular, molecular migration (mass transport) reduced shrinkage. Shrinkage of around 2% (without crosslinker) and 3% (with crosslinker) were obtained. The reduction in shrinkage was observed to increase with the spatial frequency and with the monomer diffusion velocity.

Choi et al. [26] reported a new free radical polymerisation holographic recording medium, based on low shrinkage cyclic allylic sulfides (LS-CASs) ring-opening monomers. For comparison, the LS-CAS monomer was replaced with 4-bromostyrene. In this material system, 6-methyl-3-methylene-1,5-dithiacyclooctane was used as monomer. The percentage volume shrinkage measured was 0.02% , a fivefold decrease in volume shrinkage compared to 4-bromostyrene monomer system.

Hata et.al [27] reported a novel nanocomposite to suppress shrinkage in photopolymer material using thiol-ene step-growth polymerisation mechanism. Due to the effect of crosslinked thiol-ene, polymerisation proceeded very rapidly but did not reach the gel point until high functional group conversions took place, that is, reaching the gelation point later during conversion in the mixtures accelerated the mutual diffusion and phase separation of the monomer molecules and nanoparticles during recording. This resulted in an increase in the material

sensitivity. Low shrinkage of as 0.3% was observed for a nanoparticle concentration of 35 vol.%.

3.6 Zeolite nanocomposites

One type of nanoparticle that is found to be compatible with acrylamide-based photopolymers developed at IEO is the Si-MFI zeolite. Zeolite nanoparticles can be dispersed in IEO's water soluble photopolymer with little loss in optical quality. It was found that there was a 70% increase in the refractive index modulation and substantially lower shrinkage was obtained [18]

It has been shown that nanoparticles can be spatially redistributed during the holographic recording, and the use of nanoparticles with appropriate refractive index will lead to significant improvement in the ultimate refractive index modulation. It has been observed that the nanoparticles are expelled from the bright to the dark fringes areas, in the opposite direction to monomer diffusion [28].

Zeolites are crystalline aluminosilicates or silicate materials with different framework structures that form pores with uniform sizes [29-31].

Structurally, the zeolites are aluminosilicates based on a connected framework of SiO4 and AlO4 tetrahedrals that are connected to each other by shared oxygen atoms [32]. In addition to the zeolites there is another class of inorganic materials consisting of alternating Al3+ and P5, generally described as microporous aluminophosphates or 'zeo-type materials' [33]. Zeolites and zeo-type materials are classified according to their framework type, pore dimensions and Si/Al or Al/P ratios. The framework density of the zeolites is related to the number of tetrahedral atoms (T = Si, Al) per 1000 A° [33]. The tetrahedra are linked together to form

cages connected by pore openings of defined sizes. Depending on the structural types, the pore size of the molecular sieves (zeolites) ranges from 0.3 to 2 nm [34]

Up to now there has not been a detailed experimental study of shrinkage in holographic photopolymers, taking account of layer thickness and recording parameters, i.e. slant angle, intensity and spatial frequency to give information about the process in polymer layers [35, 36]. The aim of this project is to determine shrinkage in acrylamide photopolymer using different techniques and to find the effect of incorporation of nanozeolites in photopolymer layers.

References

[1] L.Dhar, M.G.Schnoes, T.L.Wysocki, H.Bair, M.Schilling and C.Boyd, "Temperature-induced changes in photopolymer volume holograms," Appl. Phys. Lett. 73, 1337–1339 (1998).

[2] R.M.Shelby, D.A.Waldman and R.T.Ingwell, "Distortions in pixel-matched holographic data storage due to lateral dimensional change of photopolymer storage media," Opt. Lett. 25 ,713-715 (2000)

[3] D.H.R.Vilkomerson and D.Bostwick., "Some Effects of Emulsion Shrinkage on a Hologram's Image Space," Appl. Opt. 6, 1270-1272 (1967)

[4] J.T.Gallo and C.M.Verber, "Model for the effects of material shrinkage on volume holograms," Appl.Opt.33, 6797-6804(1994)

[5] M.P.Jordan and L.Solymar " A note on volume holograms," Electron. Lett. 14, 271-272 (1978)

[6] P.Fiala, J.Ruzek, and T.Jerie, "Behavior and properties of real holographic recording materials," in Practical Holography II, T. H. Jeong, ed., Proc. Soc. Photo-Opt. Instrum. Eng. 747, 74-81 (1987)

[7] A.Belendez, I.Pascual, and A.Fimia, “Model for analyzing the effects of processing on recording material in thick holograms,” J. Opt. Soc. Am. A. 9, 1214-1223 (1992)

[8] T.Kubota, “The bending of interference fringes inside a hologram,” Opt.Acta. 26,731-743 (1979)

[9] D.A.Waldman, H.Y.S. Li, and M.G.Horner, “Volume shrinkage in slant fringe gratings of a cationic ring-opening holographic recording material,” J. Imaging Sci. Technol. 41 497-514 (1997)

[10] H.Kogelnik, “Coupled Wave Theory for Thick Hologram Gratings,” The Bell System Technical Journal.48, 2909-2947 (1969)

[11] P.Hariharan, Optical Holography: Principles, Techniques and Applications, 1st ed, Cambridge University Press (1984).

[12] A.Belendez, “Influences of recording material on the characteristics of holographic optical elements,” Ph.D. dissertation (Valencia University, Valencia, Spain, (1990)

[13] C.Zhao, J.Liu, Z.Fu, and R.T.Chen, “Shrinkage correction of volume phase holograms for optical interconnects,” Proc.SPIE. 3005 (1997)

[14] C.M.Cheah, J.Y.H.Fuh, A.Y.C.Nee and L.Lu, “Mechanical characteristics of fiber-filled photo-polymer used in stereolithography,” Rapid Prototyping Journal. 5, 112-119 (1999)

[15] T.J.Trentler, J.E.Boyd and V.L.Colvin, “Epoxy resin-photopolymer composites for volume holography,” Chem. Mater. 12, 1431- 1438 (2000)

[16] Y.C.Jeong, S.Lee and J.K.Park, “Holographic diffraction gratings with enhanced sensitivity based on epoxy-resin photopolymers,” Opt. Express. 15, 1497-1502 (2007)

[17] R.Vaia, C.Dennis, L.Natarajian, V.Tondiglia, D.Tomlin and T.Bunning, "One-step,micrometer-scale organization of nano and mesoparticles using holographic photopolymerization: A generic technique," Advanced Materials.13, 1570-1574 (2001)

[18] I.Naydenova, H.Sherif , S.Mintova , S.Martin and V.Toal "Holographic recording in nanoparticle doped photopolymer," Proc. SPIE. 6252 (2006)

[19] N.Suzuki, Y.Tomita and T.Kojima, Holographic recording in TiO2 nanoparticle-dispersed methacrylate photopolymer films, Applied Physics Letters 81, 4121-4123 (2002)

[20] C.Sanchez, M.Escuti, C.van Heesch, C.Bastiaansen, D.Broer, J.Loos and R. Nussbaumer, "TiO_2 nanoparticle-photopolymer holographic recording", Advanced Functional Materials 15, 1623-1629 (2005)

[21] Y.Tomita, K.Furushima, K.Ochi et al., "Organic nanoparticle (hyperbranched polymer)-dispersed photopolymers for volume holographic storage," Appl. Phys.Lett. 88, (2006).

[22] M.A.Hoque, Y.H.Cho, Y.Kawakami, "High performance holographic gratings formed with novel photopolymer films containing hyper-branched silsesquioxane," Reactive & Functional Polymers 67 , 1192–1199 (2007)

[23] S.Lee, Y-C.Jeong, Y.Heo, S.Kim, Y-S.Choi and J-K.Park, "Holographic photopolymers of organic/inorganic hybrid interpenetrating networks for reduced volume shrinkage,"J. Mater. Chem. 19, 1105–1114(2009)

[24] J.-H.Chen, C-T.Yang, C-H.Huang, M-F.Hsu, and T-R.Jeng, "Study of Optical Properties of Glass-Like Polymer Material for Blue Laser Holographic Optic Data Storage Recording," IEEE Transactions on Magnetics. 45 , 2256-2259 (2009)

[25] S.Gallego, A.Marquez, D.Mendez, "Analysis of PVA/AA based photopolymers at the zero spatial frequency limit using interferometric methods," Applied Optics. 47, 2557–2563 (2008).

[26] K.Choi, J.W.M.Chon, M.Gu, N.Malic, and R.A.Evans, "Low-distortion holographic data storage media using free-radical ring-opening polymerization," Advanced Functional Materials. 19, 3560–3566 (2009).

[27] E.Hata and Y.Tomita, "Order-of-magnitude polymerization-shrinkage suppression of volume gratings recorded in nanoparticle-polymer composites," Optics Letters, 35,396–398 (2010).

[28] Y.Tomita, K.Chikama, Y.Nohara Y.N.Suzuki, K.Furushima and Y.Endoh, "Two-dimensional imaging of atomic distribution morphology created by holographically induced mass transfer of monomer molecules and nanoparticles in a silica-nanoparticle-dispersed photopolymer film," Optics Letters. 31, 1402-1404 (2006)

[29] T.Maesen and B.Marcus, "Introduction to zeolite science and practice, included in Studies in Surface Science and Catalysis" 137, Eds. H.Van Bekkum, E. Flanigen, P.Jacobs and J.Jansen, Elsevier, 1 (2001)

[30] S.Kallus, J.M.Condre, A.Hahn, G.Golemme, C.Algieri, P.Dieudonne, P. Timmins and J.Ramsay, "Colloidal zeolites and zeolite membranes," Journal of Materials Chemistry 12, 3343-3350 (2002)

[31] J.Cejka, H.van Bekkum, A. Corma and F.Schuth (ed) Introduction to Zeolite Science and Practice (Studies in Surface Science and Catalysis .168) 3rd edition. 2007

[32] A.Dyer, "An Introduction to Zeolite Molecular Sieves," (New York: Wiley) 1988

[33] X.Bu and P.Feng , “Crystalline microporous and open framework materials The Chemistry of Nanostructured Materials,” ed P Yang (Singapore: World Scientific)2003

[34] S.Kallus, J.M.Condre, A.Hahn, G.Golemme, C.Algieri, Ph.Dieudonne, P.Timmins and J.D.F.Ramsay, “Colloidal zeolites and zeoilite membranes,” J. Mater.Chem. 12 3343–3350 (2002)

[35] C. Neipp and A. Belendez, S. Gallego, M. Ortuno and I. Pascual, J. T. Sheridan, “Angular responses of the first and second diffracted orders in transmission diffraction grating recorded on photopolymer material,” Opt. Exp. 11, 1835-1843(2003).

[36] H.Sherif, I.Naydenova, S.Martin, C.McGinn and V.Toal, “Characterization of an acrylamide based photopolymer for data storage utilizing holographic angular multiplexing,” J. Opt. A: Pure Appl. Opt. 7, 255–260 (2005)

CHAPTER 4

STUDIES OF SHRINKAGE IN ACRTYLAMIDE PHOTOPOLYMER FILMS AFTER HOLOGRAPHIC RECORDING

4.1 Introduction

In this chapter we studied the shrinkage in acrylamide based photopolymer by measuring the Bragg detuning of transmission diffraction gratings recorded at different slant angles and at different intensities for a range of spatial frequencies. Transmission diffraction gratings of spatial frequencies 500, 1000, 1500 and 2000 lines/mm were recorded in an acrylamide based photopolymer film having 60±5 μm thickness. The grating thickness and the final slant angles were obtained from the angular Bragg selectivity curve and hence the shrinkage caused by holographic recording was calculated. The shrinkage of the material was evaluated for three different recording intensities 1, 5 and 10 mW/cm^2 over a range of slant angles, while the total exposure energy density was kept constant at 80 mJ/cm^2 in order to avoid overmodulation effects.

4.2 Experimental Procedures

4.2.1 Sample preparation

The composition of the photopolymer solution used in the study is shown in Table.4.1

Table 4.1.Photopolymer composition

Acrylamide	0.6g
Methylenebisacrylamide	0.2g
Polyvinyl alcohol (10% wt./v stock)	17.5ml
Triethanolamine	2ml
Erythrosine B dye (0.11%wt./wt.)	4ml

The photopolymer layer was prepared as described in [1]. Briefly, 0.6g of acrylamide monomer was added to 17.5 ml stock solution of polyvinyl alcohol (10% wt). Then 2ml of triethanolamine was added. To this solution 0.2 g of N, N-Methylene-bis-acrylamide and finally 4ml of Erythrosin B dye (0.11 %wt/wt stock solution) were added. Of this solution, 1.2 ml was spread on a 25 mm × 120 mm glass plate. The samples were dried for 24 h by gravity-settling method at room temperature. Sample thickness after drying was approximately 60 μm.

4.2.2 Holographic recording setup

The basic setup for recording holographic gratings is shown in Fig.4.1. The 532 nm beam from a frequency doubled Nd-YVO_4 laser was spatially filtered, expanded and collimated to around 1 cm cross sectional diameter by a lens. The expanded beam was split into two beams using a beamsplitter. The beams were made to overlap completely at the sample of photopolymer at equal and opposite angles of incidence.

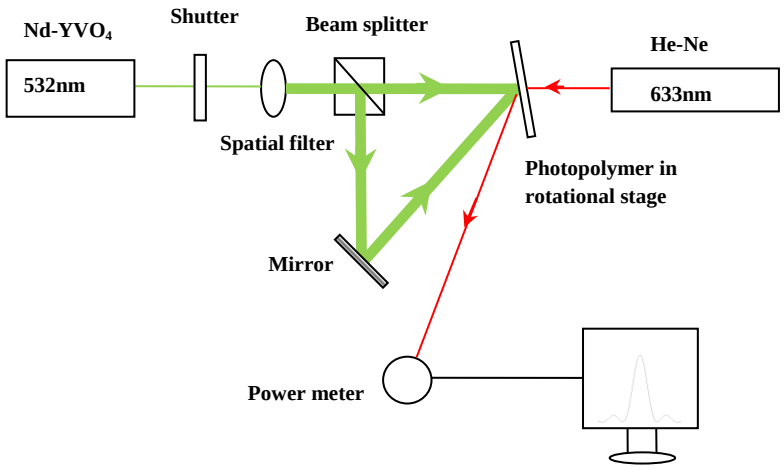

Figure 4.1. Optical set-up for recording transmission phase holographic gratings

In order to determine the spatial frequency dependence of shrinkage during grating formation, angles of incidence 15°, 30°, 47° and 64° were chosen so that the spatial frequencies were approximately 500, 1000, 1500 and 2000 lines/mm respectively. The photosensitive layer was mounted on a high-precision computer controlled rotational stage (Newport M-URM100ACC) and the plate normal bisected the angle between the beams. This ensured that the beam intensity ratio was constant across the illuminated area and the grating was unslanted. The diffraction efficiencies of the gratings were monitored using a He-Ne beam which was diffracted by the recorded grating but not absorbed by the photopolymer. The intensity of the He-Ne laser incident on the grating and the diffracted intensity were both measured using a power meter (Newport Optical Power Meter .Model 1830-C). It was necessary to ensure that the He–Ne laser was incident at the Bragg angle for 633-nm light although there was a small change (± 0.17°) in the position of maximum diffracted intensity outside the photopolymer layer for the unslanted gratings due to imperfections in setting the Bragg angle. The experimental measurements were corrected for this initial misalignment.

4.3 Study of the influence of recording intensity on photopolymer shrinkage

Gratings were recorded using intensities of 1, 5 and 10 mW/cm^2 and exposure times of 80, 16 and 8 sec. over a range of slant angles while the total exposure energy density was kept constant at 80 mJ/cm^2. After recording the unslanted gratings and obtaining the angular selectivity profiles we also measured the profiles of gratings recorded with slant angles of +5°, +10°,-5° and -10°. Angular

selectivity curves were fitted to the data from which we obtained the positions of the Bragg peaks and hence the shrinkage of the gratings as explained in [2, 3].

Figure 4.2(a) shows the growth curves of a 10° slanted grating for three different intensities. Fig. 4.2(b) shows the angular selectivity curves of the gratings of 1000 lines/mm for the same slant angles. From the graphs we can see a shift in the peak position of the curve due to shrinkage and the shift is greater for gratings recorded with lower intensities and longer exposure times, i.e. 1 mW/cm^2 and 80s. The same is true for all other slant angles.

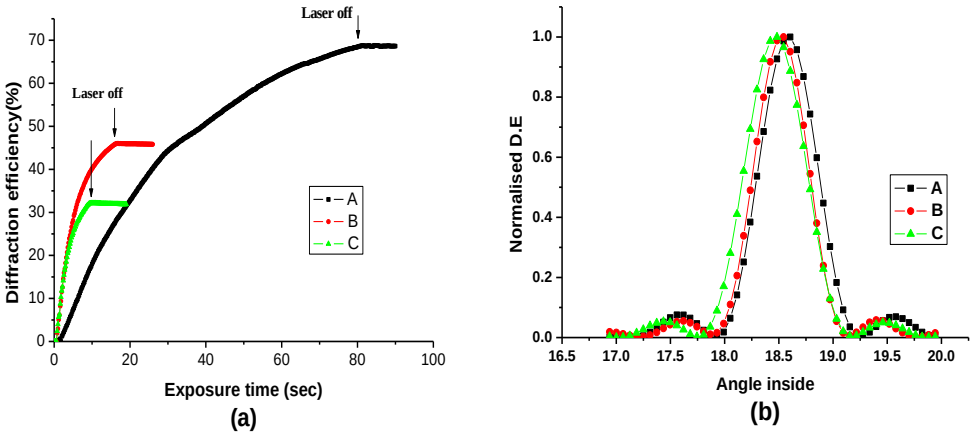

Figure 4.2 Diffraction efficiency growth (a) and angular selectivity curves (b) for gratings recorded at A - 1 mW/cm^2, 80 sec; B - 5 mW/cm^2, 16 sec, C - 10 mW/cm^2, 8 sec. The corresponding Bragg peak positions in (b) are A - 18.525°; B - 18.483° ; C - 18.468°

4.4 Study of the influence of spatial frequency on photopolymer shrinkage

Transmission diffraction gratings of spatial frequencies 500, 1000, 1500 and 2000 lines/mm were recorded in acrylamide based photopolymer film having 60±5μm thickness with angles of incidence of 15.29°, 30.85°, 47.03° and 64.28° respectively.

Figure 4.3 (a) shows growth curves of 5° slanted gratings for four different spatial frequencies. Figure 4.3 (b) shows the angular selectivity curves of these gratings. The Bragg peak shift for recordings is greater at higher spatial frequencies of 2000 lines/mm than at 500 lines/mm

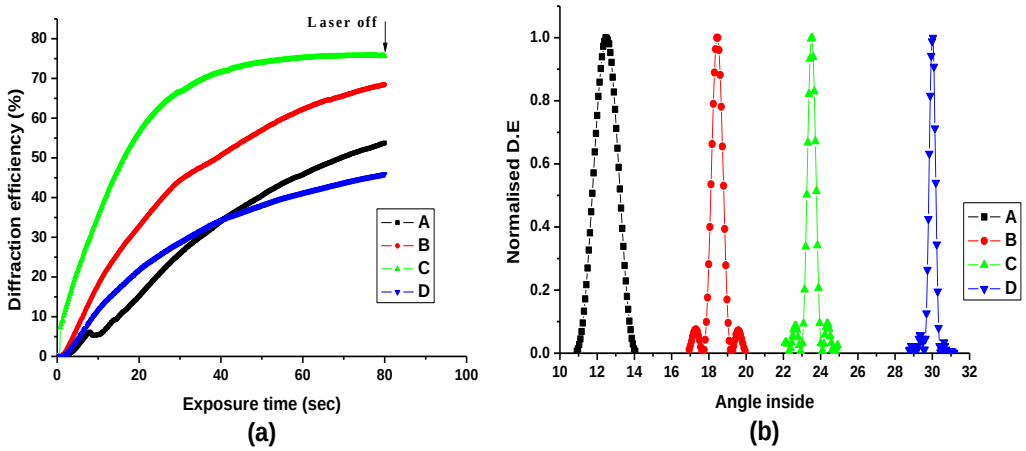

Figure 4.3. Diffraction efficiency growth (a) and angular selectivity curves (b) for gratings slanted at 5° and recorded at A- 500 lines/mm; B- 1000 lines/mm, C- 1500 lines/mm, D-2000 lines/mm. The corresponding shift in Bragg peak in (b) is A - 0.08°; B-0.12°; C-0.15°; D- 0.3°

Fig 4.4 shows the corresponding shift in Bragg curve for the range of slant angles at different intensities and at different spatial frequencies. We can determine the shrinkage due to holographic recording using Equation 3.23 as described in section 3.3.

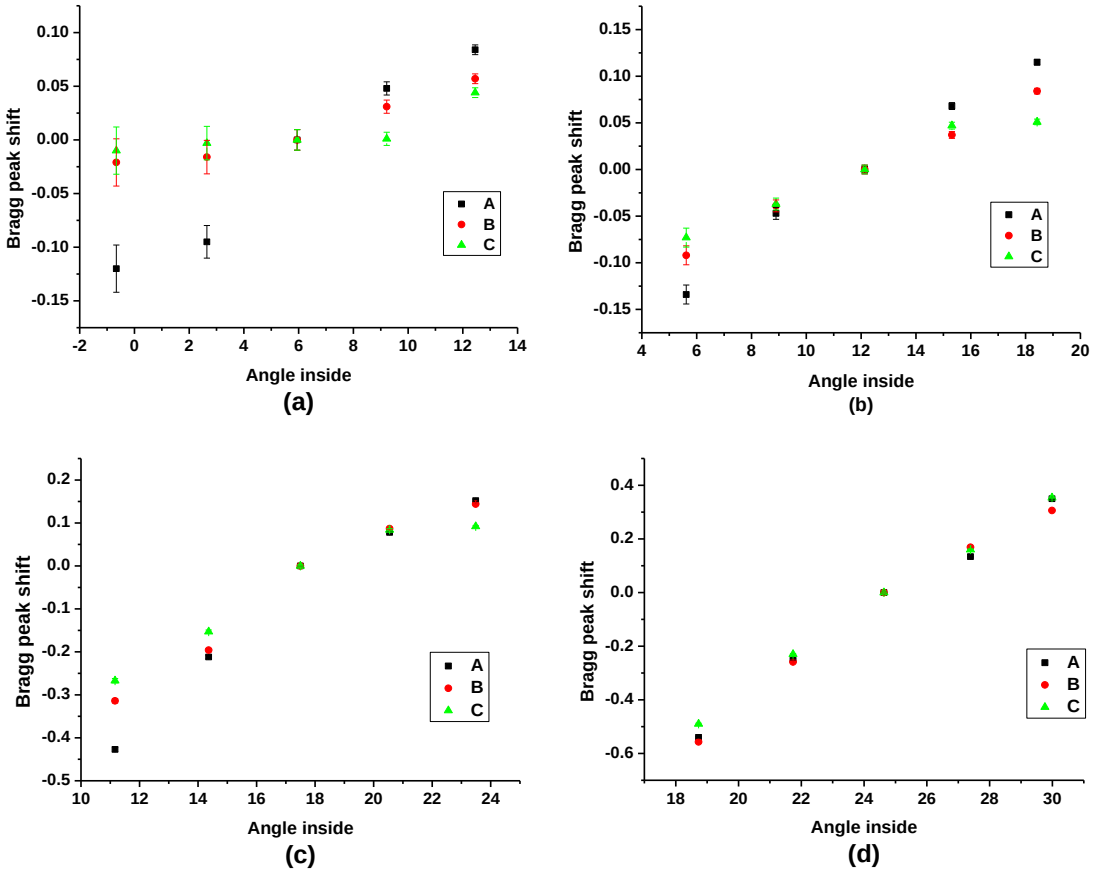

Figure 4.4. Bragg peak shift with respect to the initial slant angles for spatial frequencies (a) 500 lines/mm (b) 1000 lines/mm (c) 1500 lines/mm and (d) 2000 lines/mm for gratings recorded at A-1 mW/cm^2; B- 5 mW/cm^2, C- 10 mW/cm^2

Fig 4.5 shows the tangent of final slant angle versus tangent of initial slant angle for gratings recorded at 10 mW/cm^2 at 1000 lines/mm and the slope of the graph gives the percentage shrinkage of the material. The percentage shrinkage evaluated from the curve is 1.08%. Similarly the shrinkage can be calculated for different recording intensities and spatial frequencies.

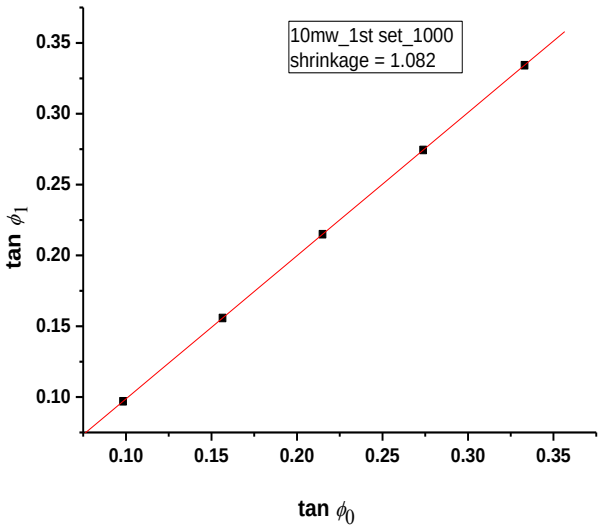

Figure 4.5. Dependence of the final slant angle on the initial slant angle for recording intensity 10 mW/cm^2 at 1000 lines/mm shrinkage- 1.08%

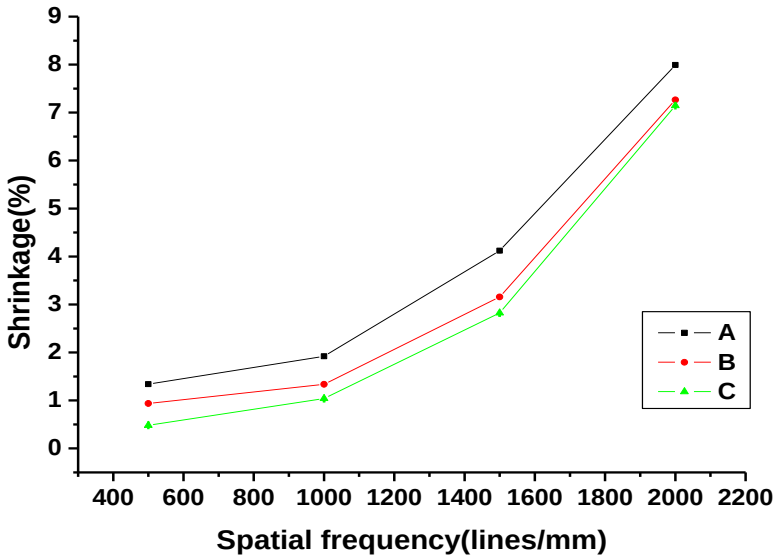

Figure 4.6. Dependence of shrinkage on spatial frequency for recording intensities A- 1 mW/cm^2, B- 5mW/cm^2, C- 10 mW/cm^2

Figure 4.6 shows plots of shrinkage versus spatial frequency for three different recording intensities. An average of 10 measurements is taken in order to obtain the value of shrinkage for each intensity and spatial frequency

4.5 Study of the influence of sample thickness on photopolymer shrinkage

We also obtained the angular selectivity curves for gratings recorded at 3 different thicknesses 30, 60 and 120 μm at 1000 lines /mm with recording intensity 10 mW/cm^2 and exposure time of 8 sec [2]

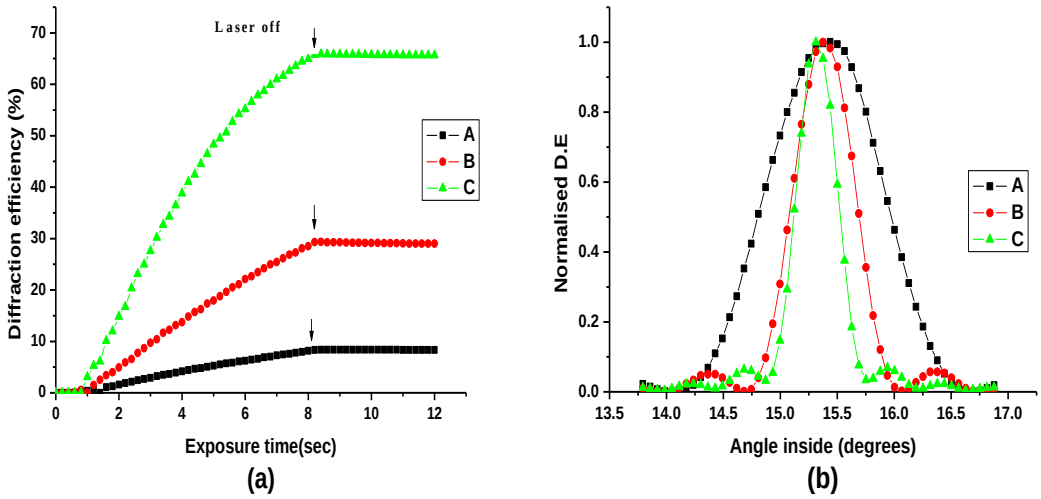

Figure 4.7. Diffraction efficiency growth (a) and angular selectivity curves (b) for gratings recorded in layers of thickness A- 30 μm; B- 60 μm, C- 120 μm. The corresponding positions of Bragg peaks in (b) are A -15.441°, B-15.375°, C- 15.31°.

The percentage shrinkage of the material is higher for recording with smaller thickness. Higher diffraction efficiencies are obtained for samples recorded with large thickness. Although the layers are with different thickness (Fig 4.7.a) and lower percentage shrinkage (Fig 4.7 b), the same refractive index modulation is

obtained, Fig 4.8 (a), suggesting the same monomer molecule conversion extent per unit volume and thus the same shrinkage. Fig 4.8(b) shows the percentage shrinkage versus thickness.

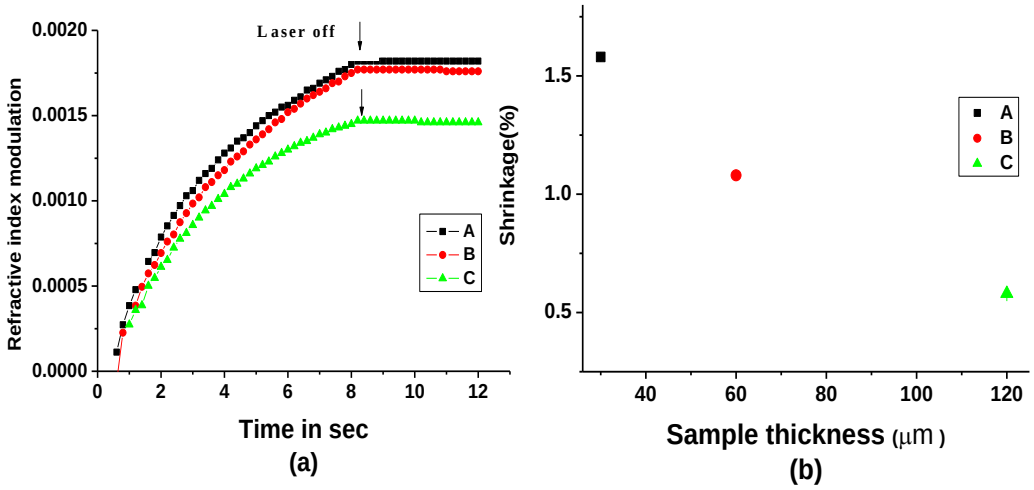

Figure 4.8. Graphs showing the refractive index modulation vs time of exposure for gratings recorded in layers of thickness A- 30 µm; B- 60 µm, C- 120 µm (a) and the corresponding percentage shrinkage (b)

4.6 Discussion and conclusions

- It was observed that the shrinkage is greater for gratings recorded with lower intensities and longer exposure times and also increases with spatial frequency. The reason for the higher shrinkage at low intensity can be related to the fact that at lower intensity the rate at which the free radicals are generated is smaller and thus the volume concentration of free radicals is lower. This leads to a lower rate of termination and the ultimate result is the creation of longer polymer chains each comprising a larger number of monomer molecules. It is known that the polymerised material has higher density due to the morphology

of the polymer material made of entangled polymer molecules. For a greater extent of polymerization the final density and thus the total dimensional change of the layer will be greater.

- Higher intensities and lower spatial frequencies are recommended but the maximum achievable diffraction efficiency is lower in these cases.
- In order to confirm the larger shrinkage at high spatial frequency of recording, gratings were recorded at 2000 lines/mm in 50μm and 105μm thick layers exposed to 5 mW/cm^2 for 16 sec. The dimensional changes of the layers after recording of the holographic gratings were measured using a white light interferometric profiler. [20]. It was calculated that the shrinkage of these layers respectively was 8.2 % (4.1 μm absolute shrinkage) and 3.14% (3.3μm absolute shrinkage). These values for the shrinkage are consistent with the result obtained in Fig. 4.6, where for the same recording conditions (curve B) in 60μm thick layers the shrinkage was evaluated to be 7.27% (4.4μm absolute shrinkage).
- One possible explanation for the large values of the observed shrinkage at high spatial frequency is the larger number of monomer molecules converted into polymer molecules, causing larger density change. At high spatial frequency the distance travelled by the monomer molecules from the dark to the bright fringes is smaller. During a given exposure time a larger number of monomer molecules will manage to reach the bright fringes at higher spatial frequency of recording than at lower spatial frequency. Thus a larger number of monomers will be polymerised at higher spatial frequency of recording and larger dimensional change (shrinkage) is expected.

- The increased shrinkage at higher spatial frequencies due to faster monomer diffusion times is also supported by the fact that at high spatial frequency there is almost no dependence on the intensity while at low spatial frequency there is definitely a dependence on the intensity.
- By taking account of the amount of polymerisation occurring in the photopolymer layers we can explain the shrinkage in layers having different thicknesses, recorded with the same intensity and exposure time, by the fact that for thicker layers the polymerisation process and hence the shrinkage is not completed on the assumption that the shrinkage occurring is proportional to the extent of polymerisation. In the case of slanted gratings the modulation of refractive index and the shift in Bragg curve resulting from the photopolymer shrinkage will continuously increase until the polymerisation is finished.
- The same refractive index modulation is obtained for layers of thickness 30, 60 and 120 μm suggesting the same extent of monomer molecule conversion and polymer density change per unit volume and thus the same absolute shrinkage.

4.7 Study of the influence of zeolite nanoparticles on photopolymer shrinkage

An acrylamide based photopolymer doped with pure silica MFI-type zeolite (silicalite-1) [4] and BETA nanoparticles has been characterised for holographic recording purposes. The concentrations of the nanoparticles in the photopolymer layers were 1, 2.5, 5 and 7.5 wt. %. Transmission diffraction gratings were recorded in nanoparticle doped photopolymer films having thickness 40 ± 3μm in order to avoid overmodulation effects. The diffraction efficiencies and the final slant angles were obtained and the shrinkage caused by holographic recording was

calculated. The shrinkage of the material was evaluated for recording intensity of 5 mW/cm^2 over a range of slant angles.

4.7.1 Experimental technique

4.7.1.1 Sample preparation

The photopolymer solution was prepared as in section 4.2.1. Instead of 17.5 ml polyvinyl alcohol (10% wt) stock solution, 9 ml (20% wt) stock solution was used. To 1 ml of photopolymer solution silicalite-1 (Si MFI) nanoparticles were added as colloidal aqueous suspensions in volumes of 0.18, 0.46, 0.94 and 1.44 ml containing 1.5 wt.% of nanoparticles. Similarly 0.067, 0.169, 0.347 and 0.531 ml containing 4.9 wt.% zeolite BETA nanoparticles were added to 1ml of photopolymer solution. More water was added to equalize the solid substance concentrations in all stock solutions and to obtain the same thickness of the final nanocomposite layers. Finally, 1.1 ml of MFI nanocomposite and 0.918 ml of BETA nanocomposite was spread on 25 mm x 120 mm glass plates, and allowed to dry for 24 h. After drying, the samples were 40 ± 3 μm thick. The final concentrations of zeolite nanoparticles were 1, 2.5, 5 and 7.5 wt.%.

4.7.1.2 Influence of zeolite nanoparticles on photopolymer refractive index

The dynamic light scattering (DLS) curve of silicalite-1 nanoparticles prior to mixing with the photopolymer is shown in Fig. 4.9. As can be seen the hydrodynamic diameter of the crystals is about 30 nm. The DLS curve is very narrow, confirming monomodal particle size distribution of the zeolite nanocrystals. A TEM image of the crystalline silicalite-1 nanoparticles is shown in the inset in Fig. 4.9.

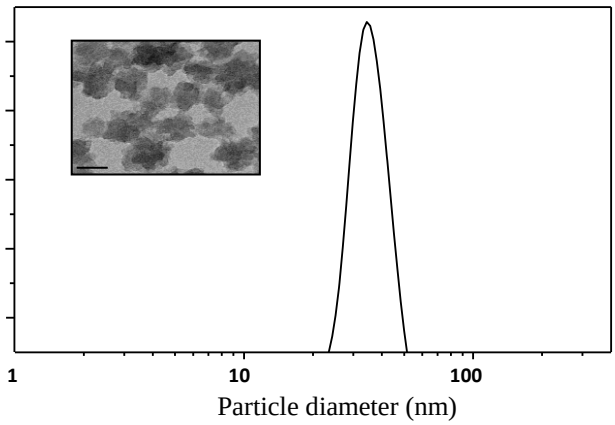

Figure 4.9. Dynamic light scattering curve of silicalite-1 nanocrystals in water suspension prior mixing with the photopolymer; the inset shows a TEM picture of the nanocrystalline particles (d=30 nm).

The incorporation of zeolite nanoparticles in photopolymer layer introduces refractive index change and the refractive index used to determine the Bragg angle inside photopolymer layers with different nanoparticle concentrations is recalculated from the initial investigations [6, 7] and is shown in Fig. 4.10

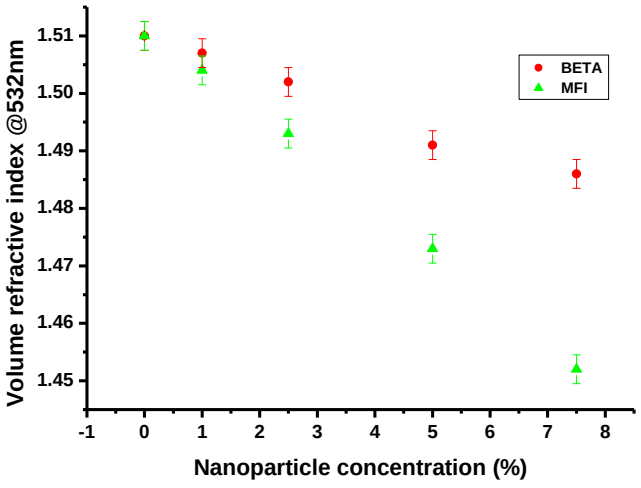

Figure 4.10. Refractive index of nanocomposite films versus nanoparticle concentration

4.7.2 Study of the influence of Si-MFI nanoparticles on photopolymer films

Figure 4.11(a) shows the growth curves of 10° slanted gratings with different MFI concentrations. Figure 4.11(b) shows the angular selectivity curves for these samples. From the graphs we determined the shift of the Bragg curve due to shrinkage and we noticed that the shift decreases with increasing concentration of zeolites. The same dependence was observed for all other slant angles (+10°, -5°,-10°). The change in the average refractive index of the layers due to the inclusion of the nanoparticles must be taken into account when the analysis of the Bragg selectivity curves of slanted gratings is carried out. The shift in the Bragg curve in the undoped case is 0.094° whereas for Si-MFI doped layers having concentrations 1 wt.%, 2.5 wt.%, 5 wt.%, 7.5 wt.% the shifts are 0.063° , 0.058°, 0.051°, 0.049° respectively.

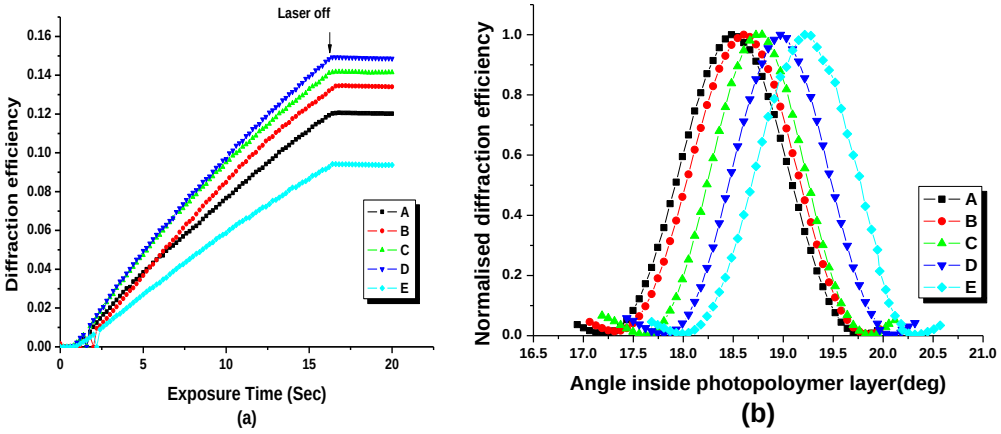

Figure 4.11. Diffraction efficiency growth (a) and angular selectivity curves (b) for gratings recorded at slant angle +5° A- Undoped, B- 1 wt.%, , C-2.5 wt.%, D-5 wt.%, E- 7.5 wt.% Shifts of peak positions in (b) are A-0.094°; B-0.063° ; C- 0.058°; D- 0.051°; E-0.049°.

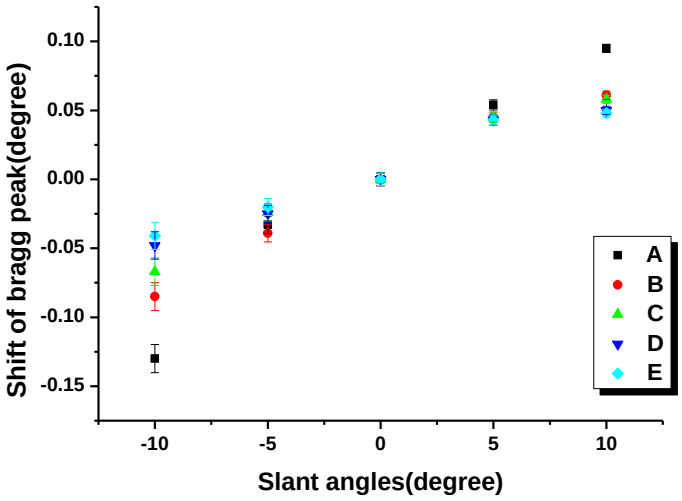

Figure 4.12. Bragg peak shift with respect to the initial slant angles for gratings recorded at A-Undoped ; 1% , C- 2.5% ; D-5% ; E-7.5%.wt Si-MFI doped layers

We determined the shrinkage due to holographic recording using Equation 3.23 in Section 3.3.

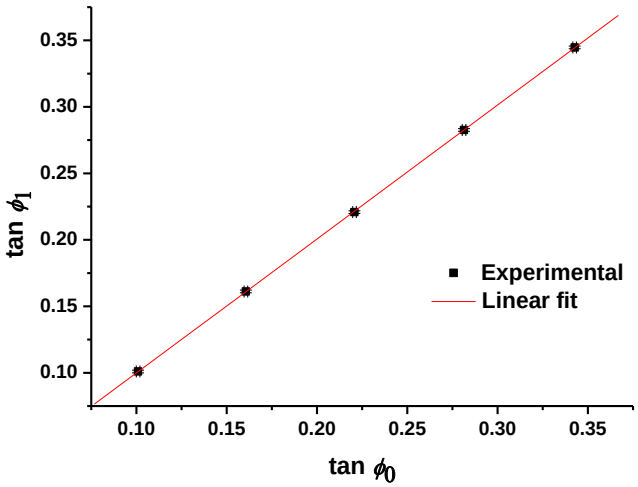

Figure 4.13. Dependence of the final slant angle on the initial slant angle for gratings recorded with 5%.wt Si-MFI doped layer having shrinkage (0.75±0.004)%.

Figure. 4.13 shows the tangent of final slant angle versus tangent of initial slant angle for gratings recorded with 5 wt.% zeolite at 1000 lines/mm and the slope of the graph again gives the percentage shrinkage of the material. The percentage shrinkage evaluated from the curve is 0.75 %. Similarly the shrinkage can be calculated for different zeolite concentrations and for the undoped layers. Results are shown in Fig.4.14 which shows that shrinkage decrease progressively with increasing concentration of nanoparticles.

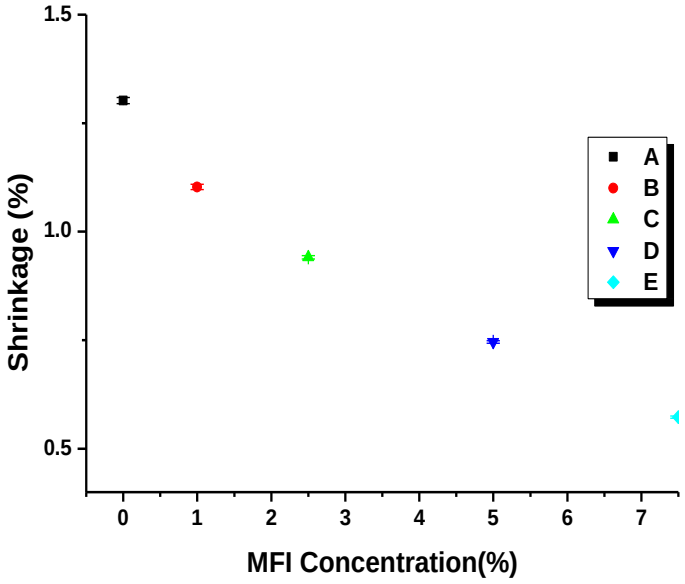

Figure 4.14. Dependence of shrinkage on nanoparticle concentration, A-Undoped; B- 1 wt.%, C- 2.5 wt.% ; D-5 wt.% ; E-7.5 wt. %. Si-MFI doped layer

4.7.3 Study of the influence of sample thickness on photopolymer nanocomposite

Recordings with 2.5 wt.% silicalite-1 nanoparticles in layers with different thicknesses were made. We choose 2.5 wt.% nanoparticles to reduce scattering

effects caused by the incorporation of nanoparticles. Gratings with slant angle of 5° were recorded in layers of thickness 45, 85 and 125 μm at a recording intensity of 10 $mWcm^{-2}$ and exposure time of 8 sec. Figure 4.15(a) shows the diffraction efficiency growth curves and Figure 4.15(b) shows the corresponding Bragg curves. Higher diffraction efficiency was measured in the thicker layers but the percentage shrinkage was the same for all thicknesses. The percentage shrinkage was 0.79, 0.78, and 0.8% for layers with thickness of 45, 85 and 125 μm, respectively. The absolute shrinkages, shown in Fig.4.16 (b), were 0.35μm, 0.66 μm and 1 μm.

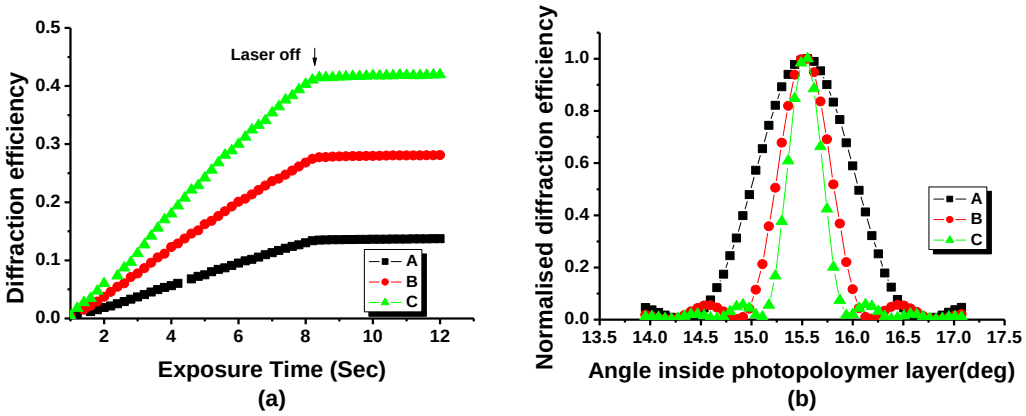

Figure 4.15. (a) Diffraction efficiency growth and (b) angular selectivity curves for gratings with 5° slant angle recorded in layers having thickness of: A- 45 μm, B- 85 μm, C- 125 μm. The corresponding positions of the Bragg peak in (b) are A -16.114°, B- 16.111°, and C- 16.116°

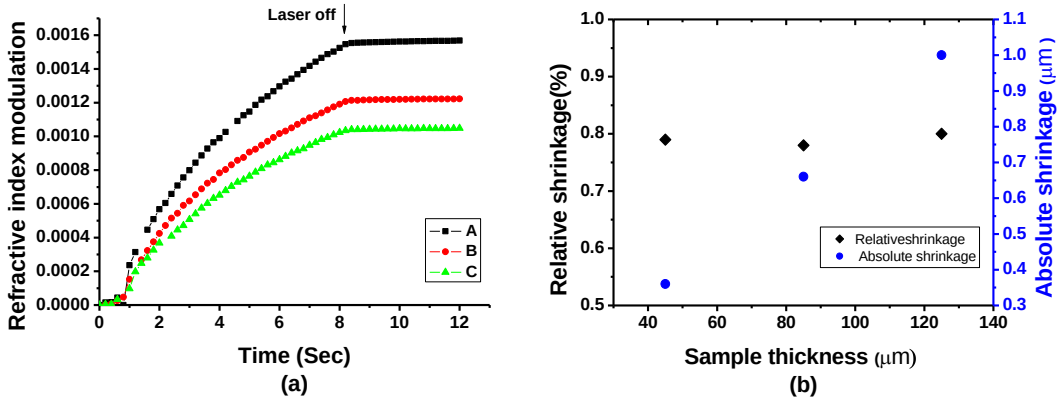

Figure 4.16. (a) Dependence of refractive index modulation on exposure time and (b) shrinkage of layers with thickness of A-45 µm , B-85 µm , and C-125 µm

The dependence of the percentage shrinkage of the nanoparticle doped layers on their thickness differs from that observed previously in undoped layers [3], in which the percentage shrinkage decreased by a factor of three as layer thickness was increased from 30 to 120 µm. The refractive index modulation was calculated from the diffraction efficiency data and found to decrease with thickness (Fig.4.16 (a)). A similar decrease in refractive index modulation with thickness was observed in undoped layers [3], but the effect was pronounced only above 60 µm layer thickness. This effect is probably due to attenuation of the recording beam intensity within the layer and, although the diffraction efficiency of gratings in thicker layers is higher, their average refractive index modulation is lower. So we investigate the effect of dye concentration on the refractive index modulation induced during holographic recording in nanocomposites.

4.7.4 Study of the influence of dye concentration on photopolymer nanocomposite

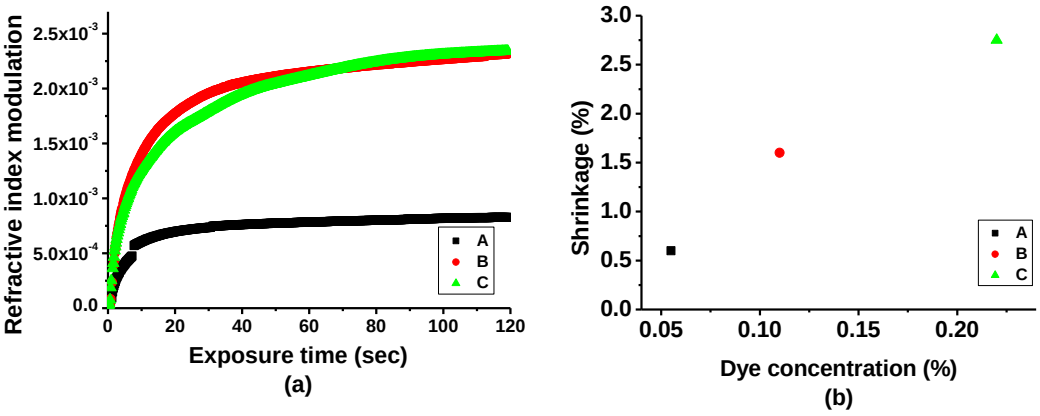

Figure 4.17. Dependence of refractive index modulation on dye concentration (a) and percentage shrinkage dependence on dye concentrations (b) for dye concentrations A-0.055 %.wt, B-0.11 %.wt , C-0.22 %.wt

Results from experiments with layers with 2.5% MFI concentration and dye concentrations of 0.055 %, 0.11 % (the optimized concentration used in all previous experiments) and 0.22 % are shown in Fig.4.17. Exposure was at an intensity of 5 $mWcm^{-2}$ for 120 s. The refractive index modulation obtained (Fig. 4.17(a)) is significantly lower in layers with dye concentration of 0.055 % and a dye concentration of 0.22 % doesn't lead to any obvious improvement in the refractive index modulation. At the same time the shrinkage is seen to increase with dye concentration. The reason for this is that the number of monomer molecules that are polymerized is greater and the excited state quenching can happen if the dye concentration is higher. Also due to high rate of generation of free radicals due to the high concentration of dye molecules the rate of termination will also be faster.

4.7.5 Study of influence of zeolite nanoparticles on photopolymer shrinkage at long exposure times

We also have studied the influence of higher exposure times in Si-MFI and BETA doped layers. Recordings were made at 1000 lines /mm with an exposure intensity of 5 $mWcm^{-2}$ for 80s. Figure 4.18(a) shows the growth curves of 10° slanted gratings recorded with different Si-MFI concentrations. Figure 4.18(b) shows the angular selectivity curves for these gratings. The shift in the position of the peak of the Bragg curve at all slant angles (+10°,+5°, -5°,-10°) for the undoped and for layers doped with Si-MFI at concentrations of 1%, 2.5%, 5%, 7.5% is shown in Fig.4.19.

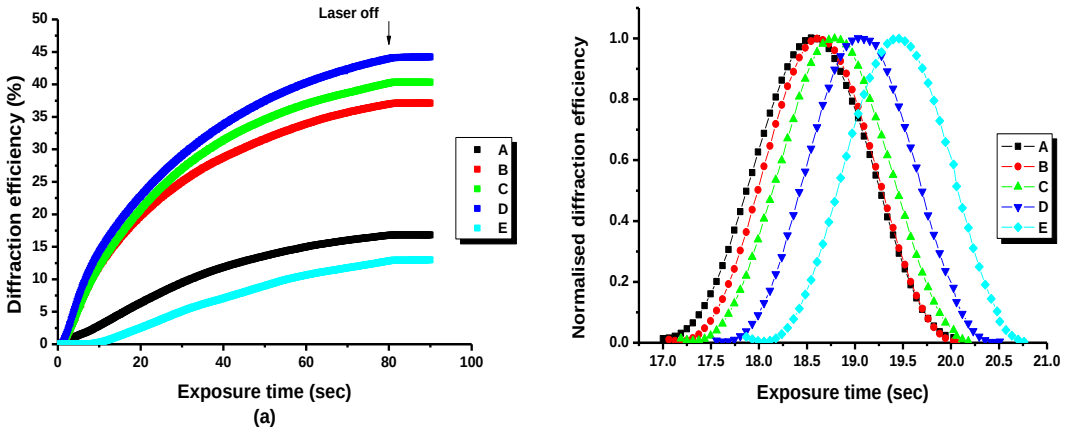

Figure 4.18. Diffraction efficiency growth (a) and angular selectivity curves (b) for gratings recorded at slant angle +10° A- Undoped, B- 1 wt.%, , C-2.5 wt.%, D-5 wt.%, E- 7.5wt.% Si-MFI doped layers, Peak positions in (b) are A-18.564°; B-18.586° ; C- 18.75°; D- 19.032°; E-19.286°

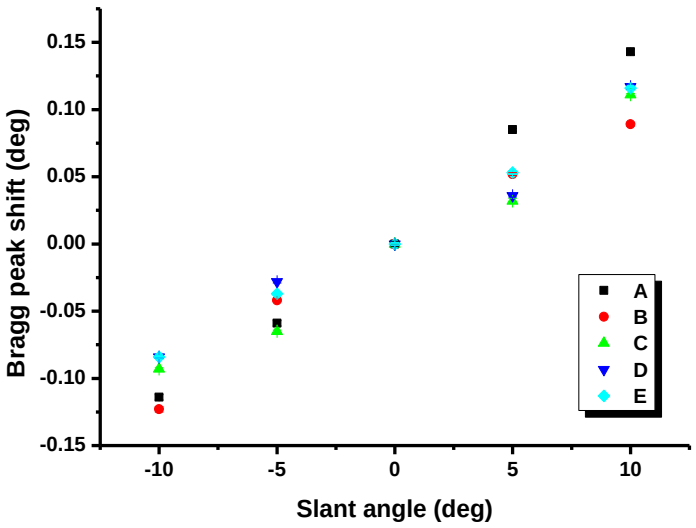

Figure 4.19. Bragg peak shift with respect to the initial slant angle for gratings recorded at A-Undoped ; B-1 wt.% , C- 2.5wt.% ; D-5 wt. % ; E-7.5 wt.%.wt Si-MFI doped layers

Similarly, Figure 4.20(a) shows the growth curves of 10° slanted gratings recorded with different BETA concentrations. Figure 4.20(b) shows the angular selectivity curves for these samples. The shift in the position of the peak of the Bragg curve at all slant angles (+10°,+5°, -5°,-10°) in the undoped and layers doped with BETA at concentrations of 1 wt. %, 2.5 wt.%, 5 wt.%, 7.5 wt.% is shown in Fig.4.21

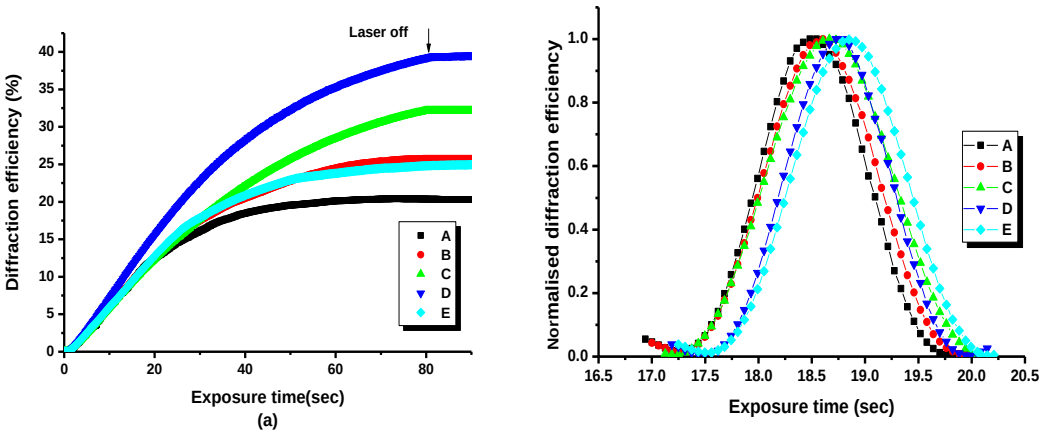

Figure 4.20. Diffraction efficiency growth (a) and angular selectivity curves (b) for gratings recorded at slant angle +10° A- Undoped,, B- 1 wt.%, , C-2.5 wt.%, D-5 wt.%, E- 7.5 wt.% BETA doped layers, Peak positions in (b) are A-18.525°; B-18.58° ; C- 18.615°; D- 18.672°; E-18.836°.

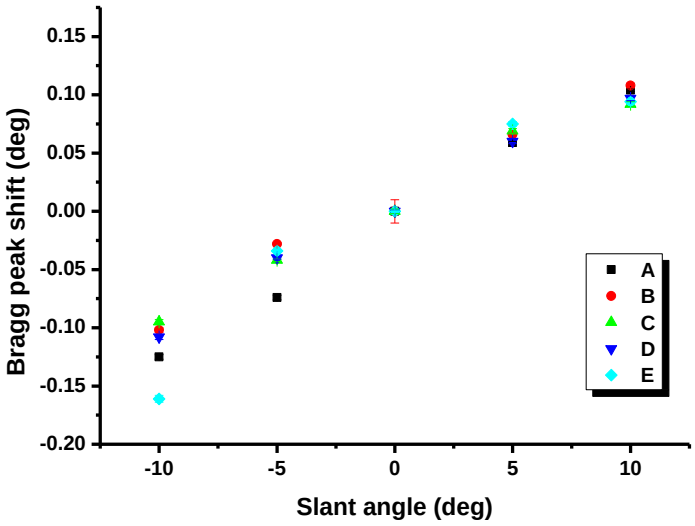

Figure 4.21. Bragg peak shift with respect to the initial slant angles for gratings recorded at A-Undoped ; B- 1 wt.% , C- 2.5 wt.% ; D-5 wt.% ; E-7.5 wt.%.wt BEA doped layers

Shrinkage versus zeolite concentration is plotted in Fig.4.22.

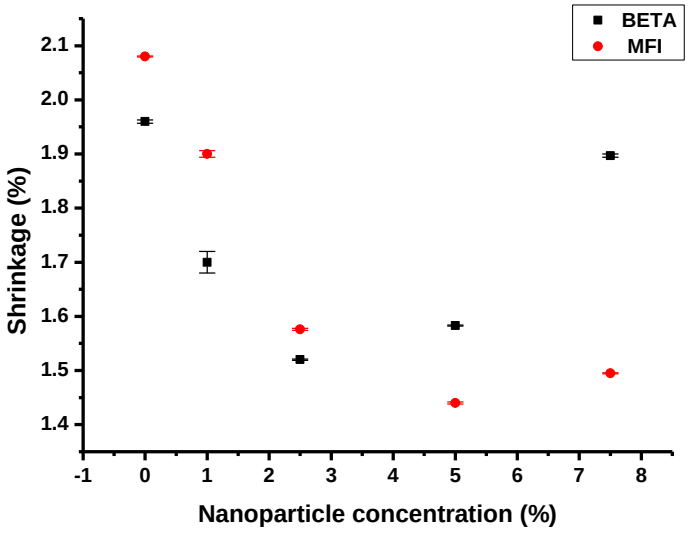

Figure 4.22. Dependence of shrinkage on nanoparticle concentration

The incorporation of nanoparticles with high concentration in photopolymer layers will result in increased scattering and increased polymerisation in the dark fringe areas. Thus the illumination pattern becomes similar to single beam exposure and homogeneous polymerisation of layers which leads to higher shrinkage.

4.7.6 Discussion and conclusions

- We have obtained lower shrinkage and increased diffraction efficiencies by doping with increasing concentrations of nanoparticles. The best results (highest diffraction efficiency and lowest shrinkage) were observed with 5 wt.% doping with Si-MFI. Increasing the concentration further will lower the diffraction efficiency and lead to increased shrinkage because of scattering effects.

- The origin of the increase in diffraction efficiency in nanoparticle doped photopolymers was attributed to a “counter diffusion” of nanoparticles during holographic exposure resulting in a spatially periodic distribution of nanoparticles [5]. The redistribution of zeolite nanoparticles in photopolymer layers were studied before [8]. The term counter diffusion means that while monomers diffuse into a “bright region” driven by a concentration gradient, the nanoparticles may migrate into a “dark region” during the holographic exposure.
- Shrinkage is reduced up to one half with increasing concentration of zeolite nanoparticles compared to undoped layers.
- Recordings made on layers of different thicknesses doped with 2.5 wt.% nanopaticles, shows no change in the shrinkage. The dependence of the percentage shrinkage of the nanoparticle doped layers on their thickness differs from that observed previously in undoped layers [3], in which the percentage shrinkage decreased by a factor of three as layer thickness was increased from 30 to 120 μm.
- The refractive index modulation was calculated from the diffraction efficiency data for 2.5 wt.% nanoparticle doping with different thickness and the refractive index modulation was found to decrease with thickness. A similar decrease in refractive index modulation with thickness was observed in undoped layers [3]. This effect is probably due to attenuation of the recording beam intensity within the layer and, although the diffraction efficiency of gratings in thicker layers is higher, their average refractive index modulation is lower.

- Experiments with layers doped with 2.5% Si-MFI concentration and different dye concentrations show that the refractive index modulation obtained is significantly lower in layers with lower dye concentration (0.055%.wt) and high dye concentration (0.22%.wt) doesn't lead to any obvious improvement in the refractive index modulation. At the same time the shrinkage is seen to increase with dye concentration. This can be related to the fact that at higher dye concentration the rate at which free radicals generated will be higher and hence the more monomer molecules will polymerise and the rate of conversion will be faster resulting in increased shrinkage.
- Recordings in Si- MFI and BETA doped layers with increased exposure time show lower shrinkage and increased diffraction efficiency with increasing concentrations of nanoparticles. The best results (increased diffraction efficiency and low shrinkage) are obtained in layers doped with 5 wt.% MFI and 2.5 wt.% BETA nanoparticles. Comparison with previous studies [4] made on Si-MFI, shows that shrinkage is predominant during the initial stage of exposure.

References

[1] S.Martin, C.A.Feely, and V.Toal, "Holographic recording characteristics of an acrylamide-based photopolymer," Appl.Opt. 36, 5757–5768 (1997)

[2] M.Moothanchery, I.Naydenova and V.Toal, "Studies of shrinkage as a result of holographic recording in acrylamide based photopolymer film," App.Physics A , 899-902, (2011)

[3] M.Moothanchery, I.Naydenova and V.Toal, “Study of shrinkage caused by holographic grating formation in acrylamide based photopolymer film,” Optics Express. 19, 13395-13404 (2011)

[4] M.Moothanchery, I.Naydenova, S.Mintova and V.Toal, “Si-MFI zeolite nanoparticle doped acrylamide photopolymer with reduced shrinkage,” Optics Express .19, 25786-25791 (2011).

[5] W.S.Kim, Y.C.Jeong, and J.K.Parka, “Organic-inorganic hybrid photopolymer with reduced volume shrinkage,” Applied Physics Letters 87, 012106 (2005)

[6] T.Babeva, R.Todorov, S.Mintova, T.Yovcheva, I.Naydenova and V.Toal, “Optical properties of silica MFI doped acrylamide-based photopolymer,” J. Opt. A: Pure Appl. Opt. 11 (2009)

[7] I.Naydenova, E.Leite, T.Babeva, N.Pandey, T.Baron, T.Yovcheva, S.Sainov , S.Martin, S.Mintova and V.Toal, “Optical properties of photopolymerizable nanocomposites containing nanosized molecular sieves,” J. Opt. 13 (2011)

[8] A.M.Ostrowski, I.Naydenova and V.Toal, “Light-induced redistribution of Si-MFI zeolite nanoparticles in acrylamide-based photopolymer holographic gratings,” J. Opt. A: Pure Appl. Opt. 11 (2009)

CHAPTER 5

HOLOGRAPHIC INTERFEROMETRY

5.1 Introduction to Interferometry

Optical interferometers are widely used in Science and Engineering for measurements of small displacements, refractive index changes and surface irregularities with high accuracy (of the order of the wavelength of the light source). The basic principle of interferometry is the superposition of light waves in space. Two waves having the same phase will interfere and will reinforce each other (constructive interference), whereas two waves with opposite phase will interfere and will cancel each other (destructive interference) assuming they are of the same amplitude. The Michelson interferometer [1], invented by Albert Michelson, is the best known type of interferometer which uses a single beam splitter for splitting and recombining light beams.

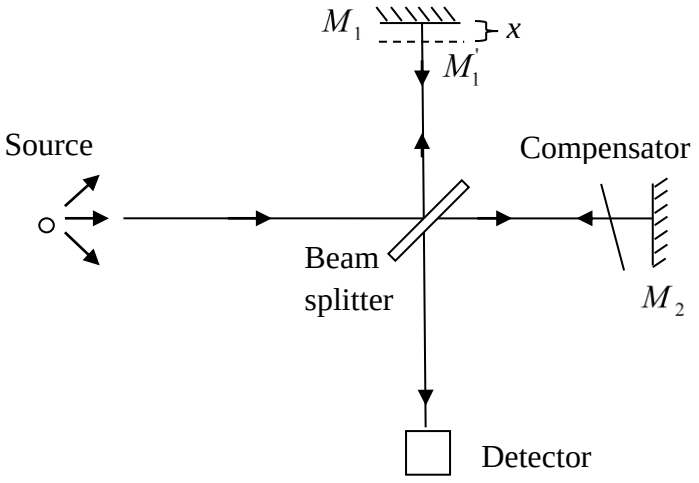

Figure 5.1. Michelson Interferometer

The basic configuration of a Michelson interferometer is as shown in Fig.6.1. Light from an extended light source is split in to two equal intensity beams which are reflected by means of mirrors M_1 and M_2 and interfere with each other at the beam splitter and the recombined wave is directed to the detector.

In order to make the optical path traversed by both the beams through glass the same, a compensator plate is used. If the mirror M_1 is moved by a distance x an interference pattern of dark and bright fringes can be observed. The intensity of the interference pattern at the detector is

$$I(X) = 2I[1+\cos(\frac{4\pi x}{\lambda})] \qquad (5.1)$$

The Michelson interferometer is used for measuring deformation and refractive index change of test objects. It is also used for measuring wavelength and coherence of optical beams.

Other interferometers are distinguished mainly by the number of interfering beams and the method used to split the beams. Different types of classical interferometers include the Mach-Zehnder interferometer , the Fizeau interferometer and the Fabry-Perot interferometer [2,3].

5.2 Holographic interferometry

Holographic interferometry is a non-contact, non-destructive evaluation technique [4] introduced in 1965 by Powell and Stetson [5]. Any movement of the optics during holographic recording will result in the formation of patterns of dark and bright fringes on the image reconstructed from the holograms. These fringes are

formed as a result of interference of scattered wavefronts from surfaces placed at slight different positions in space [6]. These fringes give information regarding any motion and this led to the development of holographic interferometry.

5.2.1 Holographic interferometry techniques

5.2.1.1 Double exposure technique

Double exposure technique is a convenient method to measure surface displacement, mainly out of plane displacement. Experimentally in double exposure technique [7] two or more holograms of the object which is under observation will be made on a photosensitive medium. The first hologram is recorded with the object in the undisplaced position and the second one with the object in the displaced position. These two holograms are recorded on the same photosensitive material and during reconstruction the hologram produces two wavefronts, one corresponding to the undisplaced position and the other correspond to the displaced position. These two wavefronts superimpose to produce interference fringes.

Let U_{O1}, U_{O2} be the complex amplitudes of the object beam before and after displacement which can be expressed as

$$U_{O1} = A_O e^{i\phi_{O1}(x,y)} \tag{5.2}$$

$$U_{O2} = A_O e^{i\phi_{O2}(x,y)} \tag{5.3}$$

ϕ_{O1} and ϕ_{O2} are the phases of the object beams before and after displacement

These two object beams will interfere with the reference beam U_R

$$U_R = A_R e^{i\phi_R(x,y)} \tag{5.4}$$

ϕ_R is the phase of the reference beam

The resultant beam incident on the photosensitive plate before and after displacement will be

$$U_B = U_{O1} + U_R = A_O e^{i\phi_{O1}(x,y)} + A_R e^{i\phi_R(x,y)} \tag{5.5}$$

$$U_A = U_{O2} + U_R = A_O e^{i\phi_{O2}(x,y)} + A_R e^{i\phi_R(x,y)} \tag{5.6}$$

Assume the exposure time for both these to be the same and set to unity for simplicity. The recorded light intensity on the hologram is given by

$$\begin{aligned} I &= U_B U_B^{*} + U_A U_A^{*} \\ &= 2(A^2{}_O + A^2{}_R) + A_O A_R e^{i(\phi_{O1}-\phi_R)}(1+e^{i(\phi_{O2}-\phi_R)}) \\ &\quad + A_O A_R e^{-i(\phi_{O1}-\phi_R)}(1+e^{-i(\phi_{O2}-\phi_R)}) \end{aligned} \tag{5.7}$$

After developing properly, the hologram is illuminated by the reference beam. The transmittance of the hologram can be defined as the ratio of the transmitted light amplitude to the incident light amplitude. The transmittance is assumed to be a linear function of recording intensity. For simplicity the constant of proportionality is set to unity.

The amplitude of the reference beam transmitted through the hologram is given by

$$U_T = U_R T = U_R I \tag{5.8}$$

Inserting equation (5.4) and equation (5.7) in equation (5.8) gives

$$\begin{aligned} U_T &= 2A_R(A^2{}_O + A^2{}_R)e^{i\phi_R} + A_O A^2{}_R e^{i\phi_{O1}}(1+e^{i(\phi_{O2}-\phi_{O1})}) \\ &\quad + A_O A^2{}_R e^{-i(\phi_{O1}-\phi_R)}(1+e^{-i(\phi_{O2}-\phi_R)}) \\ &= U_1 + U_2 + U_3 \end{aligned} \tag{5.9}$$

where U_1 is the undiffracted beam, U_2 is the image beam and U_3 be the conjugate image beam.

A small displacement will change the phase of the object beam.

Intensity distribution of the image beam is given by

$$\begin{aligned} I &= |U_2|^2 \\ &= 2A_O^2 A_R^4 [1+\cos(\phi_{O2}-\phi_{O1})] \end{aligned} \tag{5.10}$$

where $(\phi_{O2}-\phi_{O1})$ is the additional path length introduced due to object displacement.

A bright fringe is produced when the phase difference is $2n\pi$, where n=0,1,2…

A dark fringe is produced when the phase difference is $(2n+1)\pi$, where n=0,1,2..

Change in optical path length δ is related to the phase difference Δ by

$$\Delta = (\phi_{O2}-\phi_{O1}) = \frac{2\pi}{\lambda}\delta \tag{5.11}$$

λ is the wavelength of the laser.

The vector displacement (*L*) at a point on the surface of the object can be determined using holographic interferometry, since the vector displacement is proportional to the phase difference between two interfering beams [9]. The phase difference Δ in Fig.5.2 is given by

$$\begin{aligned} \Delta &= 2\pi/\lambda \left(\hat{k}_2 - \hat{k}_1\right) * L \\ &= K * L \end{aligned} \tag{5.12}$$

Where $\hat{k}_1$ and $\hat{k}_2$ are unit vectors in the direction of illumination and observation. *K* is known as the sensitivity vector [10, 11].

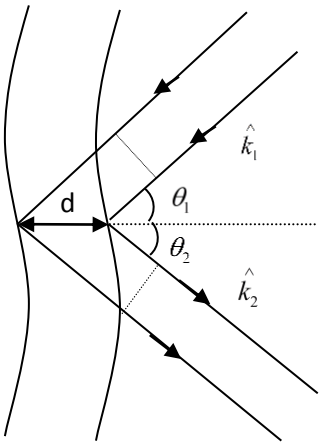

Figure 5.2. Optical path difference diagram

The change in optical path length δ of the beam due to change in the position *d* of the surface with respect to angles of illumination and observation is

$$\delta = d(\cos\theta_1 + \cos\theta_2) \tag{5.13}$$

where θ_1 and θ_2 are the angle of illumination and observation respectively. The optical path length can also be expressed in terms of wavelength λ

$$\Delta = \frac{2\pi}{\lambda} d(\cos\theta_1 + \cos\theta_2) \tag{5.14}$$

Application of this technique includes study of engineering structures [8] and detection of detached regions of ancient paintings [12].

5.2.1.2 Live fringe / Real time technique

In live fringe technique [7] the hologram of an object in the undisplaced position is recorded on a photosensitive plate. The plate is developed and is replaced exactly in its original position. The plate is now illuminated by both object and reference beam and any displacement in the object will change the path length of the object

beam so that an interference fringe pattern can be observed. The interference fringe pattern changes with change in the object displacement.

Let U_{O1} be the complex amplitude of the object beam from the hologram when the object is at rest (undisplaced state) and U_{O2} be the complex amplitude of the object beam from the hologram when the object is in the displaced or deformed state , as in equations (5.2) and (5.3). Let U_R be the complex amplitude of the reference beam as in equation (5.4)

The intensity incident on a photographic plate before displacement is as in equation (5.5)

and the resultant intensity of the undisplaced object will be

$$\begin{aligned} I &= U_B U_B^* \\ &= A^2{}_O + A^2{}_R + A_O A_R [e^{i(\phi_{O1}-\phi_R)} + e^{-i(\phi_{O1}-\phi_R)}] \end{aligned} \tag{5.15}$$

The plate is now placed back exactly in its original position and is been illuminated again by the object and reference beam. When the object is displaced the transmitted intensity through the plate can be expressed as

$$\begin{aligned} U_T &= (U_{O2} + U_R) I \\ &= U_1 + U_2 + U_3 \end{aligned} \tag{5.16}$$

U_2 is related to the object beam before and after displacement and is expressed as

$$U_2 = A_O \left[(A_O^2 + A_R^2) e^{i\phi_{O2}} + A_R^2 e^{i\phi_{O1}} \right] \tag{5.17}$$

The intensity of U_2 can be expressed as

$$\begin{aligned} I_2 &= |U_2|^2 \\ &= A_O^2 \left[(A_O^2 + A_R^2)^2 + A_R^4 + 2A_R^2 (A_O^2 + A_R^2) \cos(\phi_{O2} - \phi_{O1}) \right] \end{aligned} \tag{5.18}$$

When $A_R^2 \gg A_O^2$ equation above reduces to

$$I_R = 2A_O^2 A_R^4 \left[1 + \cos\Delta\right] \tag{5.19}$$

The formation of dark and bright fringes is similar to that in the case of the double exposure technique. The experimental difficulty regarding real time technique is in replacing the developed plate exactly in its original position.

5.2.1.3 Time average technique

In this technique the hologram of the object is recorded when it is in vibratory motion [13].

Considering a point on the object vibrating sinusoidally with angular frequency ω and time *t* according to the expression $A\cos\omega t$.

where *A* - amplitude of oscillation.

The phase change of light scattered from the particular point is given by

$$\Delta = \frac{2\pi A\cos\omega t}{\lambda}(\cos\theta_i + \cos\theta_r) \tag{5.20}$$

θ_i and θ_r are the angles of incident and reflected lights with the direction of vibration.

Let *T* be the exposure time and U_{OT} and U_R be the complex amplitude of the object and reference beam at the hologram plane.

$$U_{OT} = A_O e^{i(\phi_o + \Delta)} = U_O e^{i\Delta} \tag{5.21}$$

U_O is the object wave for the stationary sample and Δ is as in equation (6.20)

The intensity of the transmitted light through the hologram at time *t* is given by

$$\begin{aligned} I(t) &= U_R U_R^* + U_{OT} U_{OT}^* + U_{OT} U_R^* + U_R U_{OT}^* \\ &= (A_O^2 + A_R^2) + U_R^* U_O e^{i\Delta} + U_R U_O^* e^{-i\Delta} \end{aligned} \tag{5.22}$$

In equation (5.22) the second term is important because it is associated with the image beam.

Considering average of the image term over a period [12]

$$\begin{aligned} I_{av} &= \frac{U_R^* U_O}{\tau} \int_0^{\tau} e^{i\phi} dt \\ &= \frac{U_R^* U_O}{2\pi} \int_0^{2\pi} e^{i(2\pi A/\lambda)(\cos\theta_i + \cos\theta_r)\cos\omega t} d(\omega t) \\ &= U_R^* U_O J_0 \left[\frac{2\pi A}{\lambda} (\cos\theta_i + \cos\theta_r) \right] \end{aligned} \tag{5.23}$$

where J_0 is the Bessel function of zeroth order of first kind.

After developing the plate the hologram is illuminated by the reference beam

Using equation (5.8) the real image beam is given by

$$U_2 = U_R I_{av} = U_R^2 U_O J_O \left[\frac{2\pi A}{\lambda} (\cos\theta_i + \cos\theta_r) \right] \tag{5.24}$$

The intensity of the reconstructed wavefront is

$$I_2 = U_2 U_2^* = I_0 J_0^2 \left[\frac{2\pi A}{\lambda} (\cos\theta_i + \cos\theta_r) \right] \tag{5.25}$$

I_0 is the intensity of the reconstructed wavefront when the object is stationary

If $\theta_i = \theta_r = 0$ equation (5.25) reduces to

$$I_2 = I_O J_0^2 \left[\frac{4\pi A}{\lambda} \right] \tag{5.26}$$

Areas with maximum brightness in the fringe pattern vibrate with zero amplitude and are called nodes of vibration. Whereas the areas vibrating with maximum amplitude are called antinodes of vibration.

The disadvantage of time averaged technique is that the phase information is lost during averaging of displacement over a cycle so time average technique cannot be used for scanning the full range of frequency especially in real time which is useful for detecting higher order modes and light intensity decreases with increasing vibrational amplitude therefore higher order fringes are not clearly visible. In order

to overcome this problem time averaged technique is often combined with double exposure or real time technique [13-16].

5.2.2 Sensitivities

Formation of holographic fringes is a result of the path length change of object beam. The displacement of the object can be measured by analysing the fringe pattern. These displacements can be resolved in two directions.

1) Along the direction normal to test object called out of plane displacement
2) Along the direction parallel to the test object surface called in-plane displacement

5.2.2.1 Out of plane sensitivity

In an out of plane sensitive holographic interferometric system the object surface is illuminated along the surface normal and is viewed along surface normal through the hologram during reconstruction as shown in figure 5.3.

$$n\lambda = 2d \qquad (5.27)$$

is the fringe equation for the out of plane sensitive technique [17]

where, n-number of fringes counted ; d -out of plane displacement ; λ -wavelength of laser.

Since it is not always practical to illuminate and view the object along the surface normal the object is viewed at an angle θ to the surface normal as shown in figure 5.3.

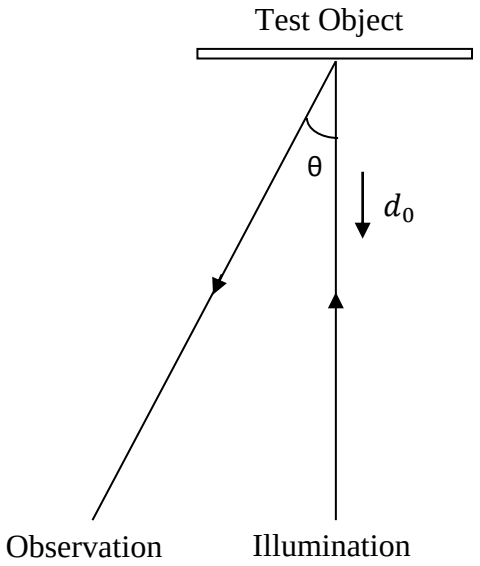

Figure 5.3. Out of plane sensitivity

The equation (5.27) thus can be modified as

$$n\lambda = d(1+\cos\theta) \tag{5.28}$$

where θ is the angle between illumination and observation

5.2.2.2 In-plane sensitivity

In case of an in-plane sensitive system the component displacement is parallel to the object surface i.e the component of displacement and the surface normal are perpendicular to each other. In-plane motion of the object can be measured by illumination and observation at an angle to the surface normal [18], and can be calculated from the equation

$$d_i = \frac{n\lambda}{\sin\alpha + \sin\beta} \tag{5.29}$$

α and β are the angles of illumination and observation to the surface normal

n is the number of fringes counted in the field of view. This technique is more suitable when the object is flat.

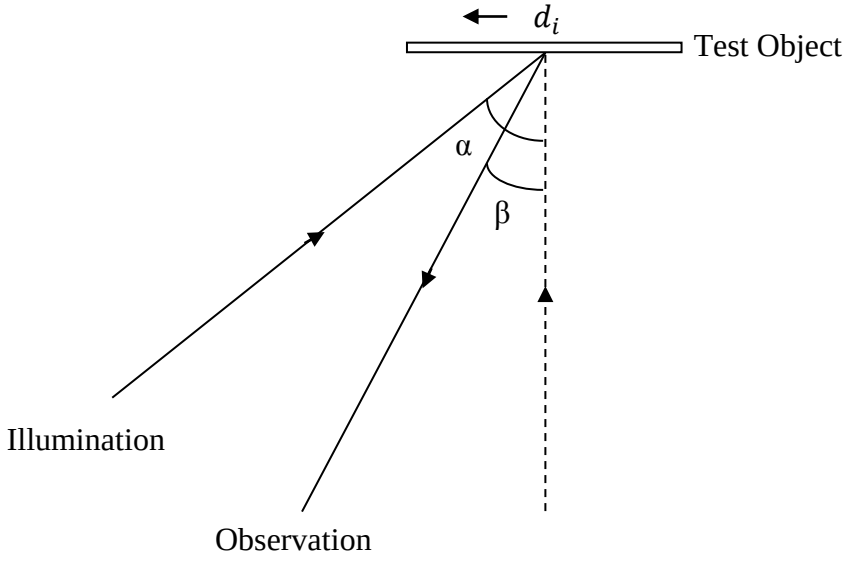

Figure 5.4. In-plane sensitivity

If the object is not flat some part of the object will be in shadow. Therefore in the case of non flat surfaces the test surface is illuminated at angles from two sides of the surface normal, so the fringes can be viewed along the surface normal.

with $\alpha = \beta$ equation (5.29) can be modified as

$$d_i = \frac{n\lambda}{2\sin\alpha} \tag{5.30}$$

where 2α is the angular separation between the two beams.

An In-plane sensitive interferometer has been used to determine the shrinkage in photopolymer films. Since the shrinkage in lateral direction is small. The system we developed is mainly sensitive to out-of-plane displacement only. The holographic interferometric technique we used and the results on shrinkage in photopolymer layers are discussed in the next chapter.

References

[1] F.G.Smith, T.A.King, "Optics and Photonics" John Wiley and Sons Ltd, England (2000)

[2] F.L.Pedrotti.S.J, L.S.Pedrotti, "Introduction to optics," 2nd edition,Prentise-Hall Inc. New Jersey(1993)

[3] J.R.Meyer-Arendt, "Introduction to classical and modern optics" 4th edition,Prentice-Hall Inc. New Jersey(1995)

[4] R.K Erf, "Holographic non-destructivetesting,"Academic Press. Inc, London, (1974)

[5] Powell & Stetson, "Interferometric vibration analysis by wavefront reconstruction." JOSA, 55, 1593-1598 (1965)

[6] R.Jones, C.Wykes, "Holographic and Speckle interferometry,"Cambridge University Press, Cambridge (1983)

[7] P.K.Rastogi, "Optical measurement technique and applications,"Artech House Inc, Norwood, USA (1997)

[8] R.C.Samson, "Holographic interferometry applications in experimental mechanics," Exp. Mech.10, 312-320(1970)

[9] P.Hariharan, B.F.Oreb, and N.Brown, "Real-time holographic interferometry: microcomputer system for the measurement of vector displacements," App. Opt. 22, 876-880 (1983)

[10] E.B.Aleksandrov and A.M.Bonch-Bruevich, "Investigation of surface strains by the hologram technique.," Sov. Phys.Tech.Phys. 12, 258-265 (1967).

[11] A.E.Ennos, "Measurement of in plane surface strain by hologram interferometry," J.Phys.E, 1, 731-734 (1968)

[12] S.Amadesi, F.Gori, R.Grella, G.Guattari, “Holographic method for painting diagnostics,”Appl.Opt.13, 2009-2013 (1974)

[13] K.A.Stenson, R.I.Powell, “Interferometric hologram evaluation and real time vibrational analysis of diffuse objects,” J.Opt. Soc. Am.55,1694-1695 (1965)

[14] C.M.Vest, “Holographic Interferometry,”John Wiley and Sons Ltd. New York (1974)

[15] H.Bjelkhagen, “Holographic time average vibration study of a structure dynamic model of an airplane fin,” Opt.Laser.Tech.6, 117-123(1974)

[16] K.Biedermann, N.E.Molin, “Combining hyper sensitisation and rapid insitu processing for time average observation in real time holographic interferometry,” J.Phys.E:Sci.Instrum, 3.669-680(1970)

[17] N.Abramson, “The making and evaluation of holograms,” Academic Press Inc, London (1981).

[18] A.E.Ennos, “Measurement of in-plane surface strain by hologram interferometry,” J.Phys.E: Sci.Instrum,1,731-734(1968)

CHAPTER 6

STUDY OF SHRINKAGE IN PHOTOPOLYMER FILMS BY HOLOGRAPHIC INTERFEROMTRY

6.1 Introduction

Real time holographic interferometry is used to determine minute changes in an object in real time by superimposing the image reconstructed from the hologram of the object, on the object itself while it is undergoing change. This chapter explains in detail the evaluation of shrinkage in acrylamide photopolymer layer during holographic recording using holographic interferometry. Using the interferometric technique, shrinkage in photopolymer layers can be determined by real-time capture of holographic interferograms during holographic recording [1]. The interferograms are produced by interference between a light wave reflected from the photopolymer layer surface, recorded in a separate hologram before photopolymerisation begins and a wave reflected from the photopolymer surface during the photopolymerisation process, which is insensitive to the hologram recording light. A Virtual instrument (VI) developed in LabVIEW (Version 8.2) was used to capture interferograms using a CMOS camera at regular intervals. One can determine the optical path change and hence the shrinkage from the captured fringe patterns. The important feature of holographic interferometry is that the fringes corresponding to the displacement of the object are produced in real time. The fringes produced in such a way will provide useful information regarding changes in the dimensions of the photopolymer.

6.2 Experimental Procedures

6.2.1 Sample preparation

A green sensitive photopolymer layer was prepared as described in section 4.7.2.1. Photopolymer solution volumes of 0.35, 0.55 and 0.75 ml were spread on 25 mm ×75 mm glass plates. The samples were allowed to dry for 24 hours. The sample thicknesses after drying were approximately 70, 110 and 150 μm respectively. A solution was also made up using similar amounts of acrylamide, N,N methylene-bis-acrylamide, triethanolamine, polyvinyl alcohol (10 %wt) and 4 ml of Methylene Blue dye. Of this solution 0.6 ml was spread on a 25 mm ×75 mm glass plate and allowed to dry for 24 hours. The layer thickness after drying was approximately 60 μm. These red sensitized layers were used to record holograms of the studied green sensitive layers.

6.2.2 Experimental set-up

The interferometer setup is as shown in Fig.6.1. Two separate independent sets of interfering beams, one at 633 nm and the other at 532 nm is been used. The 633nm arrangement is an interferometer designed to measure the changes occurring in the sample while a grating is recorded. Whereas the 532 nm arrangement produces the interference pattern required to record the grating. The 633 nm beam from a He-Ne Laser is spatially filtered, collimated and split into two beams using a beam splitter. One of the beams (object beam) is partially reflected from the green sensitive, Erythrosine B layer coated on a glass substrate with Matt black paint (to avoid back reflection from the glass substrate), whereas the other beam (reference beam) is partially reflected from a reflective paint coated glass plate and these beams are allowed to interfere so as to record a hologram in the red sensitive Methylene Blue

layer, of the surface of the Erythrosine B (Er. B) layer. The angles of illumination and observation of the object beam were 26.2^0 and 33.7^0 respectively. The combined intensity of the 633nm beams, reflected from the surface of the Er. B sensitized layer and from the glass plate was 0.5 mW cm^{-2}. After recording the hologram in the red sensitive layer for around 140 sec the beam from a Torus 532 nm laser, spatially filtered, and split into two beams using a beam splitter was switched on. These beams interfere with one another to record a holographic grating in the Erythrosine B sensitized layer, as a result of which the material shrinks. Due to shrinkage, a change occurs in the optical path of the beam reflected from the surface of the green sensitive layer and this change can be calculated from the number of fringes appearing as a result of the interference of the beam reflected from the green sensitive layer surface and the beam, reconstructed by the hologram recorded in the red sensitive layer. The appearance of fringes can be observed during the recording of the holographic grating in the green sensitive layer.

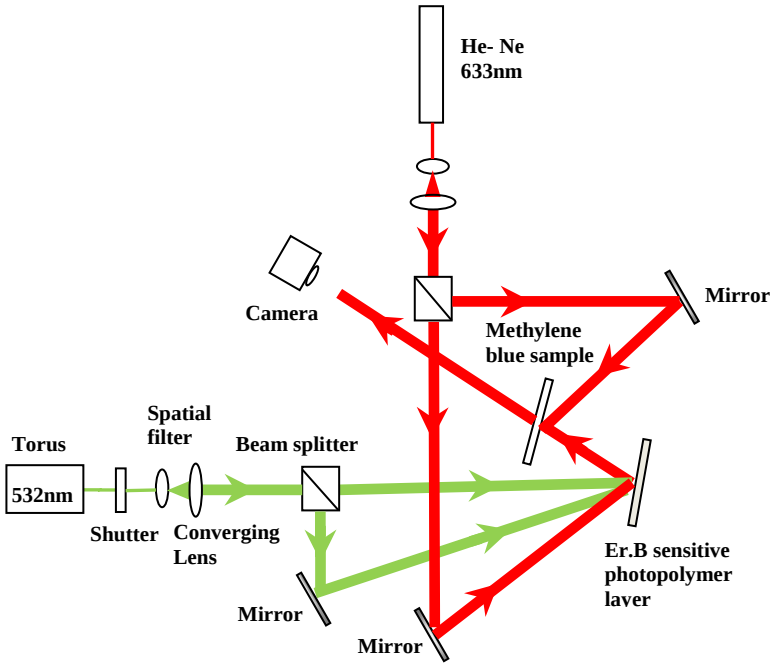

Figure 6.1. Holographic Interferometric setup

To determine photopolymer shrinkage we have used image subtraction. A CMOS camera with LabVIEW (Version 8.2) coded virtual instrument (VI) was used with a National Instruments IMAQ-1409 frame grabber card to capture images. The camera (AVT Guppy F-036B) was set in externally triggered mode and supplied by a D/A board with a digital pulse to initiate each image capture. The digital pulse frequency can be varied according to our requirement (1 to 25 Hz). A reference frame was subtracted from each incoming frame and the result, representing the change in the interferogram, displayed on the computer monitor in real time. The reference frame and other acquired frames were also stored in the computer. The movement of the interference fringes was captured as a live video which was processed using NI Vision Assistant software. The advantage of the subtraction method for the production of secondary fringes is that it can produce high contrast [2]. The reference frame was captured at the end of the recording of the hologram in the red sensitive layer, just before switching on the green laser.

6.3. Experimental Results

6.3.1 Influence of recording intensity and layer thickness on photopolymer shrinkage

A hologram of the front surface of the 70 μm thick Er. B layer was recorded in a 60 μm Methylene Blue sensitive layer using the interference of a 633 nm beam reflected from the front surface of the Er.B layer and a reference beam reflected from a glass plate. The reconstructed image from this hologram, Fig. 6.2(a), is used as the reference image for the static subtraction method. It was captured after the recording process at 633 nm was completed and the Methylene Blue sensitive photopolymer layer was fully polymerised. When the Er.B sample is not

undergoing polymerisation no fringes were produced by the subtraction of the reference image, Fig.6.2(b). The result of the subtraction was observed for 10-20 sec, confirming that the fringes, appearing at the next stage are produced only while recording a holographic grating. The interferogram shown in Fig.6.2(c) was obtained while the Er. B layer was undergoing polymerization using the 532 beam. Fig.6.2(c) clearly shows a dark fringe and the number of fringes appearing will vary depending on the exposure intensity and sample thickness.

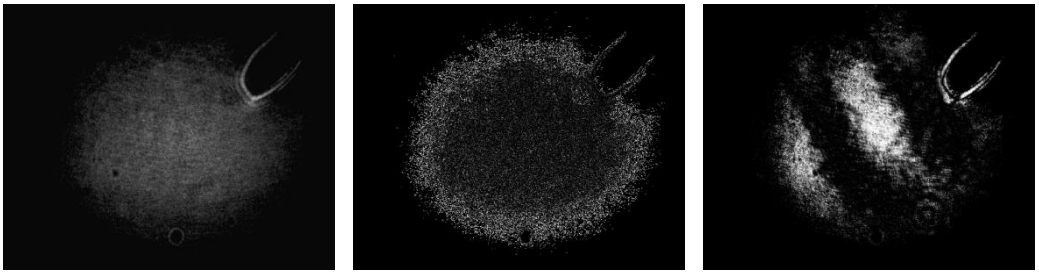

(a) **(b)** **(c)**

Figure 6.2. (a) Reference frame, produced by capturing the beam reconstructed by the hologram recorded in the red sensitive layer; (b) Result of subtraction of the reference frame from the current frame(before switching on the green laser); (c) Result of subtraction of the reference frame from the current frame (after switching on the green laser);

In order to determine the effect of shrinkage on photopolymer layer thickness and recording intensity, transmission diffraction gratings of spatial frequencies 1000 lines/mm were recorded in acrylamide based photopolymer film. Using holographic interferometry shrinkage occurring in the photopolymer is calculated using equation 5.32 in chapter 5. Figure.6.3(a), 6.3(b) and 6.3 (c) shows the relative shrinkage in 70, 110 and 160 μm thick layers for three different intensities 1, 5 and 10 mW/cm^2.

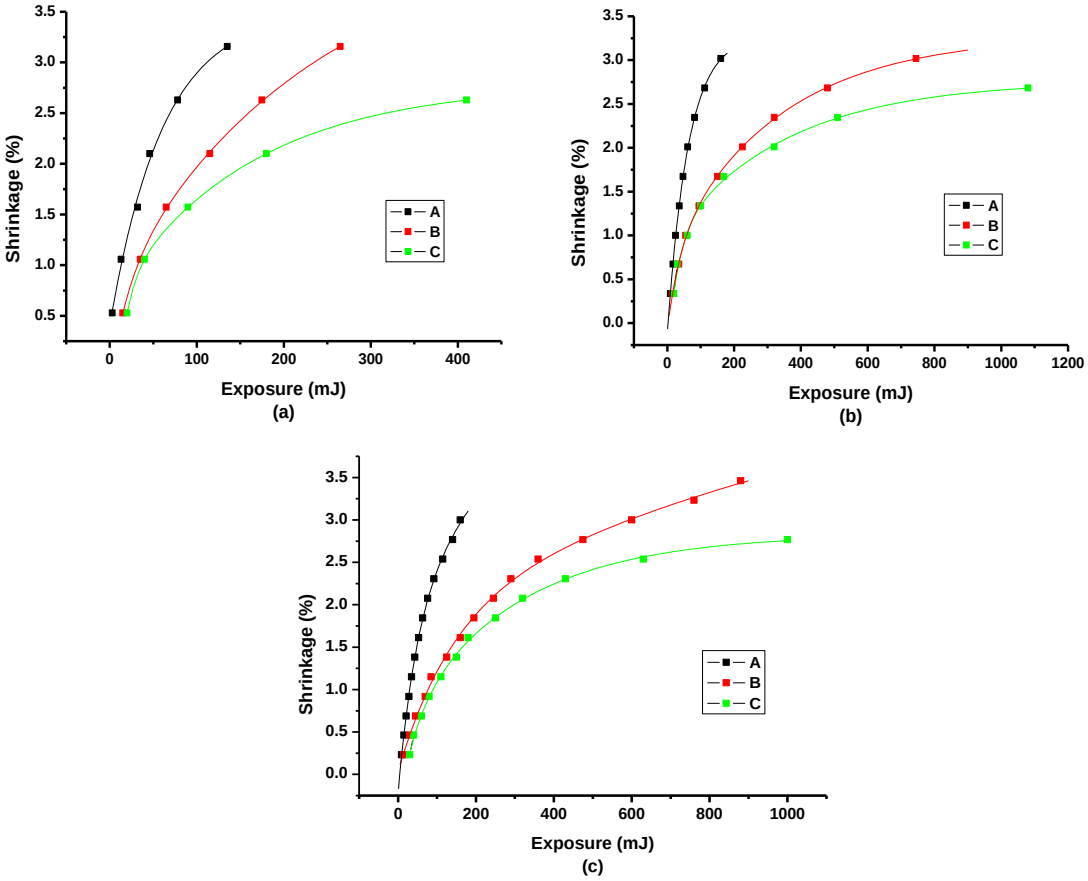

Figure 6.3. Percentage shrinkage with respect to exposure energy for spatial frequency 1000 lines/mm (a) 70 µm (b), 110 µm and (c) 160 µm thick gratings recorded at A-1 mW/cm^2; B- 5 mW/cm^2, C- 10 mW/cm^2

From Fig. 6.4 we can see that the rate of shrinkage with exposure decreases with increasing exposure. We have observed that most of the shrinkage occurs in the beginning of exposure. The same is true for all layer thicknesses.

Figure 6.4 shows the shrinkage versus exposure time for recording intensity 1 mW/cm^2

for three different layer thickness 70, 110 and 160 µm. From Fig.6.4(a) we can see that the absolute shrinkage is higher in case of thick layers and lower in case of thin layers whereas the relative shrinkage is higher for thin layers Fig.6.4(b)

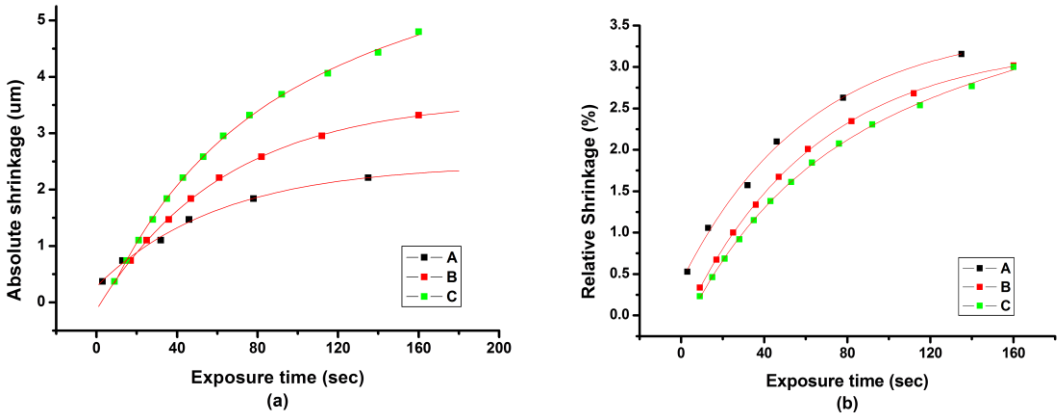

Figure 6.4. Absolute shrinkage(a) and Relative shrinkage (b) with respect to Exposure times for recording intensity 1 mW/cm^2 and spatial frequency 1000 lines/mm at A-70 µm; B- 110 µm, C- 160 µm.

Initially a single exponential asymptotic function was used to fit the curves but the curves could not be fitted with high accuracy to the data. The next step of the fitting procedure was to try data fit with a stretched exponential function. Such choice of fitting function could be justified in the present case by the fact that during the polymerization reaction which leads to the shrinkage of the sample the properties of the photopolymer and mainly its permeability will change with time. The permeability is an important factor because it will influence the mobility of the monomer molecules and thus the polymerization rate. After careful analysis of the obtained results it was concluded that the stretched exponential fit doesn't fit the experimental data better. This was a clear indication that it is not one single process, especially at higher recording intensities, that takes place and determines the dynamics of the photopolymer shrinkage. Thus we tried a double exponential asymptotic function of the form

$$y = a - b * \exp(-cx) - d\exp(-fx) \qquad (6.1)$$

to fit the curve of shrinkage versus time.

The fitted curve (for example Fig. 6.3) will give the final value of shrinkage (*a*), the amplitudes of the two exponential components in the fitting function (*b* ,*d*) and the time constants (*c*, *f*). The information about amplitudes is important because it indicates which of the two processes is having higher contribution to the final shrinkage.

Table 6.1 shows the data from the fitted curve of relative shrinkage with exposure time for three different thicknesses and intensities shown in Fig.6.3

Table 6.1. Data from the fitting of relative shrinkage VS exposure time curves

Thickness (µm)	Intensity (mW/cm^2)	Shrinkage (%)	Amplitude	τ_1 (sec)	Amplitude	τ_2 (sec)
70	1	3.5±0.16	NA	NA	3.09±0.15	58 ± 0.0002
	5	4.3±0.51	0.86±0.17	4.17 ±0.13	3.4±0.28	47.6 ± 0.007
	10	3± 0	1.34	9.09 ± 0	1.21	30 ± 0
110	1	3.3±0.03	NA	NA	3.4±0.025	62.5 ± 0.0004
	5	3.3±0.05	0.86±0.08	9.6 ± 0.014	2.44±0.05	71.4 ± 0.001
	10	2.8±0.096	1.28±0.25	3.02 ± 0.15	1.83±0.15	34.4 ± 0.006
160	1	3.4±0.59	NA	NA	3.53±0.046	71 ± 0
	5	3.5±0.09	0.48±0.0017	7.4 ± 0.07	3.06±0.1	62.5 ± 0.0017
	10	2.83 ±0.05	0.96±0.15	4.78 ± 0.075	2.28±0.2	29.4 ± 0.004

From Table 6.1 we can observe systematically in all three sets of layers of different thickness that lower shrinkage is measured when the recording is carried out with higher intensity of recording. We can correlate the increased shrinkage at lower intensities of exposure as explained previously in Section 4.6 with the fact that at lower illumination intensity the rate at which the free radicals are generated is smaller and thus the volume concentration of free radicals is lower. This leads to a lower rate of termination, the polymer chains have longer time to grow and the ultimate result is the creation of longer polymer chains each comprising a larger

number of monomer molecules. One could expect that the morphology of long polymer chains is different than the morphology of short polymer chains. If the long polymer chains are more entangled than the short polymer chains this will lead to much more dense structure of the polymerized material and higher shrinkage.

By taking account of the amount of polymerisation occurring in the photopolymer layers. We can explain the shrinkage in layers having different thicknesses, recorded with the same intensity and exposure time, by assuming that shrinkage occurring in the photopolymer layers is proportional to the polymerisation rate. From Fig. 6.4(a) we can see that the absolute shrinkage increases with layer thickness whereas percentage shrinkage is higher for thinner layers Fig.6.4 (b). It is clearly seen form fig. 6.4 (a) that while the absolute shrinkage in the thin layers have reached saturation the shrinkage in thick layers is still growing. It is possible that when saturation of shrinkage is achieved in thick layers the same level of relative shrinkage will be reached for all three set of layers with different thicknesses.

In analyzing the dynamics of the shrinkage we have seen two different time constants associated with two processes occurring in the photopolymer layers recorded with higher intensity (5 and 10 mW/cm^2). The first process is characterised by time constant of few seconds while the second process is characterised by time constant in order of tens of seconds. The process characterised by shorter time constant was not evident in case of recording with low intensity of $1mW/cm^2$. The process characterised by the longer time constant can be associated with the rate of polymerization of monomer molecules. The second process is definitely influenced by the exposure intensity and as one can see

from the table the time constants become shorter as the polymerization rate is faster with the increase of the intensity. This trend is observed in thicknesses. By comparing the amplitudes of the two exponential components in Table 6.1 one can see that consistently the relative contribution of the faster process to the overall shrinkage is significantly smaller than the contribution of the slower process.

In order to determine the physical meaning of the first process characterised by the shorter time constant and its influence on the shrinkage of photopolymer layers of thickness 90 and 180 μm were polymerised using a single beam of intensity 4 mW/cm^2 and a grating was also recorded using two beams with combined beam intensity of 4 mW/cm^2, Fig. 6.5. This experiment was carried out in order to determine if the diffusion of monomer molecules from dark to bright fringes could be responsible for the fast exponential component in the shrinkage dynamics. If this was the case one would observe a difference between single and double beam exposure, since in the first case no such diffusion is expected. As one can see from Fig. 6.5 even in the case of bulk polymerisation using a single beam exposure the shorter time constant is present. This is an indication that the lateral diffusion from dark to bright fringes is not responsible for the short time constant process. We have also observed that illumination with a single instead of double beams leads to significant increase of the rate of polymerisation in the 90 μm layers and the difference between the two modes of illumination is less pronounces in 180 μm layers

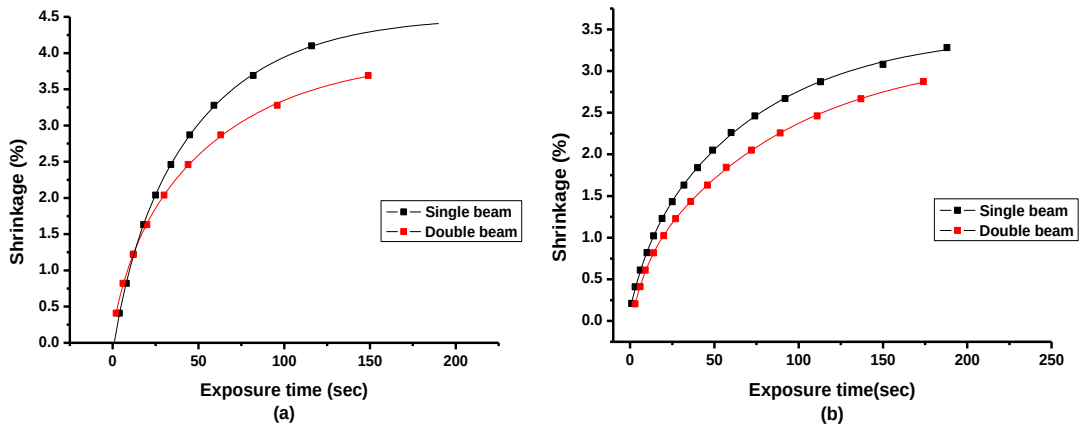

Figure 6.5. Relative shrinkage with respect to exposure times for recording intensity 4 mW/cm^2 using single and double beam in (a) 90 µm; (b) 180 µm thick layer

Table 6.2. Data from the curve fitting of Figure 6.5

Polymerisation	Thickness (µm)	Shrinkage (%)	Amplitude	τ_1 (sec)	Amplitude	τ_2 (sec)
Single beam	90	4.5±0.08	0.76±0.021	10 ±0.13	3.89±0.17	50± 0.007
	180	3.48±0.04	0.6±0.14	11.2±0.093	2.82±0.08	77±0.003
Double beam	90	3.97±0.08	0.75±0.2	11.1 ±0.03	3.01±0.15	62.5 ± 0.002
	180	3.24±0.04	0.6±0.03	8.3±0.014	2.7±0.02	91±0.005

We have observed faster polymerization rate and increased shrinkage in case of single beam polymerisation. This can be related to the fact that more monomer molecules will be converted to polymer in the case of single beam illumination whereas in the case of double beam recording some of the monomers in the dark fringe regions will remain unpolymerised. Some of the monomer molecules will diffuse from dark to bright regions and results in reduced shrinkage.

As in the case of the double beam exposure, in the single beam exposure the relative contribution of the faster process to the overall shrinkage is smaller than the contribution of the slower process.

6.3.2 Influence of zeolite nanoparticles on photopolymer shrinkage

We also have studied the effect of incorporating nanozeolites at different concentration in photopolymer films. The nanocomposites were prepared as described in section 4.7.2.1. The layers were coated on a glass slide painted matt black at the back (to avoid back reflection). Fig. 6.6(a) shows the relative shrinkage versus exposure time for undoped photopolymer layers and photopolymer layers doped with MFI nanoparticles.

Fig.6.6 (b) shows relative shrinkage versus exposure time for undoped photopolymer and BETA doped photopolymer layers. From the figure we can see that the shrinkage is lower in doped photopolymer compared with undoped layers.

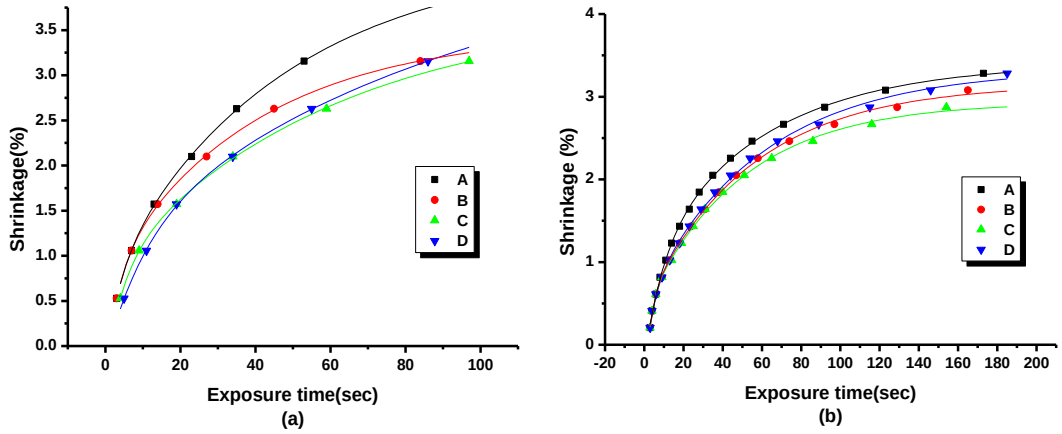

Figure 6.6. Percentage shrinkage with respect to Exposure time (a) 70 µm MFI doped layers concentrations, A- undoped; B- 2.5 wt.% ; C- 5 wt.%; D- 7.5 wt.%(b) 160 µm BETA doped photopolymer with different doping concentrations A- undoped; B- 1 wt.% ; C-2.5 wt.%; D-5 wt.%

The curves shown in Fig. 6.6 were fitted using a double exponential asymptotic function as explained before and the values obtained from the fitted curve are shown in Table 6.3. As explained before the fitted curves will give a final value of

shrinkage and two time constants associated with the shrinkage. We regard the longer time constant as characteristic of the rate of polymerisation and from the table we can see that the faster the rate of polymerisation the lower the shrinkage. In the case of MFI doped layers the fastest rate of polymerisation is noted for 2.5 wt.% layers and the observed shrinkage is also lower in these layers.

Similarly in case of BETA doped layers the polymerisation rate is faster in the case of 2.5 wt.% and the shrinkage is also lower in this case.

Table 6.3. Data from curve fitting of Figure 6.6

Nanoparticle concentration (wt.%)		Shrinkage (%)	Amplitude	τ_1 (sec)	Amplitude	τ_2 (sec)
MFI	0	4.3±0.51	0.86±0.17	4.17 ±0.13	3.4±0.28	47.6 ± 0.007
	2.5	3.48±0.09	0.99±0.14	3.8±0.093	2.7±0.08	40±0.003
	5	3.72±0.21	1.07±0.21	4.9±0.088	2.91±0.11	58.8±0.003
	7.5	4.59±1.6	1.3±0.53	10.5±0.048	3.43±1.04	100±0.01
BETA	0	3.4±0.05	1.19±0.12	9.5 ±0.016	2.39±0.1	62.5 ± 0.002
	1	3.15±0.04	1.15±0.3	2.7±0.09	2.69±0.04	55.5±0.001
	2.5	2.94±0.04	1.39±0.5	2.2±0.13	2.5±0.04	50±0.001
	5	3.34±0.05	0.88±0.18	4.3±0.084	2.7±0.07	58.8±0.001

The lower shrinkage in nanoparticle doped layers can be attributed to a counter diffusion of nanoparticles resulting in spatially periodic distribution of nanoparticles during holographic exposure [3]. The term counter diffusion means that while monomers diffuse into a bright region driven by a monomer concentration gradient, the nanoparticles may migrate into a dark region during the holographic exposure. The redistribution of zeolite nanoparticles has been observed by Raman spectroscopy before [4-7].

6.4. Discussion and conclusions

- We observed that the shrinkage is greater for gratings recorded with lower intensities of recording. The reason for the higher shrinkage at low intensity can be related to the fact as explained before in chapter 4 (section 4.6) that at lower intensity the rate at which the free radicals are generated is smaller and thus the volume concentration of free radicals is lower. This leads to a lower rate of termination and the ultimate result is the creation of longer polymer chains each comprising a larger number of monomer molecules. It is known that the polymerised material has higher density due to the morphology of the polymer material made of entangled polymer molecules. For a greater extent of polymerization the final density and thus the total dimensional change of the layer will be greater.
- By ruling out the influence of the lateral diffusion of monomer molecules on shrinkage we can assume that both process influencing the shrinkage are related to polymerization. We can ascribe the two time constants associated with shrinkage to the rate of polymerisation of monomer molecules (the process characterised by the longer time constant) and the rate of crosslinking of polymer chains (the process characterised by the shorter time constant). At lower illumination intensity the rate at which free radicals are generated will be lower and hence the crosslinking process will be slower and its rate similar to the rate of monomer polymerisation. For this reason a single exponential fit is sufficient to fit the dynamics of the shrinkage process at low intensity of recording. In case of higher intensities of recording the rate of free radicals generation is faster and the density of free radicals in unit volume will be higher, this will lead to faster and greater extend of crosslinking of polymer

chains which is reflected in the faster process observed in the shrinkage dynamics.

- By taking account of the amount of polymerisation occurring in the photopolymer layers we can explain the shrinkage in layers having different thicknesses, while recording with the same intensity and exposure time, by the fact that for thicker layers the polymerisation process and hence the shrinkage is not completed on the assumption that the shrinkage occurring is proportional to the extent of polymerisation. In thin layers most of the monomer molecules will be converted to polymer compared to thick layers which result in increased relative, but not absolute shrinkage.
- We have observed faster polymerization rate and increased shrinkage in case of single beam polymerisation. The increased shrinkage in the case of single beam illumination can be related to the fact that the amount of monomer molecules converting to polymer will be faster and homogeneous across the illuminated area which results in uniform polymerisation. Whereas in the case of double beam recording the monomer will diffuse from dark to bright regions and the diffusion results in non homogeneous polymerisation and resulting in reduced shrinkage.
- We have obtained lower shrinkage and increased diffraction efficiencies by doping with increasing concentrations of nanoparticles. The lowest shrinkage was observed with 2.5 wt.% doping with zeolite Si-MFI and zeolite BETA nanoparticles. Increasing the concentration increases the scattering of the layers, this leads to illumination closer to the single instead of the double beam exposure and thus further increased shrinkage.

- The reason for reduced shrinkage in nanoparticle doped photopolymers was attributed to a “counter diffusion” of nanoparticles during holographic exposure resulting in a spatially periodic distribution of nanoparticles [3]. The redistribution of zeolite nanoparticles on photopolymer layers was confirmed before [4-7]. The term counter diffusion means that while monomers diffuse into a “bright region” driven by a concentration gradient, the nanoparticles may migrate into a “dark region” during the holographic exposure. The increase shrinkage while doping with higher concentration can be related to the increased scattering occurring in the layers.

References

[1] M.Moothanchery, I.Naydenova, V.Bavigadda, S.Martin, V.Toal, Real-time shrinkage studies in photopolymer films using holographic interferometry, Proc. SPIE 8437, (2012)

[2] V.Bavigadda, R.Jallapuram, E.Mihaylova and V.Toal, “Electronic speckle pattern interferometer using holographic optical elements for vibrational measurements,” Optics Letters.35, 3273-3275 (2010)

[3] W.S.Kim, Y.C.Jeong, and J.K.Parka, “Organic-inorganic hybrid photopolymer with reduced volume shrinkage”, Applied Physics Letters **87**, 012106 (2005)

[4] A.M.Ostrowski, I.Naydenova and V.Toal, “Light-induced redistribution of Si-MFI zeolite nanoparticles in acrylamide-based photopolymer holographic gratings,” J. Opt. A: Pure Appl. Opt. 11 (2009).

[5] E.Leite, I.Naydenova, S.Mintova, L.Leclercq, V.Toal, "Photopolymerisable Nanocomposites for Holographic Recording and Sensor Application," Appl. Opt. 49, 3652-3660 (2010)

[6] E.Leite, T.Babeva, E.P.Ng, V.Toal, S.Mintova, and I.Naydenova, "Optical Properties of Photopolymer Layers Doped with Aluminophosphate Nanocrystals," Journal of Phys. Chem. C. 114, 16767- 16775(2010)

[7] I Naydenova, E.Leite, T.Babeva, N.Pandey, T.Baron, T.Yovcheva , S.Sainov , S.Martin, S.Mintova and V.Toal, "Optical properties of photopolymerizable nanocomposites containing nanosized molecular sieves," J. Opt. 13 (2011)

Chapter 7

Electronic Speckle Pattern Interferometry

7.1 Introduction

Holographic Interferometry cannot easily separate in-plane and out of plane components of motion. The ability to measure in-plane and out of plane components independently of each other makes Electronic speckle pattern interferometry (ESPI) an important candidate for determining surface deformations. The ESPI system was initially demonstrated by Butters and Leendertz [1] using a dual beam illumination geometry. The two beams illuminate the test object at equal and opposite angles to its normal. The correlation fringe patterns were obtained using subtraction of two recorded speckle interferograms corresponding to two different object positions using a vidicon TV camera. The ESPI system was applied to measure vibrations of a disc and torsion of a square metal plate. Macovski [2] developed time-lapse speckle interferometric systems using a vidicon TV camera and measured out-of-plane or normal stress of a plastic block and surface contours of metal sheets of different shapes by subtraction of speckle interferograms. A significant development in ESPI systems was the use of digital image processing techniques for obtaining good contrast fringe patterns [3]. Speckle interferograms corresponding to two object positions were stored in a digital frame store. The displacement of the object was detected using subtraction of the stored digital speckle interferograms. The resulting fringe pattern was later subjected to nonlinear post-processing such as level slicing to improve the contrast

of the digital speckle fringes. An ESPI technique has been used in order to determine the phase map due to shrinkage in IEO's photopolymer films.

7.2 ESPI principles

7.2.1 Digital signal processing

The scanning action of the CCD arrays transforms spatial variation in intensity of light from the object into corresponding current variation in the video signal as shown in Fig.7.1. The signal is band-pass filtered to remove the DC components. The signal is rectified to invert the negative component of signals as negative signals are displayed on a TV monitor as areas of blackness.

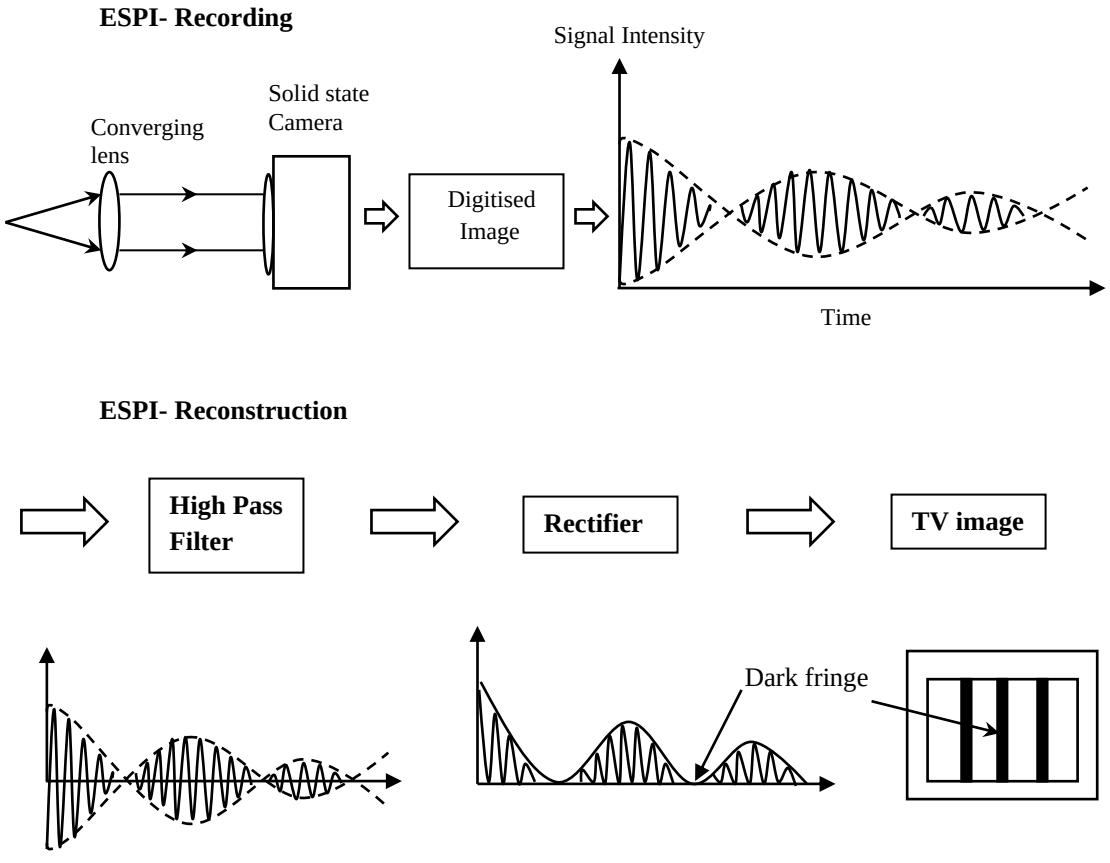

Figure 7.1. ESPI system showing signal processing steps

7.2.2 Addition fringes

When a laser illuminated object is displaced the speckle pattern changes its state. The speckle pattern change can be determined by encoding the information using the phenomenon of interference of the object beam with a smooth or diffuse reference beam [4].

Considering object and reference beams, having complex amplitudes a_1 and a_2 added coherently, the resultant intensity distribution can be expressed as

$$I = |a_1 + a_2|^2 \tag{7.1}$$

$$I = |a_1|^2 + |a_2|^2 + a_1^* a_2 + a_1 a_2^* \tag{7.2}$$

$$I = I_1 + I_2 + 2\sqrt{I_1 I_2}\cos(\phi_1 - \phi_2) \tag{7.3}$$

$$I = I_1 + I_2 + 2\sqrt{I_1 I_2}\cos(\phi) \tag{7.4}$$

where I is the intensity of the resultant speckle interference pattern,

I_1 and I_2 are the average intensities of the reference and object beams with corresponding phases ϕ_1 and ϕ_2 and ϕ is the random phase of the speckle interference pattern.

If the object is displaced then the object beam contains additional phase information about the displacement, hence the resultant intensity of the speckle interference pattern or specklegram changes to

$$I' = I_1 + I_2 + 2\sqrt{I_1 I_2}\cos(\phi + \delta) \tag{7.5}$$

where δ is the phase difference due to the object displacement. The addition of specklegrams for different object positions gives

$$I_{add} = I' + I = 2I_1 + 2I_2 + 4\sqrt{I_1 I_2}\cos\left(\phi + \frac{\delta}{2}\right)\cos\left(\frac{\delta}{2}\right) \tag{7.6}$$

The two interference patterns corresponding to displaced and undisplaced positions are recorded on a single photographic plate called a double exposure specklegram. It may be seen that the first two terms in equation (7.6) are due to the background random speckle noise and the third term indicates intensity modulation which is maximum, when $\cos\left(\frac{\delta}{2}\right)$=1 and zero when $\cos\left(\frac{\delta}{2}\right)$=0. The bright fringes correspond to correlated speckle fields (i.e whenever $\delta = 2n\pi$) and dark correspond to uncorrelated speckle fields (i.e whenever $\delta = (2n+1)\pi$). The fringe patterns in electronic speckle pattern interferometry (ESPI) can be produced by filtering the video signal corresponding to the primary speckle interferograms. In practice the addition method is applicable mainly to the time average case, for the study of vibration. The bias component of intensity is removed from the primary speckle interferograms by high-pass filtering of the video signal [5]. The filtering is implemented on the video signal with analogue electronic circuits. The addition technique does not need any image storage or processing but the fringe contrast is poor.

7.2.3. Subtraction fringes

The subtraction of speckle patterns corresponding to displaced and undisplaced positions is predominantly used in electronic speckle pattern interferometry. The intensity of speckle patterns corresponding to undisplaced and displaced positions is given in equations (7.4) and (7.5) respectively.

The resultant subtracted speckle pattern intensity is represented by

$$I_{sub} = I' - I = 4\sqrt{I_1 I_2}\sin\left(\phi + \frac{\delta}{2}\right)\sin\left(\frac{\delta}{2}\right) \qquad (7.7)$$

The dark fringes are formed whenever the two speckle patterns corresponding to displaced and undisplaced positions of the object are fully correlated (i.e whenever $\delta = 2n\pi$). The bright fringes are formed whenever the two speckle patterns are uncorrelated (i.e whenever $\delta = (2n+1)\pi$)

7.3 Sensitivities

7.3.1 In-plane sensitive ESPI system

The basic geometry of an in-plane ESPI system is as shown in Fig 7.2, consisting of two beams making equal angles with the normal being incident on the object [6, 7]. The scattered light from the object will fall on the camera which is placed along the surface normal. The coordinate axes Y, Z lie in the plane of the diagram but the X axis is directed outwards. The displacement components along the Z direction are out-of-plane components, and those along X and Y axes are in-plane components. If the surface is moved along Z direction both beams will undergo same phase change because the path length change is the same for each. So any movement normal to the surface won't make any impact on the speckle pattern. The same is the case for the movement along the X direction.

If the surface moves along the Y direction the optical path length change due to each beam will be

$$\Delta l_1 = d_Z(1+\cos\theta) + d_Y \sin\theta \qquad (7.8)$$

$$\Delta l_2 = d_Z(1+\cos\theta) - d_Y \sin\theta \qquad (7.9)$$

The effective path length change will be the sum of the path length changes for the two beams [16].

Phase change is given by

$$\Delta\phi = \left(\frac{2\pi}{\lambda}\right)\left(\Delta l_1 - \Delta l_2\right) = \left(\frac{4\pi}{\lambda}\right) d_Y \sin\theta \qquad (7.10)$$

where d_Y is the in-plane displacement along Y axis.

In order to get an interference pattern due to surface displacement a reference frame is taken and subsequent frames are subtracted from it. Speckle correlation of the combined speckle pattern with the original pattern before displacement occurs when

$$2d_Y \sin\theta = n\lambda \qquad (7.11)$$

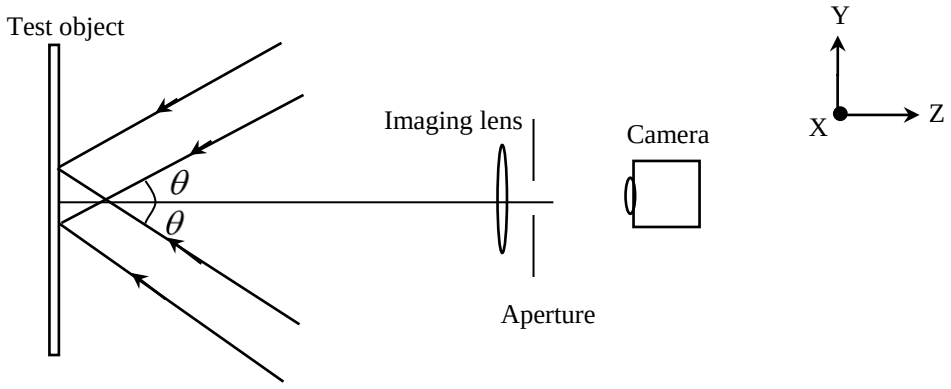

Figure 7.2. In-plane sensitive ESPI system

7.3.2 Out-of-plane sensitive ESPI system

The geometry of an out of plane sensitive ESPI system is similar to a Michelson Interferometer. One mirror in the Michelson interferometer is replaced with a test object and the other mirror with a scattering surface. The scattered beams from the object and reference will combine at the beam splitter before falling onto the

camera [8]. The basic geometry of an out-of –plane sensitive ESPI system is as shown in Fig. 7.3.

The change in optical path length due to object deformation is

$$\Delta l_1 = d_Z(1+\cos\theta) \tag{7.12}$$

The phase change is given by

$$\Delta\phi = \left(\frac{2\pi}{\lambda}\right)\left[d_Z(1+\cos\theta)\right] \tag{7.13}$$

If the angle of illumination is small the above expression can be written as

$$\Delta\phi = \left(\frac{4\pi}{\lambda}\right)d_Z \tag{7.14}$$

Since it is not practical to have the illumination and observation directions collinear, the phase change as a result of object deformation will be

$$\Delta\phi = \left(\frac{2\pi}{\lambda}\right)\left(d_Z(1+\cos\theta)\right) \tag{7.15}$$

The phase difference between two successive bright fringes is 2π. Therefore the displacement that the object undergoes is

$$d_Z = \left(\frac{\lambda}{1+\cos\theta}\right)\times n \tag{7.16}$$

where n is the number of fringes.

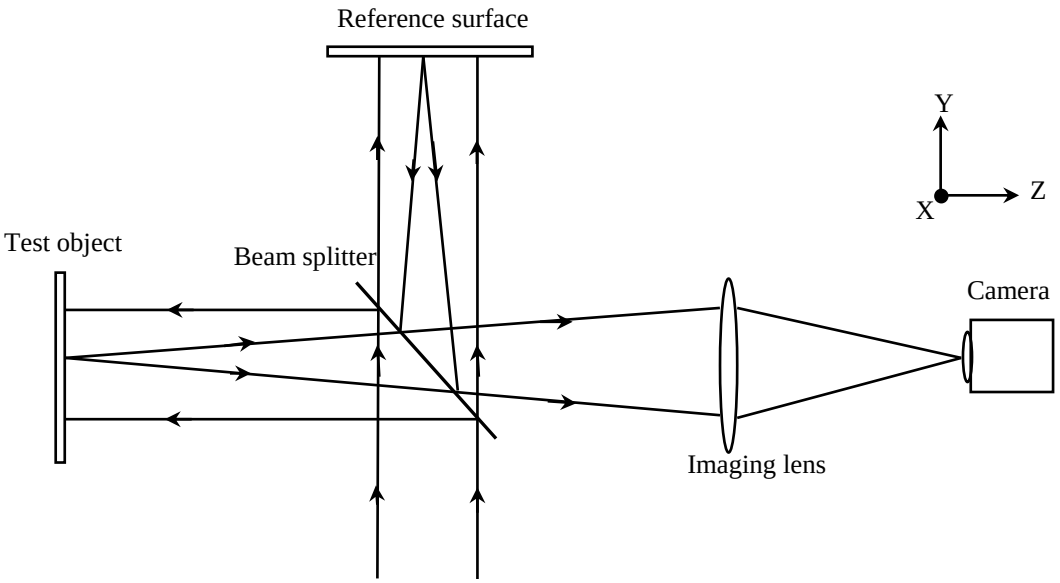

Figure 7.3. Out-of-plane sensitive ESPI system

7.4 Phase shifting techniques

In an ESPI system fringes are produced by image subtraction or addition. Fringe counting technique could not produce complete phase information relating to object deformation. Creath et al. [9] reported phase shifting technique in speckle interferometry to obtain quantitative data of the object displacement. Phase shifting methods are used to measure the phase of the object wavefront with respect to the reference wavefront at every pixel. The phase is calculated from the changes in intensity at each pixel due to the phase differences introduced between object and reference beams. The displacement at each pixel in the image of the object is measured by phase shifting technique so that a complete displacement profile of the object can be obtained. The phase information obtained from a single frame is called spatial phase modulation, whereas if the phase shifted intensities are captured at different time intervals this is called temporal phase modulation. A

wrapped phase map can be extracted if known phase shifts are introduced. The wrapped phase map will contain some phase jumps due to the random nature of speckle and the displacement itself. The former can be removed by various spatial filtering methods and the latter by a process called phase unwrapping [10].

7.4.1 Phase modulation technique

Phase shifts can be introduced by methods such as moving a mirror, tilting a glass plate etc [10]. Moving a mirror in the reference beam by means of piezo electric transducer is one of the most common techniques [11].The intensity of the interference pattern is measured at different phase shifts. The intensity of each frame is given by [12]

$$I = I_0\left[1+V\cos(\phi+\alpha)\right] \tag{7.17}$$

where I_0 - background intensity, V - visibility of the interference fringe pattern, ϕ - wavefront phase α - known phase shift between object and reference beam.

Since there are three unknowns (I_0, V, ϕ) in equation (7.17), at least three measurements are required to determine phase. In a general case, N frames are recorded as the phase is shifted. The phase shift is assumed to change during the detector integration period, but the change is assumed to be same from frame to frame.

The intensity in one recorded frame is written as

$$I_i(x,y) = \left(\frac{1}{\Delta}\right)\int_{\alpha_i-\frac{\Delta}{2}}^{\alpha_i+\frac{\Delta}{2}} I_0(x,y)\left\{1+V(x,y)\cos\left[\phi(x,y)+\alpha(t)\right]\right\}d\alpha(t) \tag{7.18}$$

where Δ - change in relative phase, $\alpha(t)$ - relative phase between object and reference beam,

α_i - average value of phase shift for i^{th} exposure.

Integrating equation (7.18) gives

$$I_i(x,y) = I_0(x,y)\left\{1+V(x,y)\sin c\left(\frac{\Delta}{2}\right)\cos\left[\phi(x,y)+\alpha_i\right]\right\} \quad (7.19)$$

Simplifying equation (7.19) gives

$$I_i(x,y) = I_0(x,y)\left\{1+V_0(x,y)\cos\left[\phi(x,y)+\alpha_i\right]\right\} \quad (7.20)$$

where V_0 is the detected fringe visibility, $\sin c\left(\frac{\Delta}{2}\right) = \frac{\sin\frac{\Delta}{2}}{\frac{\Delta}{2}}$ (7.21)

Equation (7.20) is the basic equation for finding the phase of the interferogram using different algorithms.

7.4.2 Phase shifting algorithms

7.4.2.1 Three frame technique

Using the 3 frame technique the phase steps used are $\alpha_i = 0, {}^{2\pi}\!/_{3}, {}^{4\pi}\!/_{3}$, a phase difference of 90^0 between each frame [12]. The phase of the interferogram is calculated by substituting these phase values in equation (7.20). The phase value at each detector point is given by

$$\phi = \tan^{-1}\left[\frac{\sqrt{3}(I_1 - I_3)}{2I_1 - I_2 - I_3}\right] \quad (7.22)$$

where I_1, I_2, I_3 are the intensities of the interferogram with phase steps of $0, {}^{2\pi}\!/_{3}, {}^{4\pi}\!/_{3}$ respectively.

7.4.2.2 Four frame technique

The four frame technique is the simplest algorithm that is widely used. In a four frame technique the phase step values used are $\alpha_i = 0, \frac{\pi}{2}, \pi, \frac{3\pi}{2}$ [13]. The phase is calculated by inserting these phase values in equation (7.20). The phase at each detector point is given by

$$\phi = \tan^{-1}\left[\frac{I_4 - I_2}{I_1 - I_3}\right] \tag{7.23}$$

where I_1, I_2, I_3, I_4 are the intensities of the interferogram with phase steps of $0, \frac{\pi}{2}, \pi, \frac{3\pi}{2}$

The main problem with this algorithm is that it is susceptible to errors due to miscalibration of the phase shifting device.

7.4.2.3 Five frame algorithm

The five frame algorithm was introduced as an improvement to the four frame technique to reduce calibration errors [14]. The concept of the algorithm is to eliminate the phase error by using a suitable combination of sets of phase shifted images. In the five frame technique the phase step values used are $\alpha_i = -\pi, -\frac{\pi}{2}, 0, \frac{\pi}{2}, \pi$. The phase difference is calculated as

$$\phi = \tan^{-1}\left[\frac{2(I_4 - I_2)}{I_1 - 2I_3 + I_5}\right] \tag{7.24}$$

where I_1, I_2, I_3, I_4, I_5 the intensities of the interferogram with phase steps of $-\pi, -\frac{\pi}{2}, 0, \frac{\pi}{2}, \pi$

7.4.3 Phase unwrapping

In a wrapped phase map the phase values corresponding to each pixel within the image are wrapped between $-\pi$ and $+\pi$ due to the nature of the arctangent function that has been used for phase calculations. The wrapped phase map contains 2π phase discontinuities. To obtain a smooth phase map of the object deformation, it is necessary to remove these 2π phase steps or discontinuities. The process of removing these 2π phase steps is called phase unwrapping or integrating the phase [10]. The most common method of unwrapping is by scanning pixels sequentially along a row or column. Wherever the phase jumps are detected, an offset of 2π is either added to or subtracted from the pixel's phase value depending on the sign of the jump. Starting at the top of any column in the phase map the offset is set to zero. Scanning down the pixels in the column, the phase jumps are examined by calculating the phase difference between adjacent pixels.

An out of plane sensitive ESPI system has been used to determine shrinkage in photopolymer layers. Phase shifted interferograms were captured during polymerisation of photopolymer films. These phase shifted images have been used to calculate the phase map due to shrinkage. The experimental details on determination of shrinkage in photopolymer layers using ESPI technique will be explained in detail in the next chapter.

References

[1] J.N.Butters and J.A.Leendertz, “Holographic and video techniques applied to engineering measurement,” J. Meas. Control. 4, 349-354 (1971)

[2] A.Macovski, S.D.Ramsey, and L.F.Schaefer, **,** **“**Time lapse interferometry and contouring using television systems” Appl. Opt. 10, 2722–2727 (1971)

[3] S.Nakadate, T.Yatagai and H.Saito, “Electronic speckle pattern interferometry using digital image processing techniques,” Appl. Opt. 19, 1879-1883 (1980)

[4] R.S.Sirohi, “Speckle interferometry,” Contemporary Physics.43, 161-180 (2002)

[5] P. K. Rastogi, Editor, “Digital speckle pattern interferometry and related techniques,” John Wiley & Sons Ltd. 231-234, First edition, (2001)

[6] B.Bowe, S.Martin, V.Toal, A.Langhoff, M.Whelan, “Dual in-plane electronic speckle pattern interferometry system with electro-optical switching and phase shifting,” Appl.Opt., 38, 666-673(1999)

[7] R.S.Sirohi, N.K.Mohan, “In-plane displacement measurements configuration with two fold sensitivity,” Appl.Opt. 32, 6387-6390 (1993)

[8] R.S.Sirohi, “Speckle Metrology,” Chapter 2 , Academic Press Inc, London (1978)

[9] K.Creath, “Phase shifting speckle interferometry,” Appl. Opt. 24, 3053-3058 (1985)

[10] W.H.Stevenson, “Optical frequency shifting by means of rotating a diffraction grating,” Appl.Opt. 9, 649-652 (1970)

[11] P.K.Rastogi, “Holographic Interferometry Principles and Methods,” Chapter 5, Springer series in optical sciences. 68, Springer-Verlag, Berlin (1994)

[12] J. -R. Huang, H. D. Ford and R. P. Tatam, “Phase-stepped speckle shearing interferometer by source wavelength modulation,” Opt. Lett., Vol. 21, No. 18, 1421-1423, (1996)

[13] Y. Surrel, “Phase stepping: a new self-calibrating algorithm,” Appl. Opt., Vol. 32, No. 19, 3598-3600, (1993)

[14] J. Schwider, R. Burow, K. E. Elssner, J. Grzanna, R. Spolaczyk and K. Merkel, “Digital wavefront measuring interferometry--some systematic error sources,” Appl. Opt. Vol. 22, No. 21, 3421-3432, (1983)

CHAPTER 8

STUDIES OF SHRINKAGE IN PHOTOPOLYMER FILMS BY ELECTRONIC SPECKLE PATTERN INTERFEROMETRY

8.1 Introduction

Although the fringe counting technique used in holographic interferometry gives information regarding real time shrinkage it could not produce complete phase information relating to object deformation. Creath [1] reported the use of a phase shifting technique in speckle interferometry to obtain quantitative data about object displacement. Phase shifting methods are used to measure the phase of the object wavefront with respect to the reference wavefront at every pixel. The phase is calculated from the changes in intensity at each pixel due to the phase differences introduced between object and reference beams. The displacement at each pixel in the image of the object is measured by phase shifting technique so that a complete displacement profile of the object can be obtained. This chapter deals with an Electronic Speckle Pattern Interferometric (ESPI) system used to determine the change in surface profile of acrylamide photopolymer due to shrinkage. A programme developed in LabVIEW was used to acquire phase shifted live specklegrams continuously. The programme was initiated while the sample remained unexposed and specklegram was recorded and stored while the modulating voltage used to drive a piezoelectric transducer attached to a reference surface, was zero. The modulation voltage was then changed in steps in order to capture phase shifted images which were stored on the computer.

8.2 Experiment

8.2.1 Sample preparation

The photopolymer solution was prepared as previously described in Chapter 5. For fringe counting experiments 0.2, 0.4 and 0.6 ml of photopolymer solution were spread on 25 mm ×35 mm glass plates. The samples were allowed to dry for 24 hours. The sample thicknesses after drying were approximately 90, 160 and 210 μm respectively. For phase shifting experiments 0.06 ml of photopolymer solution was spread on a circular area of 1.3 cm diameter on a 25 mm × 35 mm glass plate coated with non reflective paint. The samples were dried for 24 h. Sample thickness after drying was approximately 160μm.

8.2.2 Experimental set up

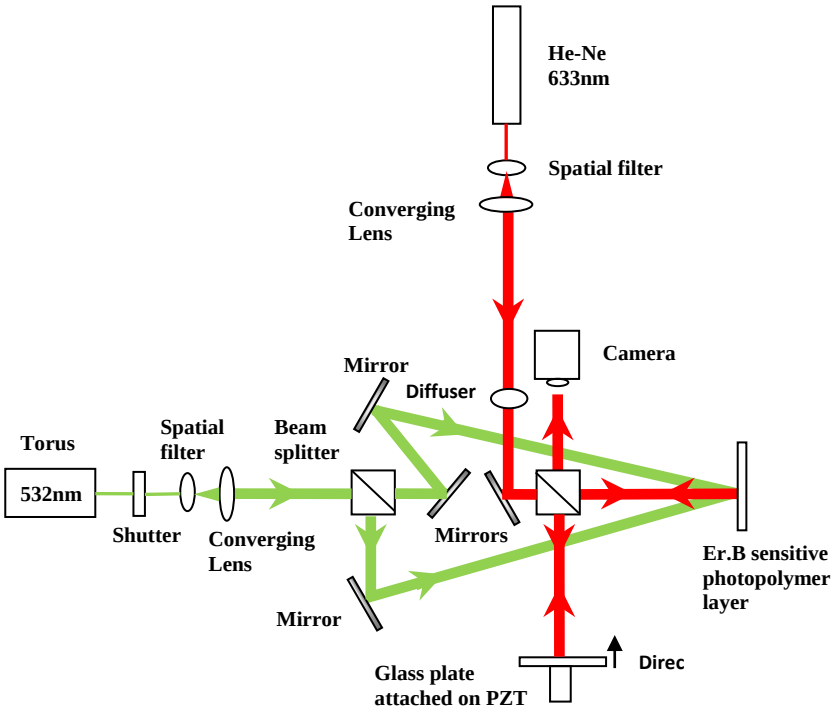

Figure 8.1. ESPI system

The ESPI system is as shown in Fig.8.1. An Er.B sensitised photopolymer film is the object under study in this system. The photopolymer substrate is the glass plate coated with non-reflective paint, to prevent back reflection of light from glass substrate. Similarly a glass plate coated with reflective paint was attached to a piezoelectric transducer whose motion can be controlled using the programme designed in Labview.

The 633nm beam from a He-Ne Laser is spatially filtered collimated and split into two beams using a beam splitter. One of the beams is partially reflected from the green sensitive, Erythrosine B sample (object beam) whereas the other beam (reference beam) is partially reflected from a glass plate attached to a piezoelectric transducer (PZT) and these two beams are allowed to interfere and fall on to a CMOS camera. The field of view of the camera was 25mm. The optical path length of the two arms in the interferometer was 11 cm. The camera (Guppy F032B) was interfaced to a laptop using an IEEE1394 firewire port. After recording the reference frame and phase shifted specklegrams of the photopolymer surface a beam from a Torus 532 nm laser, spatially filtered, and split into two beams using a beam splitter was switched on. These beams interfere with one another to record a holographic grating in the Erythrosine. B sensitized layer, as a result of which the material shrinks. Phase shifted images were captured at regular intervals during the whole recording process. The reference frame was subtracted from phase shifted frames in order to calculate the phase map due to shrinkage. The reference frame was captured before recording the grating in the green sensitive layer, just before switching on the green laser.

8.3 Experimental Results

8.3.1 Fringe counting technique

In order to compare the values of shrinkage obtained from holographic inteferometry we have done some fringe counting experiments using the ESPI system without any movement of the PZT. Frame subtraction was used in this technique. So during photopolymerisation we observed a movement of fringes due to shrinkage in photopolymer layers. A reference frame was subtracted from each incoming frame and the result representing the change in the specklegram displayed on the computer monitor in real time. The movement of the fringes was captured as a live video which was processed using NI Vision Assistant software. The appearance of each fringe normally represents a displacement of half a wavelength of the light used.

$$d = \frac{n\lambda}{2} \qquad (8.1)$$

where, n - number of dark fringe ; λ - wavelength of light

Transmission diffraction gratings were recorded in acrylamide based photopolymer films of thickness 90, 160 and 210 μm. The recording intensity was 5 mW/cm^2. The observed values of shrinkage after fitting the curves as shown in Fig. 8.2 were 3.5, 3.4, and 3.8 % respectively for 90, 160 and 210 μm layers. Whereas the result observed in a 160μm thick layer with same exposure time and intensity from holographic interferometric technique were 3.45 %.

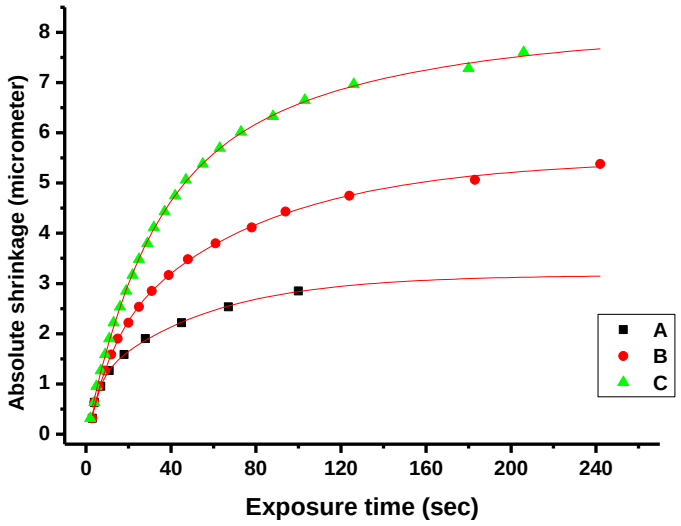

Figure.8.2. Absolute shrinkage versus Exposure times for recording intensity 5 mW/cm^2 at A-90 μm; B- 160 μm, C- 210 μm.

8.3.2 Phase shifting technique

In order to calibrate the piezoelectric transducer an external voltage was applied to the transducer in the interferometer set up with a glass plate as the object. We observed that 2.5V was needed to obtain a phase shift of 2π as shown in Fig. 8.3. The observed voltage value was divided in to four equal increments to obtain the voltage value corresponding to a constant phase difference of $\pi/2$ in the interferometric system.

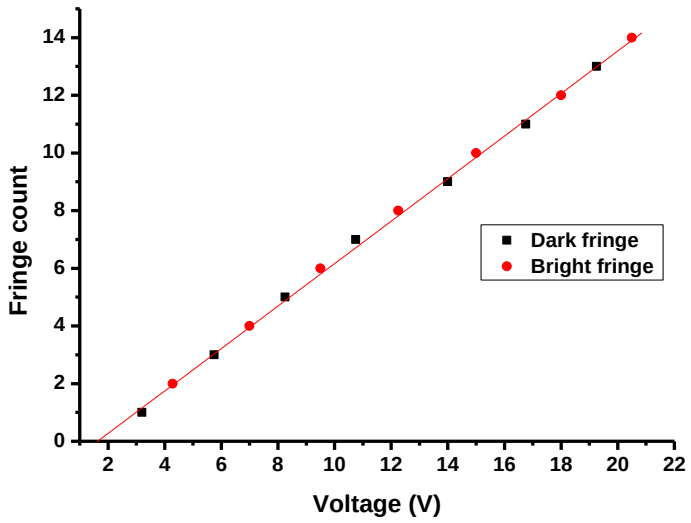

Figure 8.3. Calibration of piezoelectric transducer

In order to obtain a fringe pattern, a reference specklegram was captured before recording a grating without moving the PZT. Then 5 more phase shifted images I_1, I_2, I_3, I_4, I_5 corresponding to 0°, 90°, 180°, 270°, 360° were captured by changing the input voltage to the PZT thereby introduced a constant phase difference of $\pi/2$ between consecutive frames. These phase shifted specklegrams were used to get the wrapped phase map before polymerising the photopolymer layers.

The wrapped phase map was calculated using a five frame algorithm [2]

$$\phi = \tan^{-1}\left[\frac{2(I_4 - I_2)}{I_1 - 2I_3 + I_5}\right] \tag{8.2}$$

In a wrapped phase map the phase values corresponding to each pixel within the image are wrapped between –π and +π due to the nature of arctangent function that has been used for phase calculations. The command 'atan2' used for phase calculations assigns angles into their proper quadrants by taking account of the signs of the trigonometric functions.

The photopolymer layer was then polymerised using a green beam and phase shifted speckle patterns corresponding to shrinkage in the object position were also obtained. The beam profile of the green beam using for the recording process is shown in Fig. 8.4(b). Profile is been plotted for the area (dotted square) shown in Fig. 8.4 (a) using Image J software.

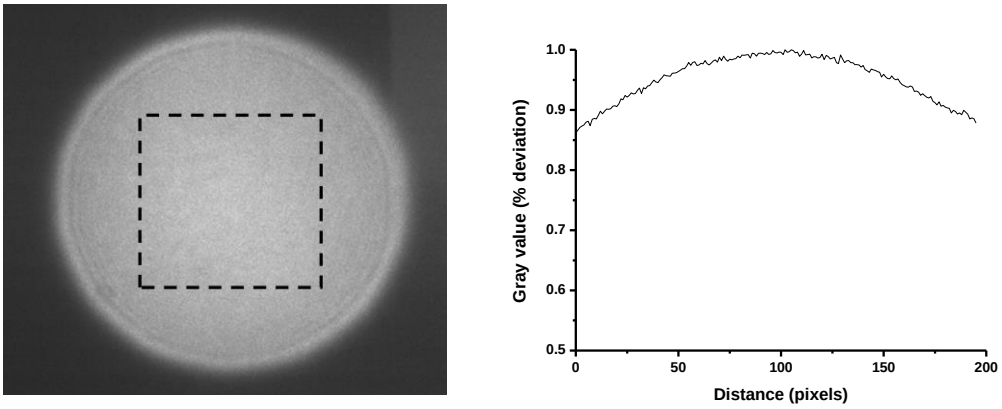

(a) (b)

Figure 8.4. Beam profile of recording beam

The wrapped phase maps before and during exposure were unwrapped using the 2D-SRNCP unwrapping algorithm [4] in order to obtain smooth phase maps. These two unwrapped phase maps were subtracted from one another in order to get the map of the shrinkage in the photopolymer.

The phase shifted specklegrams obtained at 80 seconds of exposure with 10 mW/cm^2 on a 160 μm thick photopolymer approximately 1.3cm in diameter are shown in Fig. 8.5. The recording beam overlap area is made larger than the photopolymer region and hence there is no diffusion from outside the illuminated area. The wrapped phase map calculated from these 5 phase shifted frames is shown in Fig. 8.6. The phase map is noisy because of high spatial frequency

speckles. Some points in the speckle pattern are completely dark and some others are saturated, so a low pass (average) or median filter with kernels of size 5×5 or 7×7 or 9×9 can be applied [3]. In this experiment an image averaging filter with 7×7 kernel was applied to obtain a smoothly varying wrapped phase map.

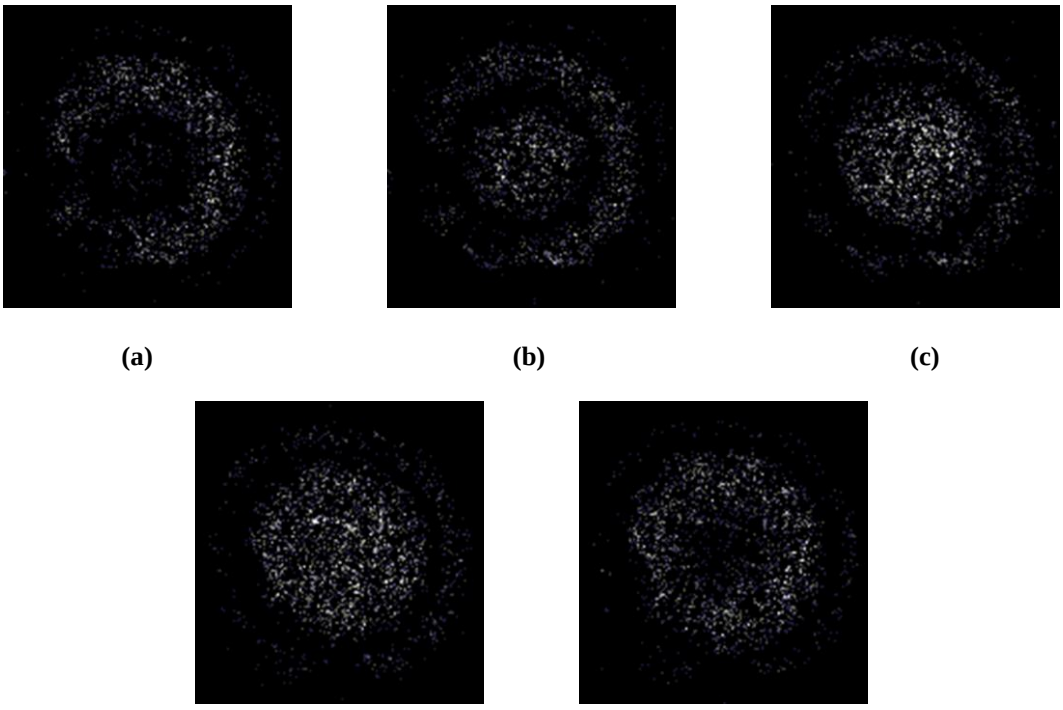

(a) **(b)** **(c)**

(d) **(e)**

Figure 8.5. Phase stepped speckle subtraction fringes (a) 0° (b) 90° (c) 180° (d) 270° (e) 360°

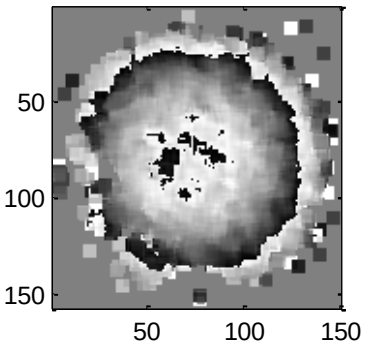

Figure 8.6 Wrapped phase map

The wrapped phase map contains 2π phase discontinuities. To obtain a smooth phase map of the object deformation, it is necessary to remove these 2π phase steps or discontinuities. The process of removing these 2π phase steps is called phase unwrapping or integrating the phase [23]. We have used a 2D-SRNCP algorithm developed at the General Engineering Research Institute (GERI) at Liverpool John Moores University, U.K [4]. This algorithm unwraps the highest quality pixels with highest reliability values first and lowest quality pixels with lowest reliability value last to prevent error propagation. In the 2D SRNCP algorithm the reliability of a pixel is defined based on the second differences (meaning difference of phase gradients) between a pixel and its neighbours. By using second differences of phase values of the adjacent pixels, detection of inconsistencies in the phase map can be improved. The unwrapping path is determined by the reliability of the pixels [4]. The reliability of a pixel is defined as the inverse of the second difference between the pixel and its neighbours. The 2D SRNCP algorithm follows non-continuous or discrete paths for unwrapping. The phase maps still contain some errors which cannot be detected, but the algorithm is very robust in practice compared to continuous path unwrapping algorithms. The 2D-SRNCP phase unwrapper is written in the C programming language. This C code is callable from Matlab using the '*mex'*- 'Matlab Executable' functionality after compiling the C code in Matlab.

The unwrapped phase map of the wrapped image (Fig.8.6) is shown in Fig. 8.7(b). The phase value of each pixel lying in the range [-π, +π] is represented by a grey level within the dynamic range of the CMOS camera enabling display of the phase map as a gray level image. The dark pixels correspond to a phase value of –π and

white pixels which are saturated correspond to phase value of +π. The unwrapped phase map of the photopolymer before exposure is shown in Fig. 8.7 (a).

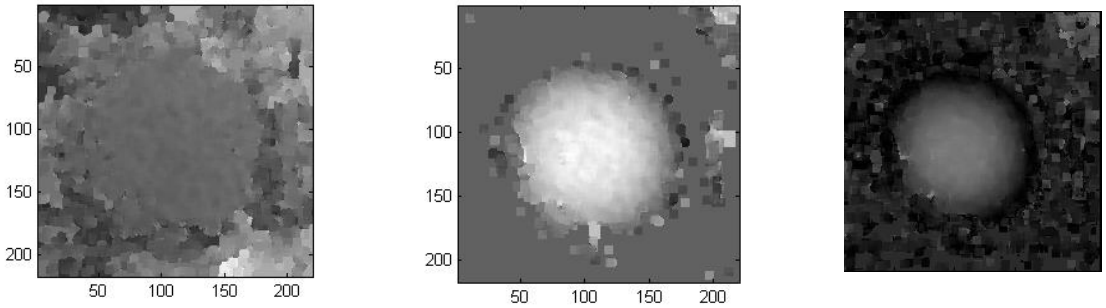

(a) (b) (c)

Figure 8.7 Unwrapped phase map (a) before exposure (b) 80s exposure (c) subtracted

In order to determine shrinkage in photopolymer layers in real time the phase map corresponding to the time of recording, in this case 80 sec, is subtracted from that before recording. The resulting unwrapped phase map is shown in Fig. 8.6(c). From the subtracted phase map, a 3D displacement map of shrinkage can be calculated

$$\Delta d = \left(\frac{\lambda}{4\pi} \right) \phi \qquad (8.3)$$

where Δd - shrinkage in photopolymer layer ; λ - wavelength of laser ; ϕ - unwrapped phase

Figure 8.8 shows an example of a 3D displacement map of shrinkage produced from the data shown in Fig. 8.7. Pixels values shown in the displacement maps corresponds to 7 mm approximately (100 pixels = 7mm).

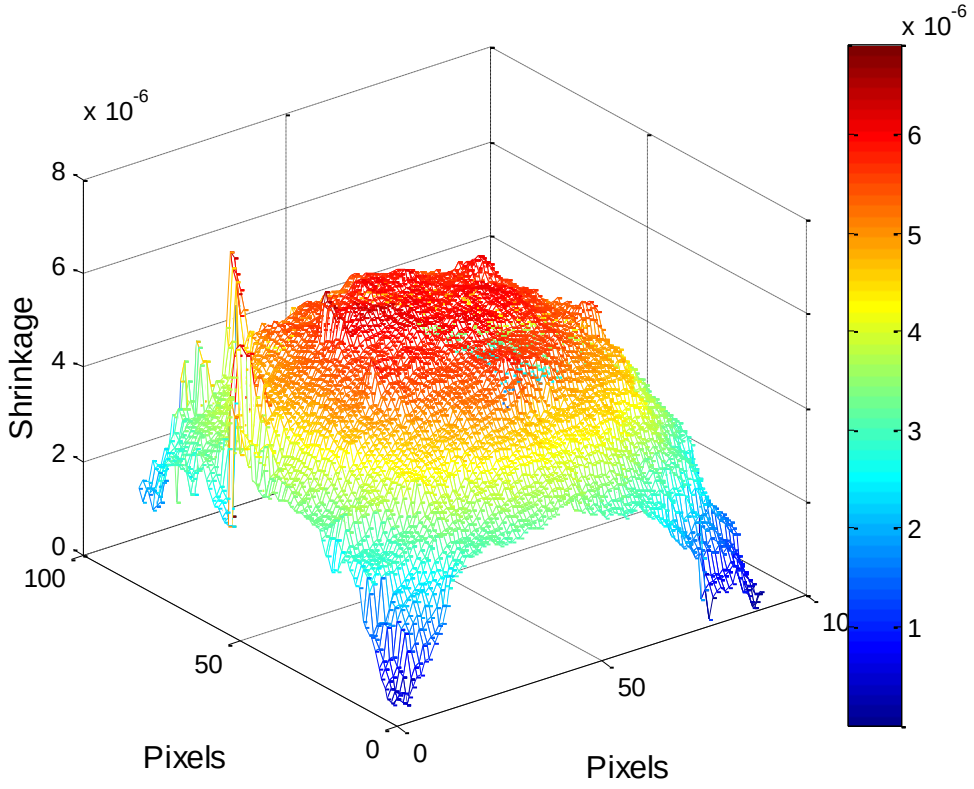

Figure 8.8. Absolute shrinkage of 160 µm sample at 80sec of exposure for recording intensity 10 mW/cm^2

Figure 8.9 shows map of shrinkage at different stages during recording a grating with 10 mW/cm^2 in a 160 µm layer. One can see from the map that the shrinkage increases with exposure time. Fig. 8.9(a) shows the shrinkage 20 s after the start of recording and we can see that the shrinkage is not uniform. This can be related to the fact that in the early stages of exposure the diffusion of monomer occurs rapidly and we believe the diffusion is uniform manner and the portion where the concentration of monomer molecule will be higher shrinks more due to the higher conversion rate of monomer to polymer.

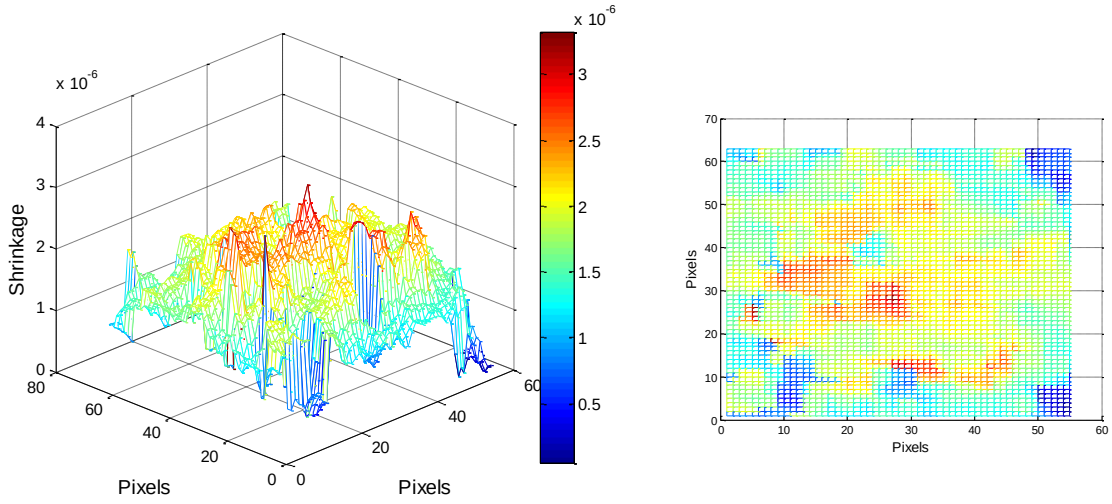
x 10^-6
Shrinkage
Pixels
Pixels
x 10^-6
Pixels
Pixels

(a)

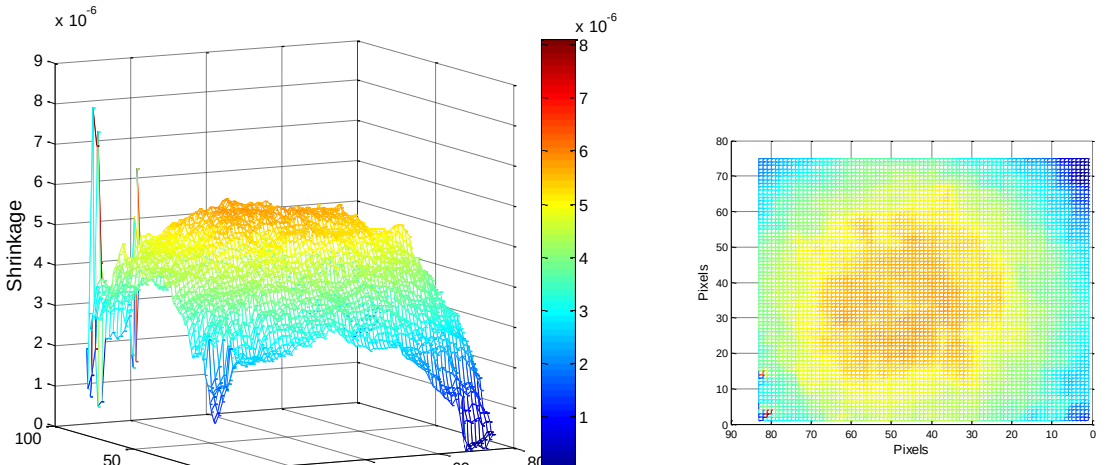
x 10^-6
Shrinkage
Pixels
Pixels
x 10^-6
Pixels
Pixels

(b)

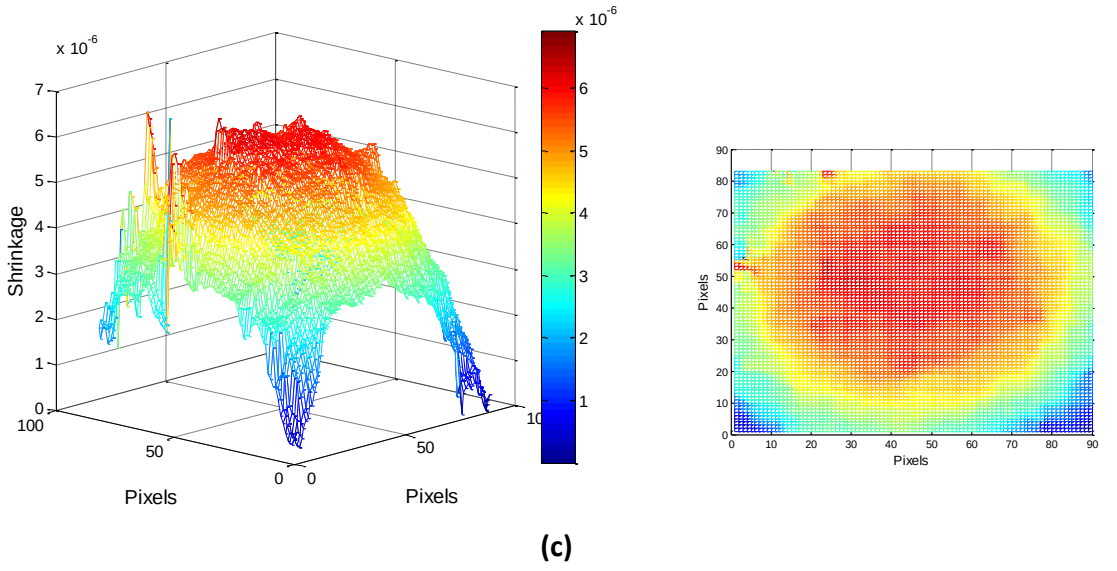

(c)

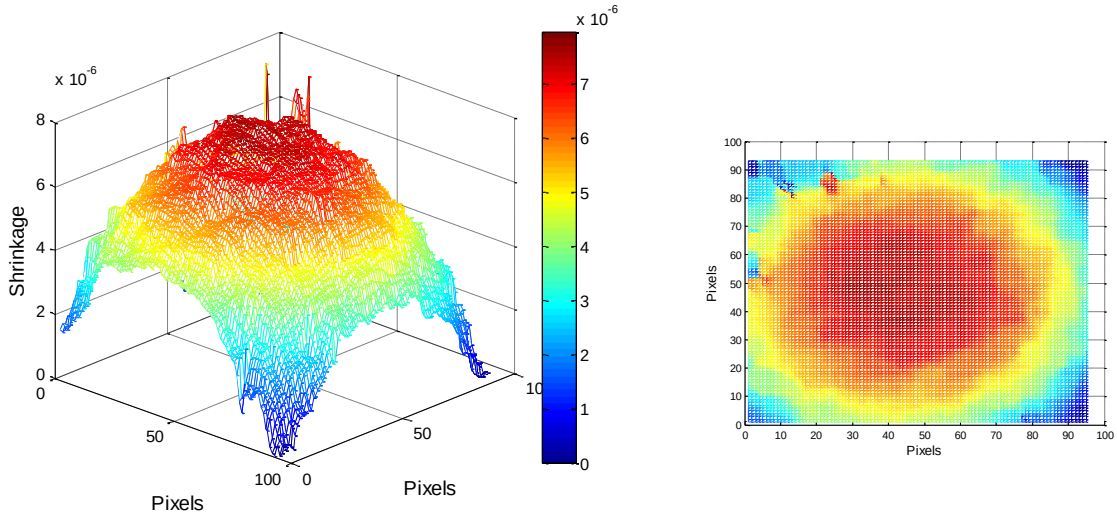

(d)

Figure 8.9. Absolute shrinkage of 160 µm sample at (a) 20s (b) 50s (c) 80sec (d) 120s of exposure for recording intensity 10 mW/cm^2

Similarly Fig. 8.9(b) shows the shrinkage after 50s, Fig. 8.9(c) shows the shrinkage after 80s exposure and Fig. 8.9(d) shows the shrinkage after 120s of exposure . From the results we can see that the shrinkage increases with exposure time.

8.3.2.1 Intensity dependence of shrinkage in photopolymer films.

The shrinkage of the material was evaluated in 160 μm thick layers for three different recording intensities 1, 5 and 10 mW/cm^2. Phase shifted specklegrams were captured before polymerising the layers and also at exposure times of 200, 40 and 20 s so as to keep the total exposure energy constant at 200 mJ/cm^2 for each of the three intensities. Fig 8.10 shows the shrinkage determined from the phase shifted specklegrams captured at the end of 20 sec for gratings recorded with 10 mW/cm^2. The maximum value of shrinkage in this sample at these recording conditions corresponds is approximately 2.4μm.

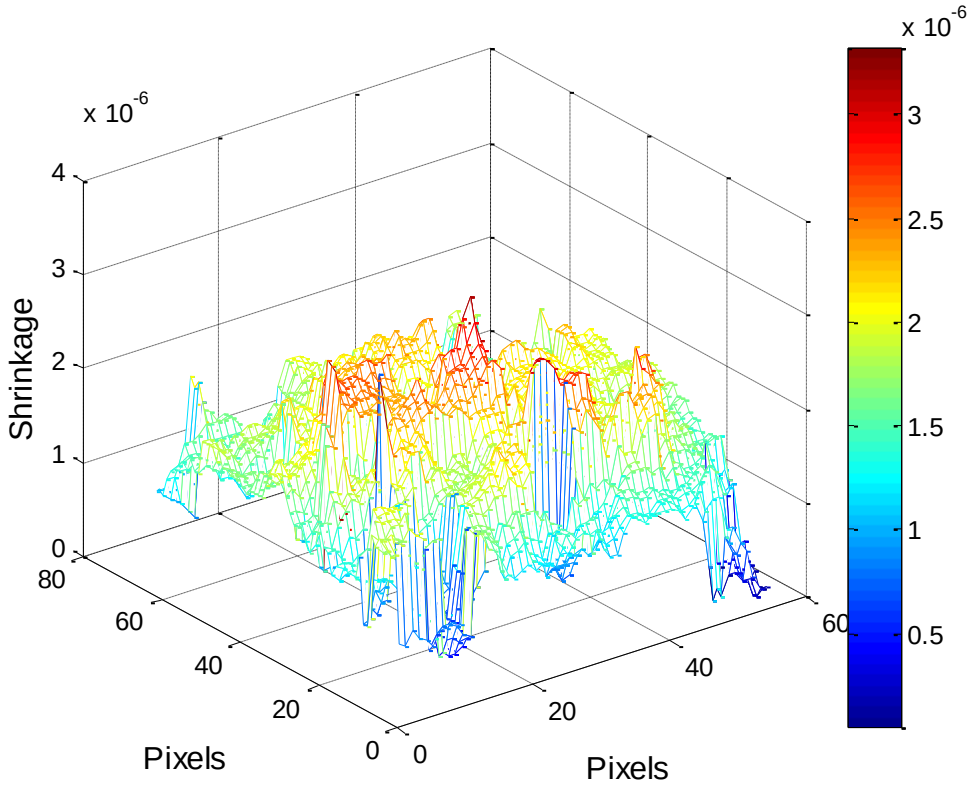

Figure 8.10. Absolute shrinkage of 160 μm sample at 200 mJ/cm^2 exposure for recording intensity 10 mW/cm^2

Figure 8.11 shows the shrinkage determined from the phase shifted specklegrams captured at the end of 40 sec for gratings recorded with 5 mW/cm^2. The maximum value of shrinkage is 4.4 μm approximately

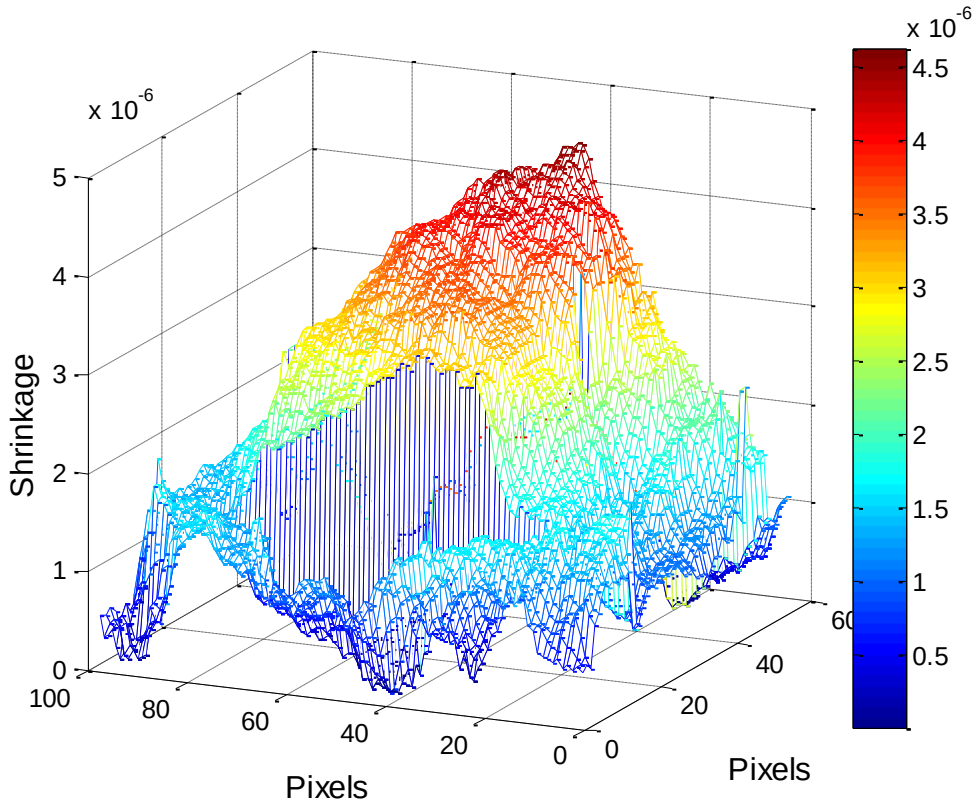

Figure 8.11. Absolute shrinkage of 160 μm sample at 200 mJ/cm^2 exposure for recording intensity 5 mW/cm^2

Fig 8.12 shows the shrinkage determined from the phase shift specklegrams captured at the end of 200 sec for gratings recorded with 1 mW/cm^2. The maximum value of shrinkage is 5 μm approximately

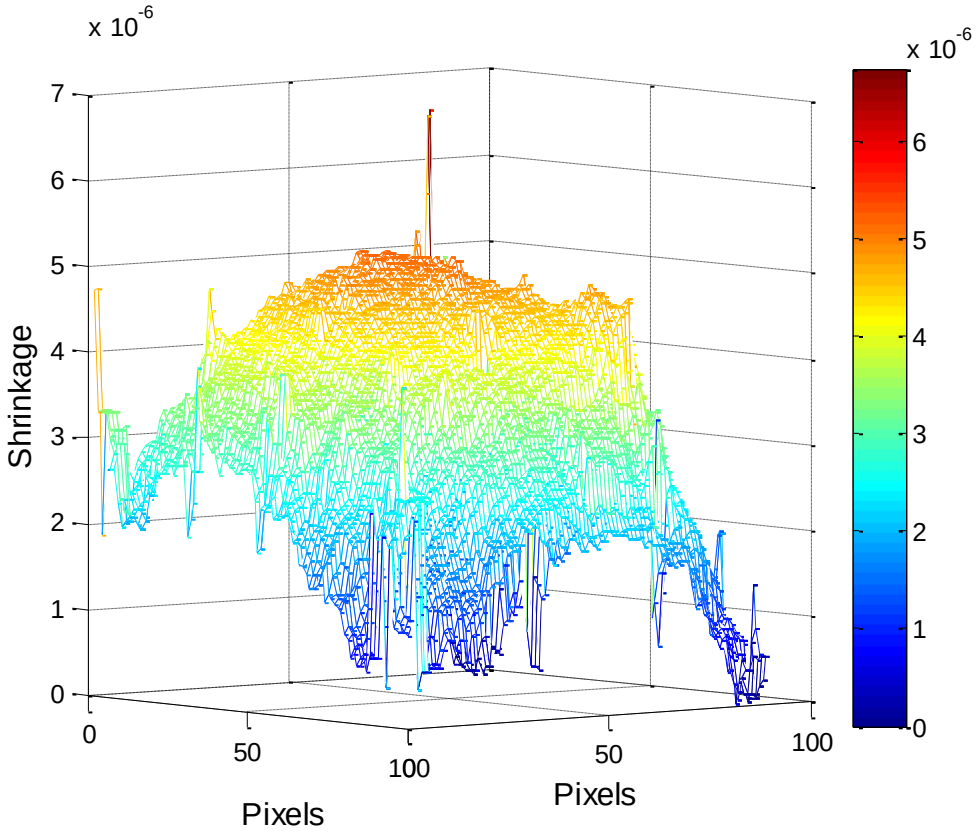

Fig.8.12. Absolute shrinkage of 160 µm sample at 200 mJ/cm^2 exposure for recording intensity 1 mW/cm^2

8.3.2.2 Discussion and conclusions

As previously observed the relative shrinkage was lower with higher intensity of recording. We can correlate the increased shrinkage at lower intensities of exposure as previously explained with the fact that at lower illumination intensity the polymer molecules formed are likely to be larger. The reason for this is that the rate at which the free radicals are generated is smaller and thus the volume concentration of free radicals is lower. This leads to a lower rate of termination and the ultimate result is the creation of longer polymer chains each comprising a larger number of monomer molecules. The observed shrinkage is higher than the previous results from holographic interferometery and Bragg curve studies. The reason for this is that the photopolymer layer is polymerizing as a whole (recording beam

overlap area is larger than the sample area) and there is no diffusion from outside which results in higher shrinkage.

8.3.2.3 Dependence of shrinkage on recordings with single and double beam exposure in photopolymer films.

We also have studied the effect of polymerising photopolymer layers using a single beam and double beam exposure. The shrinkage was measured in a 160μm thick layer for recording intensity 5 W/cm^2. Phase shifted specklegrams were captured before polymerising the layers and at exposure time of 80s. Fig 8.13 shows the shrinkage corresponding to single beam exposure and the maximum value of shrinkage corresponds to 3.7% approximately.

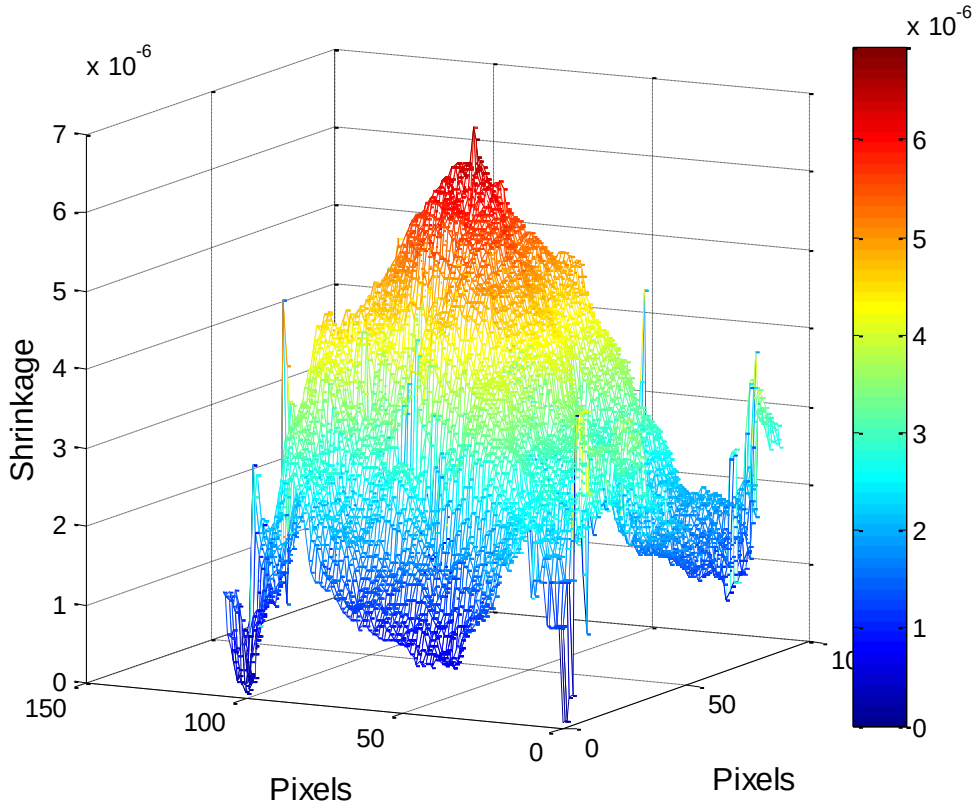

Figure 8.13. Absolute shrinkage of 160 μm sample at 80sec single beam exposure for recording intensity 5 mW/cm^2

Fig 8.14 shows the shrinkage corresponding to two beam exposure. The maximum value of shrinkage corresponds to 3.12 % approximately

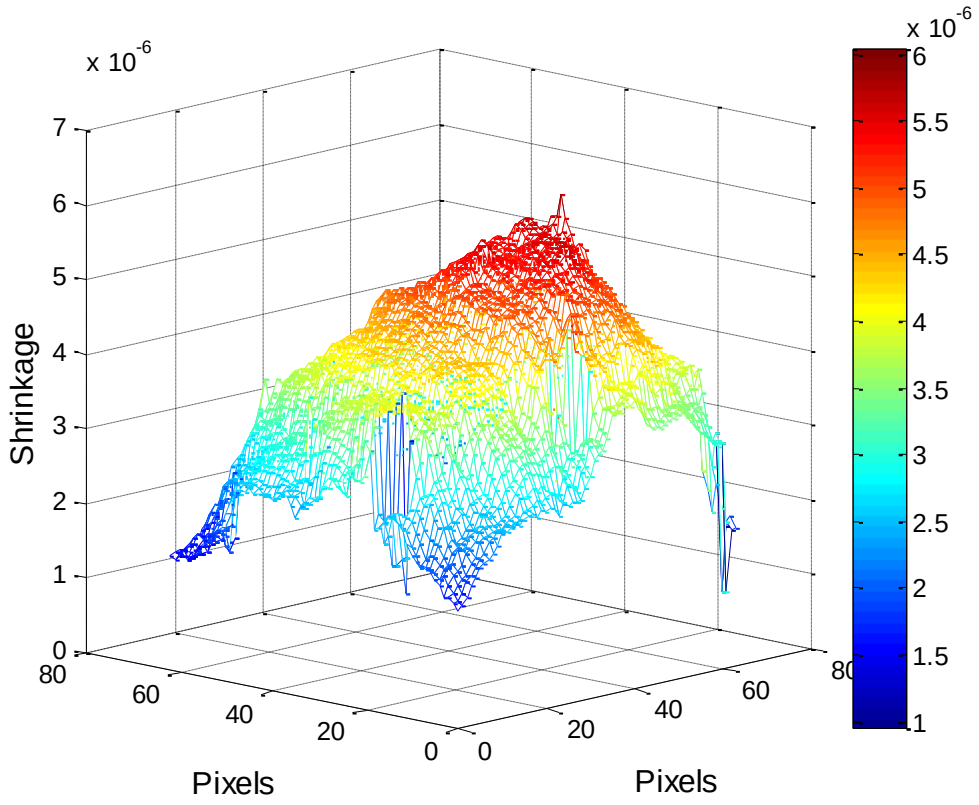

Figure.8.14. Absolute shrinkage of 160 µm sample at 80sec double beam exposure for recording intensity 5 mW/cm^2

The observed values of shrinkage show that bulk polymerisation results in higher values of shrinkage.

The reason for carrying out shrinkage studies on photopolymer coated on a small area is because we find it difficult to get complete information regarding the shrinkage for recordings made in photopolymer layers coated on the whole substrate. Recordings were made on photopolymer layers coated on the whole glass substrate. Fig 8.15 shows the shrinkage at the end of 160 sec for recording made on a 160 µm thick layer with recording intensity 1 mW/cm^2. The maximum value of

shrinkage corresponds to 3.12 %. The result is similar to the values of shrinkage obtained from holographic interferometry. Further investigation is needed to find the reason for the observed shrinkage.

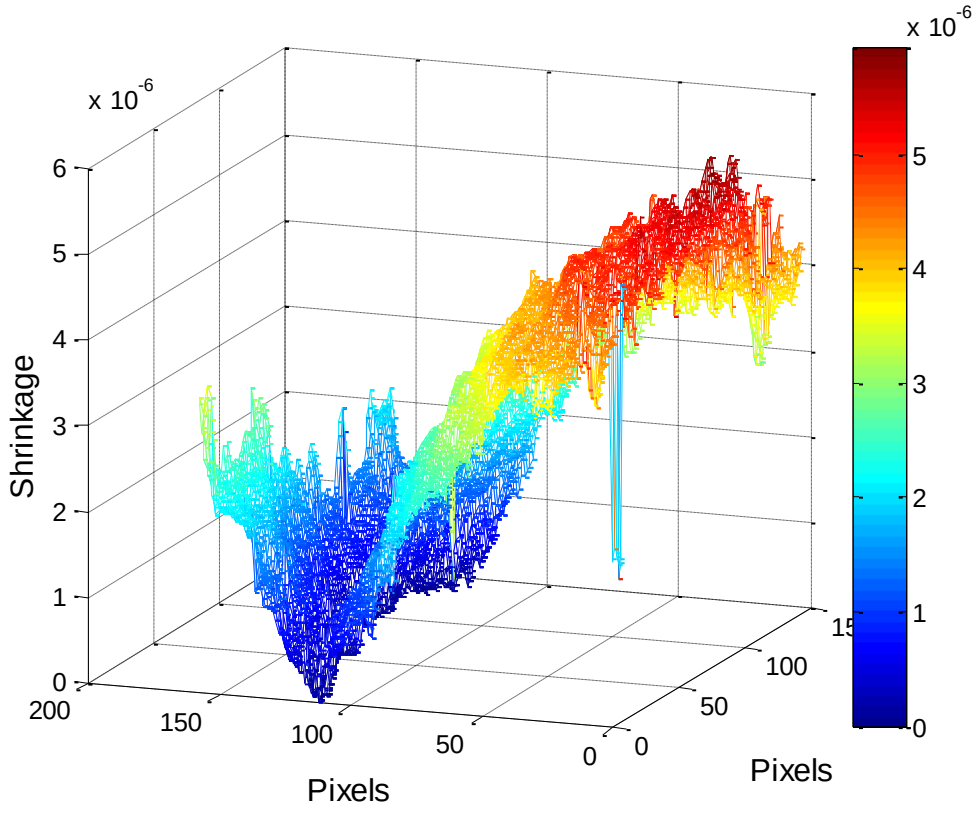

Fig.8.15. Absolute shrinkage of 160 µm sample at 160 sec exposure for recording intensity 1 mW/cm^2

8.3.2.2 Discussion and conclusions

- Fringe counting technique has been employed in order to compare the results with those obtained using holographic interferometric technique. The results were similar to those obtained using Holographic Interferometry.
- Using ESPI phase shifting technique the map of shrinkage has been calculated
- The shrinkage map has the same circular symmetry as the profile of the recording beam as expected.

- Gratings were recorded on a 160 μm layer with three different intensities. As previously observed the relative shrinkage was lower with higher intensity of recording. We can relate the increased shrinkage at lower intensities of exposure as previously explained with the fact that at lower illumination intensity the polymer molecules formed are likely to be larger. The reason for this is that the rate at which the free radicals are generated is smaller and thus the volume concentration of free radicals is lower. This leads to a lower rate of termination and the ultimate result is the creation of longer polymer chains each comprising a larger number of monomer molecules.
- The observed shrinkage is higher than the previous results from holographic interferometery and Bragg curve studies. The reason for this is that the recording beam overlap area is greater than the sample so that the photopolymer layer is polymerizing as a whole and there is no inward diffusion of monomers from outside which would effectively reduce the shrinkage.
- Experiments were done using a single beam and double beam exposure. The observed values of shrinkage show that single beam polymerisation results in higher values of shrinkage. The increased shrinkage in single beam polymerisation is due to faster polymerisation rate as observed before. This can be related to the fact that the rate of monomer conversion to polymer will be faster and the conversion will be equal in all illuminating areas which results in uniform polymerisation and increased shrinkage. Whereas in the case of double beam recording the monomer will diffuse from dark to bright regions and the diffusion can be uneven hence resulting in an spatially uneven rate of polymerisation and reduced shrinkage.

- Recordings were made on photopolymer layers coated on the whole glass substrate even though the maximum value of shrinkage was similar to the values of shrinkage obtained from holographic interferometry. Further investigation is needed to find the reason for the observed map of shrinkage. We think it might be due to clamping effect, edge effect or due to the diffusion of monomer from areas outside the polymerising region.

References

[1] K.Creath, "Phase shifting speckle interferometry," Appl. Opt. 24, 3053-3058 (1985)

[2] P.Hariharan , B.F.Oreb and T.Eiju, "Digital phase-shifting interferometry: a simple error-compensating phase calculation algorithm," Appl. Opt. Vol. 26, No. 13, (1987)

[3] A.J.Moore , J.R.Tyrer and F.M.Santoyo, "Phase extraction from electronic speckle pattern interferometry addition fringes," Appl. Opt. Vol. 33, No. 31, 7312-7320, (1994)

[4] M.A.Herraez , D.R.Burton , M.J.Lalor , M.A.Gdeisat, "Fast two-dimensional phase-unwrapping algorithm based on sorting by reliability following a noncontinuous path," Appl. Opt., Vol. 41, No. 35, 7437-7444, (2002)

CHAPTER 9

CONCLUSIONS AND FUTURE WORK

The main objective of this project was to determine and minimise the shrinkage of an acrylamide based photopolymer developed in the Centre for Industrial and Engineering Optics for holographic recording. This recording material is sensitized in the visible spectrum with Erythrosine B, a green sensitive dye. Three different experimental techniques were used to study the process of shrinkage and its dependence on the composition of the material and recording conditions. The shift of Bragg curve due to shrinkage was measured after the completion of the holographic recording process, holographic interferometry was used to study the dynamics of the shrinkage process and electronic speckle pattern interferometry was used to produce maps of shrinkage in real time. The main conclusions of this study are summarized below.

The shrinkage of the material was determined from the shift of Bragg curve for different exposure intensities, thicknesses, spatial frequencies and zeolite nanoparticle concentrations in photopolymer layers.

Influence of the exposure intensity

Transmission diffraction gratings were recorded with constant exposure energy of 80 mJ/cm^2 at varied intensity and exposure time. It was observed that the shrinkage is greater for gratings recorded with lower intensities and longer exposure times. The reason for the higher shrinkage achieved with low intensity of recording can be related to a regime of polymerisation that leads to conversion of larger number of monomer to polymer molecules and to the creation of longer polymer chains.

Influence of the spatial frequency

Transmission diffraction gratings were recorded at a range of spatial frequencies from 500 to 2000 lines/mm. It was observed that the resulting shrinkage in the photopolymer layer increases with the increase in spatial frequency. One possible explanation for the large values of the observed shrinkage at high spatial frequency is the larger number of monomer molecules converted into polymer molecules, causing larger density change. At high spatial frequency the distance travelled by the monomer molecules from the dark to the bright fringes is smaller. Thus during a given exposure time a larger number of monomer molecules will manage to reach the bright fringes at higher spatial frequency of recording than at lower spatial frequency. Thus the number of monomers that get polymerised will be higher with increasing spatial frequency of recording and larger dimensional change (shrinkage) is expected. Minimum shrinkage of 0.49 % was observed at intensity 10 mW/cm^2 and spatial frequency 500 lines/mm . Maximum shrinkage of 8 % was measured at intensity 1 mW/cm^2 and spatial frequency 2000 lines/mm.

Higher intensities and lower spatial frequencies lead to lower shrinkage of the photopolymer layer but the maximum achievable diffraction efficiency is also lower in these cases.

Influence of the thickness of the layers

Transmission gratings were recorded in layers of thickness ranging between 30 and 120 μm. The recording time and intensity were kept constant for all layer thicknesses. The total exposure was 80 mJ/ cm^2. It was observed that while the absolute shrinkage in the layers was the same, the relative shrinkage for layers of

different thickness was higher for the thinner layers. By taking account of the amount of polymerisation occurring in the photopolymer layers of different thickness for constant total exposure we can explain the difference in relative shrinkage, by the fact that for thicker layers the polymerisation process and hence the shrinkage is not completed on the assumption that the shrinkage occurring is proportional to the extent of polymerisation. The same value for absolute shrinkage in layers of different thickness can be explained by the fact that after absorbing the specific exposure energy the same amount of material was polymerized. The refractive index modulation obtained in layers of thickness 30, 60 and 120 μm was measured to be the same, thus suggesting the same extent of monomer molecule conversion and density change per unit volume and thus the same absolute shrinkage. Minimum shrinkage of 0.58 % was observed in layers of thickness of 120 μm. Maximum shrinkage of 1.57 % was measured in layers of thickness 30 μm.

Influence of nanoparticles dopants

Two different nanozeolites (Si-MFI & BETA) were used to improve the holographic recording characteristics namely higher diffraction efficiency and reduced shrinkage. Incorporation of zeolite nanoparticles shows improvement in holographic recording characteristics in the photopolymer material. Diffraction efficiency is improved up to 40% and shrinkage is reduced to one half with increased concentration of nanoparticles.

Highest diffraction efficiency and lowest shrinkage was observed with 5 wt.% doping with zeolite Si-MFI. Increasing the concentration further will lower the diffraction efficiency and lead to increased shrinkage because of scattering effects.

The origin of the increase in diffraction efficiency in nanoparticle doped photopolymers was attributed to a “counter diffusion” of nanoparticles during holographic exposure resulting in a spatially periodic distribution of nanoparticles. The term counter diffusion means that while monomers diffuse into a “bright region” driven by a concentration gradient, the nanoparticles may migrate into a “dark region” during the holographic exposure.

Recordings made on layers of different thicknesses doped with 2.5 wt.% nanopaticles, shows the same relative shrinkage as absolute shrinkage increases with the thickness of the layer. The dependence of the percentage shrinkage of nanoparticle doped layers on their thickness differs from that observed in undoped layers, in which the percentage shrinkage decreased by a factor of three as layer thickness was increased from 30 to 120 μm, but the absolute shrinkage was the same for all thicknesses.

Experiments with layers doped with 2.5% Si-MFI concentration and different dye concentrations shows that the refractive index modulation obtained is significantly lower in layers with lower dye concentration (0.055%.wt) and high dye concentration (0.22%.wt) doesn’t lead to any obvious improvement in the refractive index modulation. At the same time the shrinkage is seen to increase with dye concentration. This can be related to the fact that at higher dye concentration the rate at which free radicals generated will be higher and hence the more monomer molecules will polymerise and the rate of convertion will be faster resulting in increased shrinkage.

Recordings in zeolite Si- MFI and BETA doped layers with increased exposure time shows lower shrinkage and increased diffraction efficiency with increasing

concentrations of nanoparticles. The best results (increased diffraction efficiency and low shrinkage) were obtained in layers doped with 5 wt.% MFI and 2.5 wt.% BETA nanoparticles. Comparing the results obtained after short exposure times in order of 16 s in zeolite Si-MFI doped layers reveal that shrinkage predominantly occurs during the initial stage of exposure.

The results shows that careful consideration of the recording conditions and zeolite nanoparticles concentration is needed to attain maximum efficiency and minimum shrinkage during holographic recording.

The dynamics of shrinkage was studied by Holographic Interferometry

A photopolymer recording material which is sensitized with Methylene Blue, a red sensitive dye was used to record holograms to determine shrinkage in a photopolymer material sensitized in the green with Erythrosine B.

Influence of the exposure intensity

The observation from Bragg curve shift experiments, that the shrinkage is greater for gratings recorded with lower intensities of recording was confirmed by the real time holographic interferometry measurements.

Indentified processes contributing to the shrinkage

The shrinkage was measured in real time and it was determined that they can be best fitted with a double exponential function. Two separate processes occurring on different timescales of few seconds and few tens of seconds were identified. We propose that the two processes could be ascribed to shrinkage due to crosslinking (the process characterised by the shorter time constant) and to shrinkage due to polymerisation of monomer molecules (the process characterised by the longer

time constant). At lower illumination intensity the first process was not observed separately and this could be explained by the fact that the rate at which free radicals are generated will be significantly slower and hence the crosslinking process will be slower and its rate similar to the rate of monomer polymerization. In the case of higher intensities of recording the rate of free radicals generation is faster and hence the density of free radicals in unit volume will be higher, which leads to faster and greater extend of crosslinking of polymer chains which is reflected in the appearance of another, faster process in the shrinkage dynamics.

Influence of the thickness of the layers

The observation made by the Bragg curve shift experiments, that the relative shrinkage is greater for gratings recorded in thinner layers was confirmed by the real time holographic interferometry measurements.

By taking account of the amount of polymerisation occurring in the photopolymer layers we can explain the shrinkage in layers having different thicknesses, while recording with the same intensity and exposure time, by the fact that for thicker layers the polymerisation process and hence the shrinkage is not completed on the assumption that the shrinkage occurring is proportional to the extent of polymerisation. In thin layers most of the monomer molecules will be converted to polymer compared to thick layers during photopolymerisation which result in increased relative, but not absolute shrinkage.

Influence of the regime of exposure (single or double beam exposure)

It was observed that the polymerisation rate is faster and shrinkage is increased in case of single beam exposure. The increased shrinkage in the case of single beam

illumination can be related to the fact that the amount of monomer molecules converting to polymer will be larger and homogeneous across the illuminated area which results in uniform polymerisation and increased shrinkage. Whereas in the case of double beam recording there will be unexposed regions (the dark fringes) and the polymerisation will not be homogeneous across the area and resulting in reduced shrinkage.

Influence of nanoparticles dopants

It was observed that incorporation of nanoparticles with increasing concentration reduces shrinkage. The lowest shrinkage was observed with 2.5 wt.% doping with zeolite Si-MFI and zeolite BETA nanoparticles. Increasing the concentration increases the scattering of the layers, this leads to illumination regime that is closer to the single instead of the double beam exposure and thus further increases the shrinkage.

A 3D map of the shrinkage was studied by ESPI

Using ESPI phase shifting technique and a five frame algorithm the map due to shrinkage has been calculated at different times after the beginning of the exposure. The shrinkage map has the same circular symmetry as the profile of the recording beam as expected.

Influence of the exposure intensity

Gratings have been recorded on a 160 μm layers of diameter 1.3 cm with three different intensities. In order to avoid the influence of diffusion of monomers from the unexposed surrounding area the recording beam diameter is larger than the size

of the sample. The results are consistent with the results from the other two methods; it is observed that the relative shrinkage is lower with higher intensity of recording. The value of the measured shrinkage is higher than the one measured by Holographic Interferometry and studies of the shift of the Bragg curve. The reason for this is that the recording beam overlap area is greater than the sample so that the photopolymer layer is polymerizing as a whole and there is no inward diffusion of monomers from outside which would effectively reduce the shrinkage.

Influence of the regime of exposure (single or double beam exposure)

Experiments were done using a single beam and double beam exposure on photopolymer having same size and thickness. The observed values of shrinkage show that single beam polymerisation results in higher values of shrinkage. This is consistent with the results from Holographic Interferometry.

Future work

Following the preliminary investigations carried out in this thesis, a number of suggestions could be taken up for future projects

- ***Continue studies of shrinkage profile as a result of incorporating MFI and BETA nanoparticles***.

  The shrinkage profile as a result of incorporating nanozeolites in photopolymer films needs to be investigated in detail.

- ***Incorporating microporous nanoparticles with various shapes and structures in order to clarify the mechanism of suppression of the photopolymer shrinkage.***

  The effect of zeolite nanocrystals (pure silicate, aluminosilicates and aluminophosphate) having different channel diameter in their molecular structure incorporated in acrylamide based photopolymer layers for holographic applications needs to be investigated further. Experiments with nanozeolites like ALPO, BEA, LTA, LTL of different concentrations in acrylamide photopolymer layers in order to determine the nanoparticle with higher refractive index modulation and lowest possible shrinkage. Layers with lowest possible scattering need to be employed

- ***Studies of shrinkage of multiplexed holograms in photopolymer films***

  The test system has the ability to multiplex sets of holographic gratings with equalised diffraction efficiencies using angular multiplexing. In angular multiplexing the holographic medium is rotated using out of plane angular steps between recordings. Ten or even hundreds of holograms can be recorded in this manner depending on the available dynamic range of the recording material, thickness and spatial frequency of recording. The diffraction efficiency of

multiplexed gratings scale as $1/N^2$ [2], where N is the number of the gratings multiplexed. Therefore as the number of gratings stored in the photopolymer increases, approximate exposure scheduling become even more important. To improve the uniformity of the multiplexed gratings it is necessary to progressively increase the exposure times used for recording in such a way as to compensate for the reduced dynamic range that may exist by the time a particular grating is recorded. This technique will enable to determine the change in photopolymers refractive index in the case of a single grating recorded compared with a number of gratings recorded in a single photopolymer layer. In addition it is possible to investigate photopolymers temporal stability in terms of material shrinkage and diffraction efficiency by studying variation in the Bragg selectivity curve. Multiplexed grating technique is mainly employed to develop the photopolymer material for various holographic applications.

- ***Studies of shrinkage of multiplexed holograms in photopolymer films doped with nanozeolites***

  Optimum nanoparticle concentration giving best possible results in standard photopolymer layers could be used in these experiments. Initially each set of gratings is recorded with uniform diffraction efficiency using iterative scheduling method. New exposure times should be used to repeat the experiments for series of photopolymer layers with different concentration of nanoparticles and also different layer thickness. Multiplexed gratings recorded with uniform diffraction efficiency and lowest possible shrinkage is advantageous for employing the photopolymer material for different holographic applications.

APPENDIX-A

Diffracted Intensity and Bragg Curve measurements (VI) written in LabVIEW

This VI is been used to plot the diffraction efficiency and Bragg curve of photopolymer layers

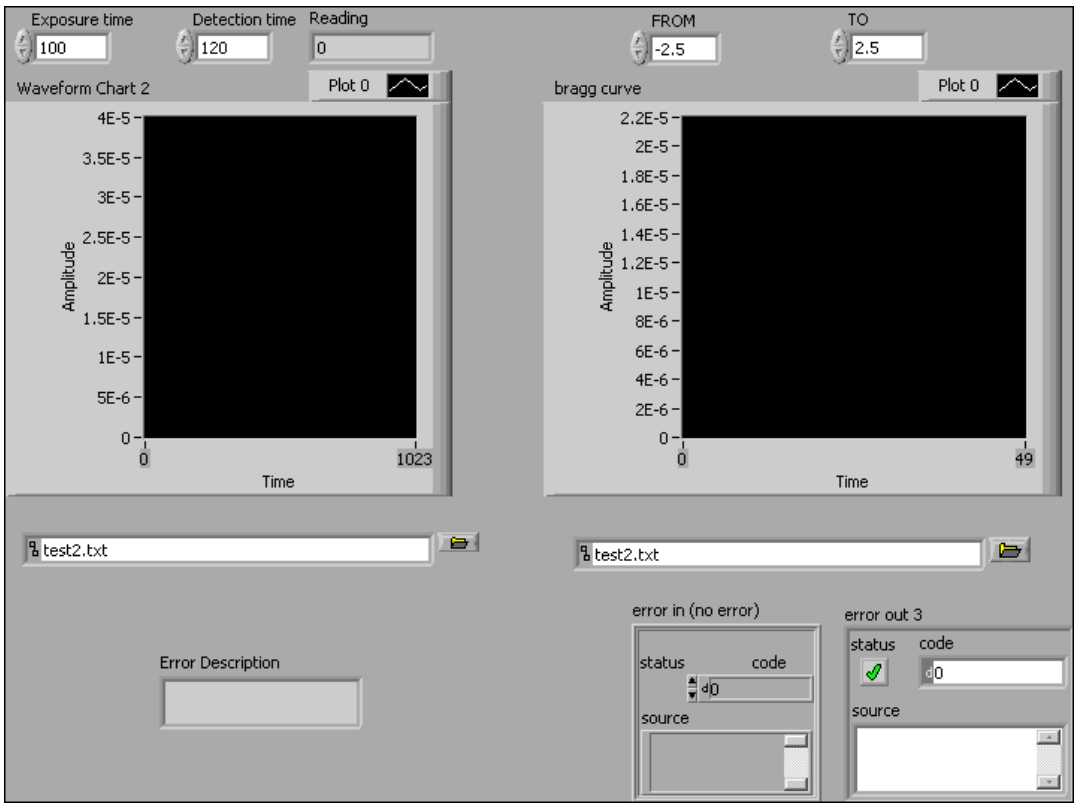

Fig 1. Front Panel for Diffracted Intensity and Bragg Curve VI

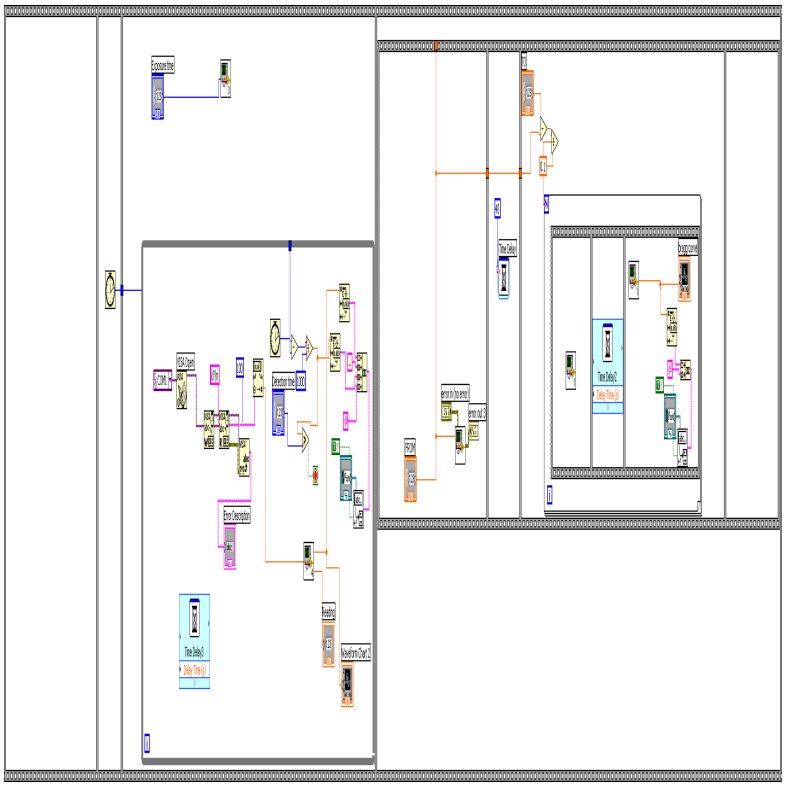

Fig 2. Block Diagram for Diffracted Intensity and Bragg Curve VI

Generation of Digital Counter Pulse for Camera External Triggering (VI) written in LabVIEW

This VI will create a counter output channel to produce a pulse in terms of frequency

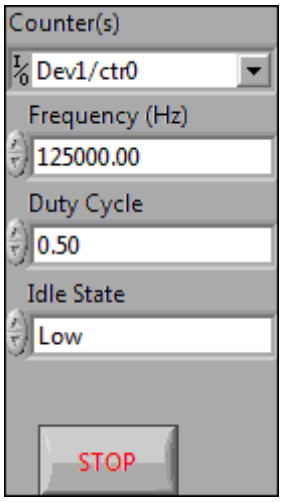

Fig 3. Front Panel of the Counter Generation code VI

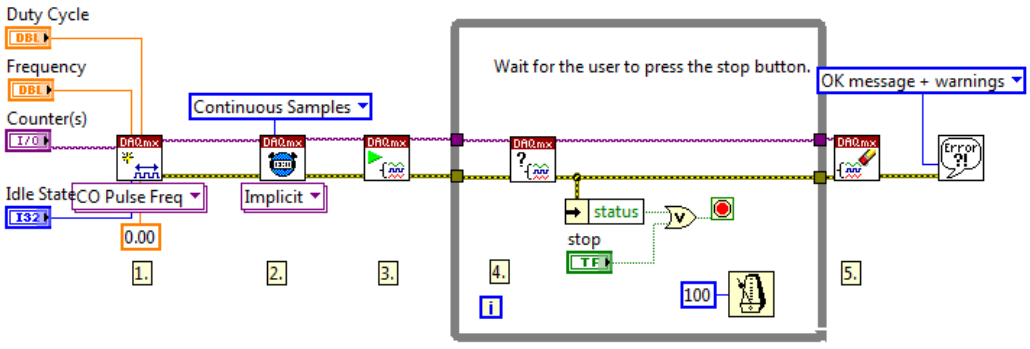

Fig 4. Block Diagram of the Counter Generation code VI

Continuous Generation of Digital Waveforms (VI) written in LabVIEW

This VI will generate digital waveform continuously using an internal sample clock of the DAQ board

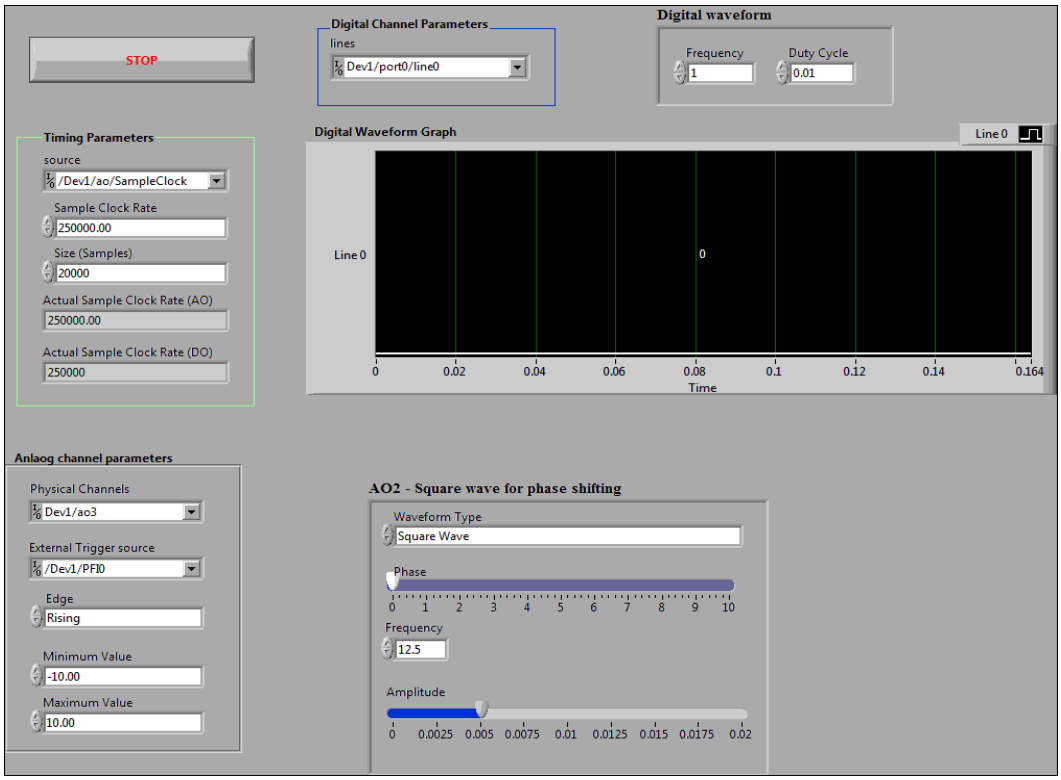

Fig 5. Front Panel of the Digital Waveform Generation VI

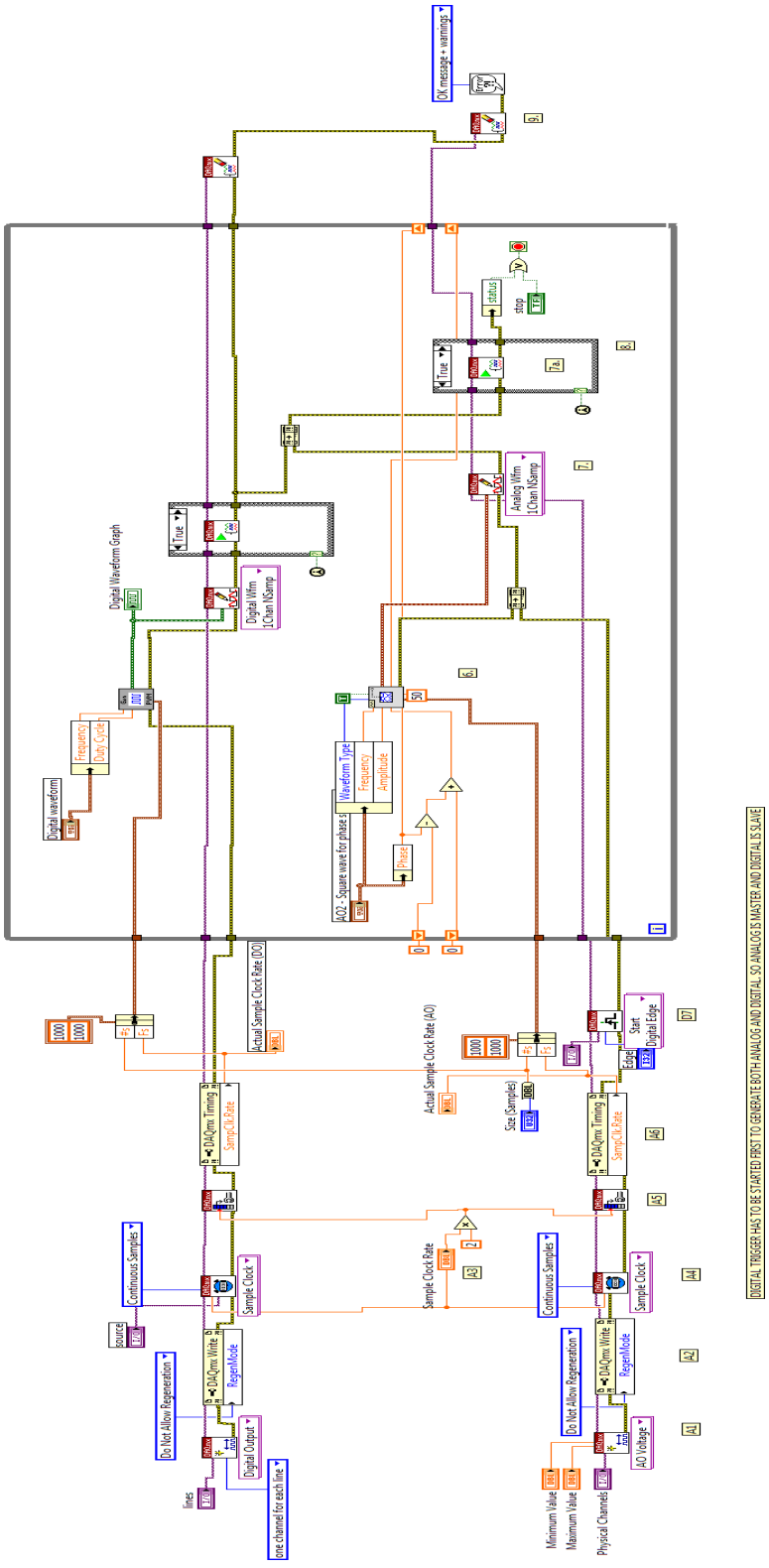

Fig 6. Block Diagram of the Digital Waveform Generation

Triggered Static Subtraction of Images (VI) written in LabVIEW

This VI will subtract a reference frame from all incoming frame and save in AVI format

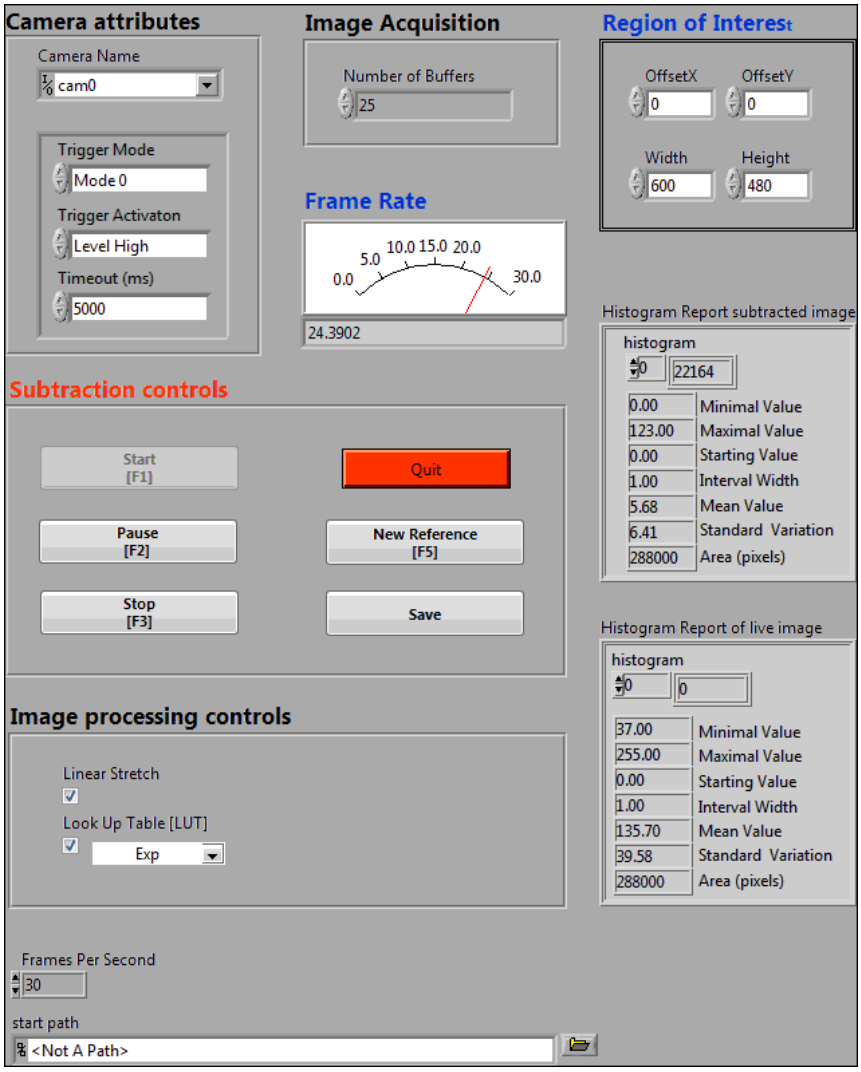

Fig 7. Front Panel Triggered Static Subtraction VI

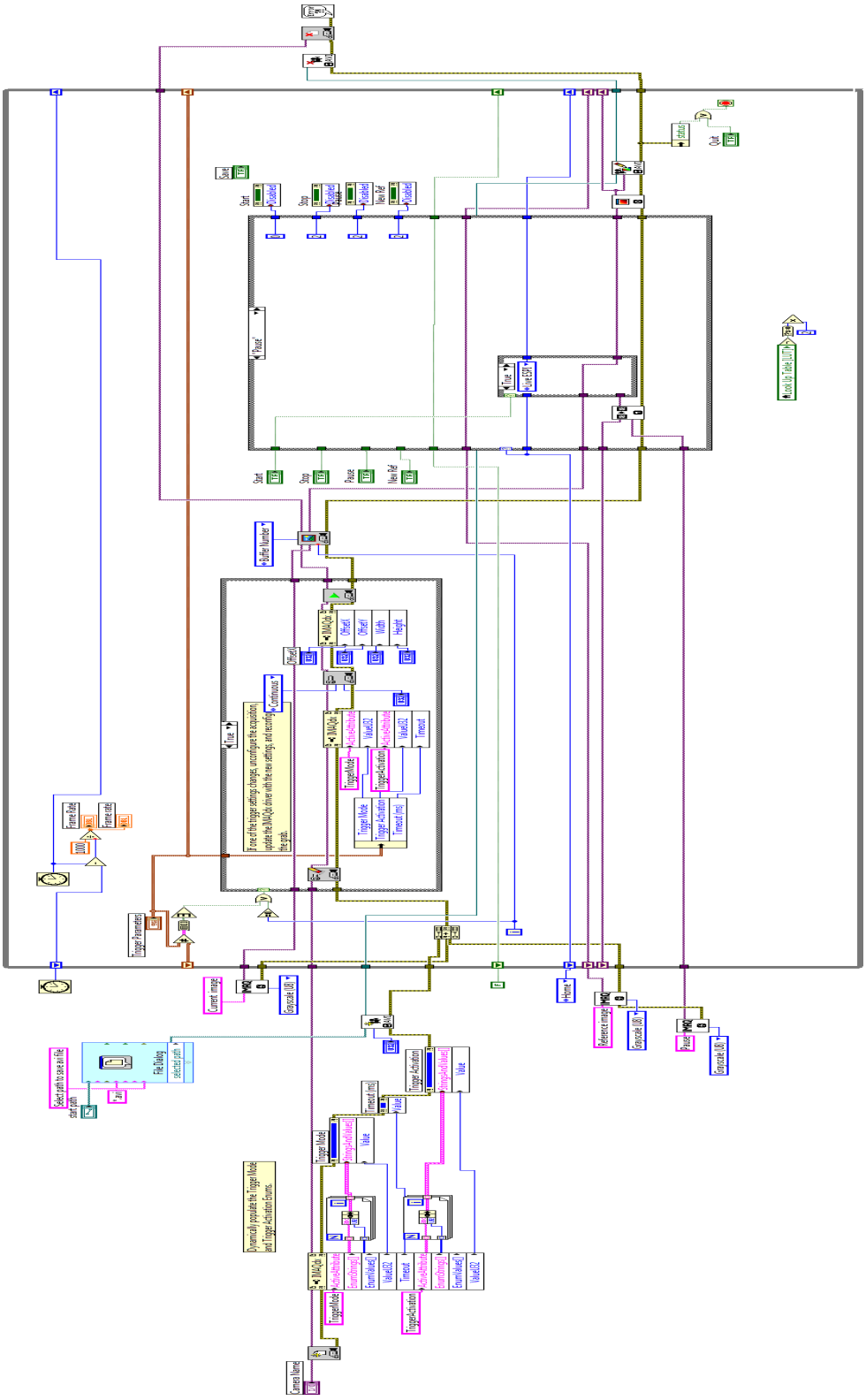

Fig 8. Block Diagram of Triggered Static Subtraction

Grab and Save Images (VI) written in LabVIEW

This VI will capture and save live images

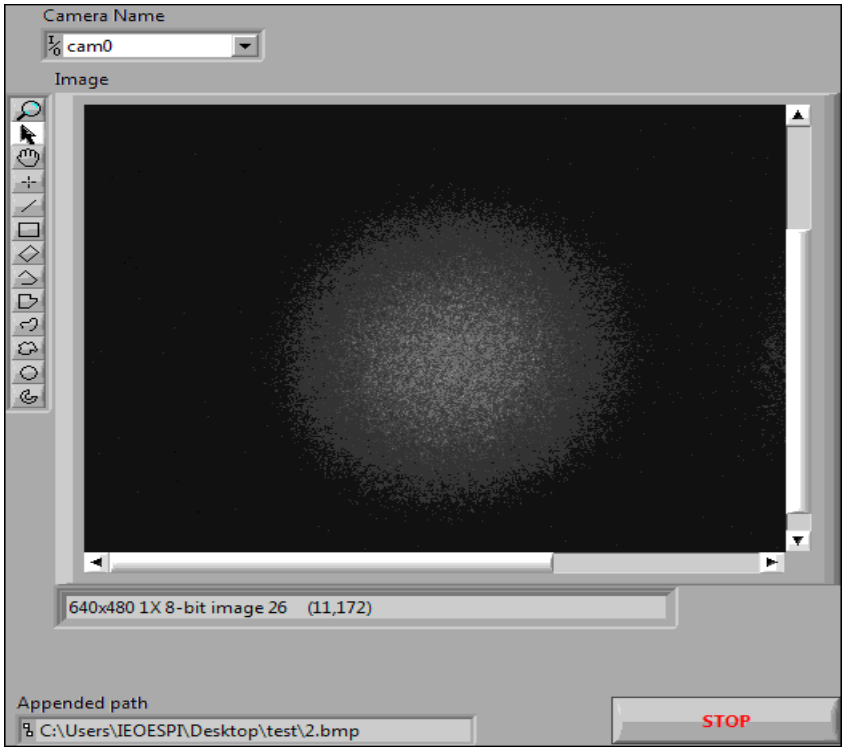

Fig 9. Front Panel of Grab and Save Image

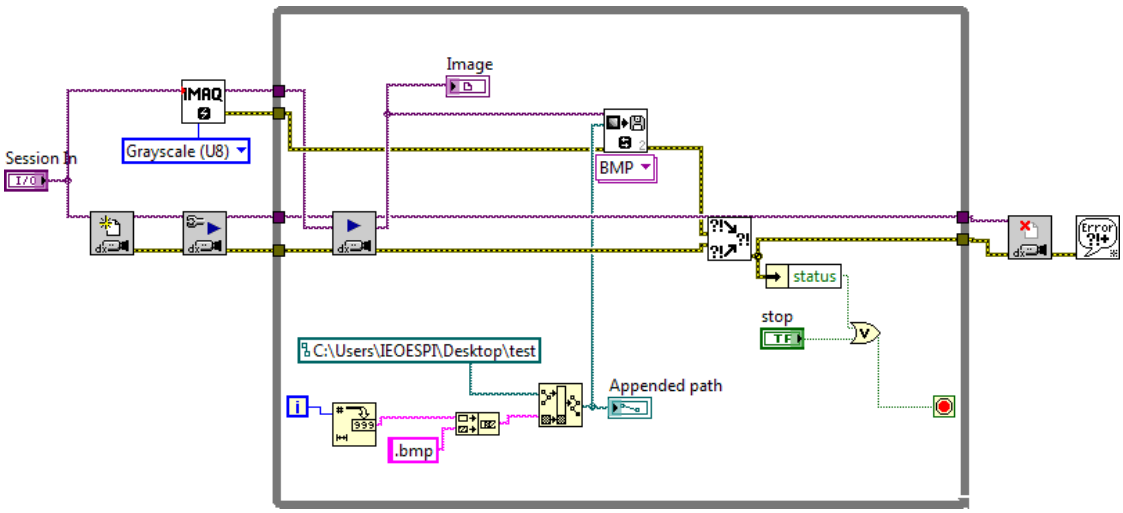

Fig 10. Block Diagram of Grab and Save Image

Trigger Camera with change in Voltage (VI) written in LabVIEW

This VI will capture and save images with a change in voltage

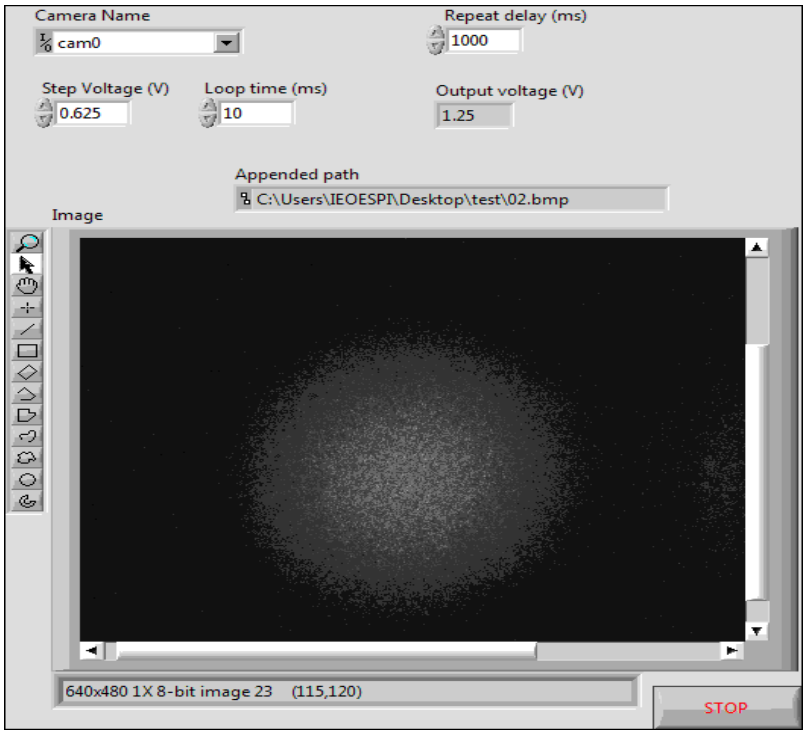

Fig 11. Front Panel Trigger Camera with change in Voltage

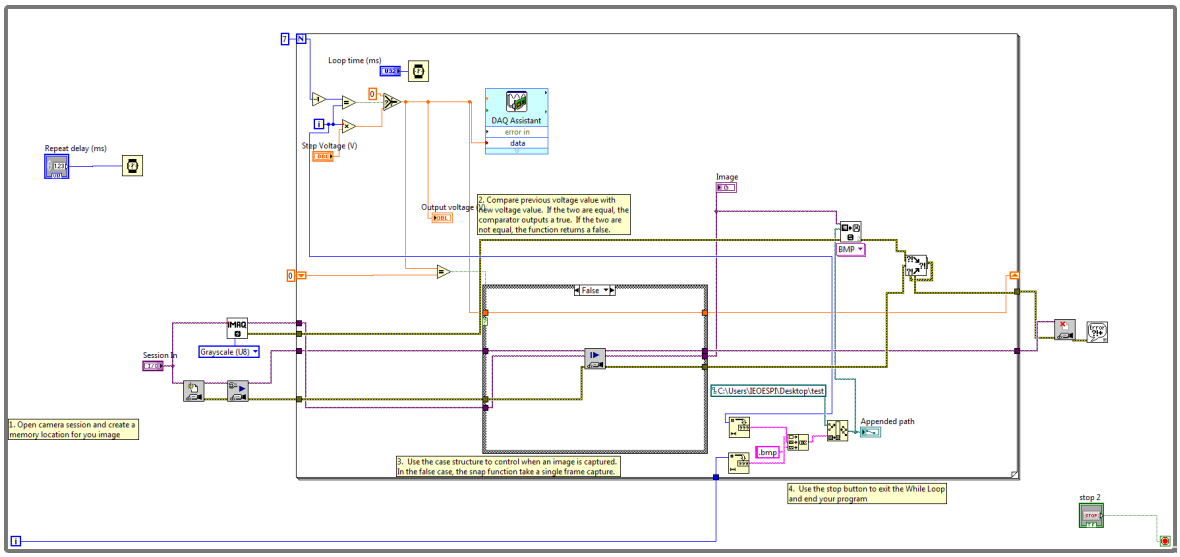

Fig 12. Block Diagram Trigger Camera with change in Voltage

Subtraction of Two Images (VI) written in LabVIEW

This VI will subtract two images

Fig 13. Front Panel of Subtraction of Two Images

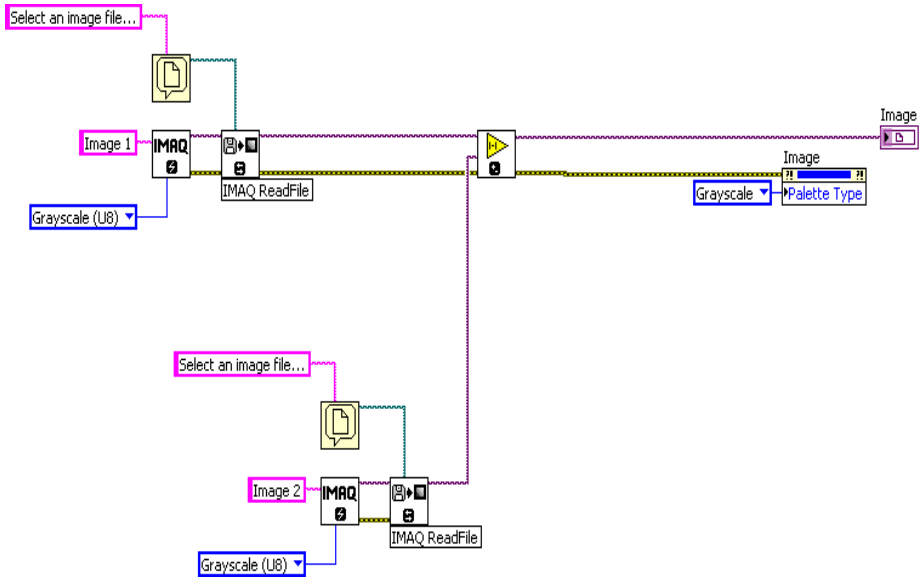

Fig 14. Block diagram of Subtraction of Two Images

APPENDIX –B

Subtraction of Phase Shifted Frames

```
A1=imread('ref.bmp');
A=double(A1);
filterImage1 = medfilt2(A,[5 5]);
i1=filterImage1;
B1=imread('01.bmp');
B=double(B1);
filterImage2 = medfilt2(B,[5 5]);
i2=filterImage2;
C1=imread('02.bmp');
C=double(C1);
filterImage3 = medfilt2(C,[5 5]);
i3=filterImage3;
D1=imread('03.bmp');
D=double(D1);
filterImage4 = medfilt2(D,[5 5]);
i4=filterImage4;
E1=imread('04.bmp');
E=double(E1);
filterImage5 = medfilt2(E,[5 5]);
i5=filterImage5;
F1=imread('05.bmp');
F=double(F1);
filterImage6 = medfilt2(F,[5 5]);
i6=filterImage6;

PSImage11=imsubtract(A,B);
PSImage12=imsubtract(A,C);
PSImage13=imsubtract(A,D);
PSImage14=imsubtract(A,E);
PSImage15=imsubtract(A,F);

S1=PSImage11;
figure(1)
image(S1)
colormap(gray)
truesize

S2=PSImage12;
figure(2)
image(S2)
colormap(gray)
truesize

S3=PSImage13;
figure(3)
image(S3)
colormap(gray)
truesize

S4=PSImage14;
figure(4)
image(S4)
colormap(gray)
truesize
```

```
S5=PSImage15;
figure(5)
image(S5)
colormap(gray)
truesize
```

Five Frame Wrapped-Unwrapped Phase Map

```
% reads an 8-bit image shifted by 0°
i1_8B=imread('01.bmp');
% converts 8-bit RGB to gray image;
A1=rgb2gray(i1_8B);
% reads  with double precision value for A1
A=double(A1);
% creates a 2D image average filter with specified kernal size
filter = fspecial('average',[7 7]);
% computes a 2D convolution between A and filter kernel provides
filtered
% image
i1 = conv2(A, filter);
% reads an 8-bit image shifted by 90°
i2_8B=imread('02.bmp');
% converts 8-bit RGB to gray image;
B1=rgb2gray(i2_8B);
% reads  with double precision value for B1
B=double(B1);
% computes a 2D convolution between A and filter kernel provides
filtered
% image
i2 = conv2(B, filter);
% reads an 8-bit image shifted by 180°
i3_8B=imread('03.bmp');
% converts 8-bit RGB to gray image;
C1=rgb2gray(i3_8B);
% reads  with double precision value for C1
C=double(C1);
% computes a 2D convolution between A and filter kernel provides
filtered
% image
i3 = conv2(C, filter);
% reads an 8-bit image shifted by 270°
i4_8B=imread('04.bmp');
% converts 8-bit RGB to gray image;
D1=rgb2gray(i4_8B);
% reads  with double precision value for D1
D=double(D1);
% computes a 2D convolution between A and filter kernel provides
filtered
% image
i4 = conv2(D, filter);
% reads an 8-bit image shifted by 360°
i5_8B=imread('05.bmp');
% converts 8-bit RGB to gray image;
E1=rgb2gray(i5_8B);
% reads  with double precision value for E1
E=double(E1);
```

```
% computes a 2D convolution between A and filter kernel provides
filtered
% image
i5 = conv2(E, filter);
% calculates wrapped phase using Schwider-Hariharan 5 frame phase
shifitng
% algorithm
WrappedPhase=atan2(2*(i4-i2),i1-2*i3+i5);
% creates an RGB graphic window
figure(1);
% creates matrix of real numbers between 0 and 1
colormap(gray(256))
% scales image data to the full range of colormap and displays
imagesc(WrappedPhase);
% compiles files written in C++ but runs in MALTLAB
mex Miguel_2D_unwrapper.cpp;
% converts wrapped phase matrix values to single precision
WrappedPhase = single(WrappedPhase);
% runs the unwrapper code on single precision wrapped phase values
UnwrappedPhase = Miguel_2D_unwrapper(WrappedPhase);
% creates an RGB graphic window
figure(2)
% creates matrix of real numbers between 0 and 1 for unwrapped
phase values
colormap(gray(256))
% scales image data to the full range of colormap and displays
imagesc(UnwrappedPhase);
```

Displacement Map

```
A=imread('C:\Users\admine\Dropbox\14-03-2013\0.3ml pp on half
plate_10mw green bigger than red\subtracted\80s_125_75.png');
% creates matrix of real numbers between 0 and 1 for unwrapped
phase values
B=rgb2gray(A);
% scales image data to the full range of colormap and displays
C=double(B);
% converts unwrapped phase values to double precision matrix
% wavelength of the laser light is defined as
lambda=633*1e-9;
% calculates displacement values from unwrapped phase map
displacement=C*(lambda/(4*pi));
% creates an RGB graphic window
% displays a 3D displacement map
mesh(displacement);
xlabel('Pixels','FontSize',12) ;
ylabel('Pixels','FontSize',12) ;
zlabel('Shrinkage','FontSize',12) ;
```

Publications and Presentations

Peer-reviewed journals:

1. Mohesh Moothanchery, Izabela Naydenova, and Vincent Toal, "Studies of shrinkage as a result of holographic recording in acrylamide based photopolymer film", Appl. Physics, A.104, 899-902, May 2011
2. Mohesh Moothanchery, Izabela Naydenova, Vincent Toal, "Holographic grating formation in acrylamide based photopolymer with shrinkage", Optics Express.19, 13395-13404, June 2011
3. Mohesh Moothanchery, Izabela Naydenova, Svetlana Mintova and Vincent Toal, Si-MFI zeolite nanoparticle doped photopolymer with reduced shrinkage, Optics Express, 19, 25786-25791, Dec.2011
4. Mohesh Moothanchery, Viswanath Bavigadda, Vincent Toal and Izabela Naydenova "Shrinkage during holographic recording in photopolymer films determined by holographic interferometry" (Submitted to Applied Optics)
5. Mohesh Moothanchery, Svetlana Mintova, Vincent Toal and Izabela Naydenova "Reduced shrinkage in photopolymer films determined by holographic interferometry" (To be submitted to Journal of Optics)
6. Mohesh Moothanchery, Viswanath Bavigadda, Vincent Toal and Izabela Naydenova, "Studies of shrinkage in photopolymer films determined by electronic speckle pattern interferometry" (To be submitted to Optics Letters)

Conference proceeding papers:

1. M. Moothanchery, I. Naydenova, V. Bavigadda, S. Martin and V. Toal, "Real-time shrinkage studies in photopolymer films using holographic interferometry," Proc. SPIE, Vol. 8437, 8437I, (2012)
2. I. Naydenova, S. Mintova, M. Moothanchery, E. Leite, T. Babeva, S. Martin, V. Toal, "Nanozeolite doped photopolymerisable composites: optical properties and holographic applications, Information Photonics, Ottawa, Canada, May 18-20, 2011.
3. Mohesh Moothanchery, Svetlana Mintova, Izabela Naydenova and Vincent Toal, Nanoparticle doped photopolymer with reduced shrinkage in photopolymer film: Photonics 2010, December 11-15 **,** Guwahatti, India

Oral Presentations:

1. Mohesh Moothanchery, Izabela Naydenova, Svetlana Mintova, and Vincent Toal, "Photopolymer films doped with zeolite nanocrystals", 10th Mediterranean workshop and Topical Meeting "Novel Optical Materials and Applications" Cetraro, Italy, June 05-11, 2011
2. I. Naydenova, S. Mintova, M. Moothanchery, E. Leite, T. Babeva, S. Martin, V. Toal, "Nanozeolite doped photopolymerisable composites: optical properties and holographic applications, Information Photonics, Ottawa, Canada, May 18-20, 2011
3. M. Moothanchery, I. Naydenova, S. Mintova, V. Toal, "Nanozeolites doped photopolymer with reduced shrinkage for holographic applications", DIT Annual research symposium, February 2011.

4. M. Moothanchery, I. Naydenova, V. Toal, “Shrinkage studies in photopolymer films using holographic interferometry”, DIT Postgraduate Research Symposium, Nov 2011.

Poster presentations:

1. Mohesh Moothanchery, Izabela, Naydenova, Viswanath Bavigadda, Suzanne Martin, Vincent Toal, “Real-time shrinkage studies in photopolymer films using holographic interferometry,” Photonics Europe, Brussels , Belgium ,April 2012
2. Mohesh Moothanchery, Izabela, Naydenova, Svetlan Mintova, Vincent Toal , “Shrinkage studies in nanozeolites doped photopolymer,” IOP Rosse Medal Competition, RCSI, 30th March 2012.
3. M. Moothanchery, I. Naydenova, S. Mintova, V. Toal, “Holographic recording in zeolite nanoparticle doped acrylamide photopolymer films”, Photonics Ireland-2011, Dublin, Ireland, September 2011 ,
4. Mohesh Moothanchery, Izabela Naydenova, Svetlana Mintova, and Vincent Toal,” Si-MFI nanozeolite doped acrylamide photopolymer films”, IoP Spring Meeting, Carlingford, Ireland, April, 2011.
5. M. Moothanchery, I. Naydenova, V. Toal, “Bragg detuning of slanted holographic gratings in photopolymer film”, COST MPO604 Meeting, Visegrad, Hungary, 2010.
6. M. Moothanchery, I. Naydenova, S. Mintova, V. Toal, “Nanozeolites doped photopolymer with reduced shrinkage for holographic recording”, “10th International Conference on Fibre Optics and Photonics: PHOTONICS-2010”, Guwahati (IIT), India, December 2010
7. M.Moothanchery , I Naydenova & V Toal, “Studies of shrinkage as a result of holographic recording in acrylamide based photopolymer film” ICPEPA-7, Copenhagen, Denmark, 2010.
8. M. Moothanchery, I. Naydenova, V. Toal, “Bragg detuning of slanted holographic gratings in acrylamide based photopolymer film”, Summer School on Optoinformatics , Maynooth, Ireland, June 2010